

Politecnico di Torino

Department of Control and Computer Engineering (DAUIN)



**Master of Science in  
Mechatronics Engineering**

Master's Thesis

**Characterization of the EBM Additive Manufacturing  
Process Parameters using Artificial Neural Networks**

Supervisor:

**Prof. LUCA IULIANO**

Co-Supervisors:

**Prof. SANTA DI CATALDO**

**Prof. ENRICO MACII**

**Dr. MANUELA GALATI**

Candidate:

**Babar Saleem**

2020



## **Abstract**

Additive manufacturing also known as 3D printing is an emerging technology as it has great potential in a large variety of applications in aerospace, biomedical and automotive industry. Additive manufacturing enables the production of complicated designs, lightweight structures and novel functional features by joining materials in a layer by layer fashion to make the objects from 3D models. Nowadays there are various technologies which can implement AM using different kinds of materials, such as Powder Bed Fusion (PBF) which includes, selective laser sintering (SLS) and Electron Beam Melting (EBM). With the rapid development of AM, more complex structures with more materials can be fabricated.

Specifically the Electron beam used to melt the powder in EBM is much more powerful than the laser and can result in strong mechanical properties of manufactured part with high density, offering minimal waste. However, ensuring AM part quality in EBM still remains the big challenge in the major industrial breakthrough of additive manufacturing technologies.

Recently, the machine learning (ML) that is a growing field of artificial intelligence (AI) is becoming more and more important not only in Additive manufacturing but in overall manufacturing industry, mainly because of ability of ML to perform the complex task such as regression and classification. The basic purpose of Machine Learning is to make a system able to learn useful features from a data set identify the patterns and accordingly make the decisions. Currently, ML is applied in various processes of additive manufacturing like for monitoring of the AM process and making it able to take decisions on the basis of data coming from different cameras and sensors, like for defects and anomaly detection. In this thesis a framework of optimizing the influential parameters impacting on the final part quality of EBM produced parts has been implemented. First, all of such important parameters have been identified by different analysis techniques. Afterwards, the co-relation analysis of these parameters was carried out in order to find the impact of variance of these parameters on different part qualification categories. Finally, using this data a regression model was developed by comparing different machine learning algorithms to find a network that could predict the process parameter anomaly, before going towards the failure of the part.

## **Acknowledgements**

First and foremost I am highly grateful and indebted to my supervisor, Prof. LUCA IULIANO and my co-supervisors who let me pursue this masters thesis at Politecnico di Torino. Specially I would like to extend my gratitude to Dr. MANUELA GALATI and OSCAR DI MAURO for being available all the time to provide their valuable feedback. Their directions and supervision facilitated me to learn beyond the scope.

I would like to dedicate this thesis and degree to my late father who was the main source of motivation and inspiration for me to achieve this goal. I am also thankful to my family for their emotional support particularly in the difficult times of COVID-19 lockdown.

---

# Contents

<b>List of Figures</b>	III
<b>List of Tables</b>	V
<b>1 INTRODUCTION</b>	1
1.1 OVERVIEW . . . . .	1
1.2 EBM THE PROCESS . . . . .	3
1.2.1 EBM TECHNOLOGY . . . . .	3
1.2.2 ELECTRON BEAM PARAMETERS . . . . .	6
1.3 ELECTRON BEAM-MATTER INTERACTION . . . . .	9
1.3.1 ELECTRONS AND MATTER . . . . .	9
1.4 REVIEW OF PROCESS DEFECTS IN EBM . . . . .	10
1.4.1 POROSITY AND LACK OF FUSION . . . . .	10
1.4.2 BALLING . . . . .	10
1.4.3 RESIDUAL STRESS, DELAMINATION AND CRACKING . . . . .	11
1.4.4 SURFACE DEFECTS . . . . .	12
1.4.5 GEOMETRICAL DEFECTS . . . . .	12
1.4.6 SMOKING . . . . .	13
1.5 REVIEW OF PROCESS MONITORING IN EBM . . . . .	13
1.5.1 IN-PROCESS MONITORING METHODS IN EBM . . . . .	13
<b>2 MACHINE LEARNING IN ADDITIVE MANUFACTURING: STATE OF THE ART</b>	20
2.1 MACHINE LEARNING TECHNIQUES . . . . .	20
2.1.1 SUPERVISED LEARNING . . . . .	20
2.1.2 UNSUPERVISED LEARNING . . . . .	21
2.1.3 REINFORCEMENT LEARNING . . . . .	21
2.2 NEURAL NETWORKS . . . . .	22
2.2.1 CONVOLUTION NEURAL NETWORKS . . . . .	23
2.3 ML APPLICATIONS IN REAL WORLD . . . . .	24
2.4 APPLICATION OF MACHINE LEARNING IN AM . . . . .	25
2.4.1 APPLICATION OF ML IN THE IN-PROCESS DEFECT MONITORING . . . . .	26
2.4.2 APPLICATION OF ML IN POWDER SPREADING CHARACTERIZATION . . . . .	28
2.4.3 APPLICATION OF ML IN PROCESS PARAMETER OPTIMIZATION . . . . .	29

<b>3</b>	<b>MATERIALS AND METHODOLOGY</b>	<b>33</b>
3.1	Material . . . . .	33
3.2	Parameter Analysis and Co-relation . . . . .	34
3.2.1	Arcam EBM® Log Studio . . . . .	34
3.2.2	Beam Current . . . . .	36
3.2.3	Bottom Temperature . . . . .	37
3.2.4	Column Temperature . . . . .	37
3.2.5	Filament Current . . . . .	38
3.2.6	Rake Current Feedback . . . . .	38
3.2.7	Left/Right Regulator Pulse Length . . . . .	39
3.2.8	Current Height . . . . .	39
3.2.9	Backing Vacuum Gauge Feedback . . . . .	40
3.2.10	Chamber Vacuum Gauge Feedback . . . . .	40
3.2.11	Column Vacuum Gauge Feedback . . . . .	41
3.3	Pearson Correlation Coefficient . . . . .	41
3.4	Prediction Models/Classifiers . . . . .	42
<b>4</b>	<b>Experiments and Results</b>	<b>47</b>
4.1	Results of Parameter Analysis and Correlation . . . . .	48
4.1.1	Build Done Case I . . . . .	48
4.1.2	Build Done Case II . . . . .	50
4.1.3	Build Done Case III . . . . .	51
4.1.4	Build Failed Case I . . . . .	53
4.1.5	Build Failed Case II . . . . .	54
4.1.6	Build Failed Case III . . . . .	56
4.1.7	Arc Trip Error Case . . . . .	57
4.1.8	Correlation Analysis Conclusion . . . . .	59
4.2	Results of Support Vector Machine (SVM) . . . . .	60
4.3	Results of Artificial Neural Networks (ANN) . . . . .	61
4.4	Python Script . . . . .	62
<b>5</b>	<b>CONCLUSION AND FUTURE WORK</b>	<b>73</b>
5.0.1	Conclusion . . . . .	73
5.1	Future Work . . . . .	74
	<b>Bibliography</b>	<b>75</b>

---

# List of Figures

1.1	Metal Additive Manufacturing processes: ISO-ASTM 52900 [2]	2
1.2	Schematic of an EBM apparatus (Source: Arcam)	3
1.3	Schematic of important parts of EBM build chamber (Source: Arcam)	4
1.4	Flow chart of a general AM production cycle	5
1.5	Phases of EBM process (Galati and Iuliano, [57])	6
1.6	By products of electron beam – matter interaction	9
1.7	Process induced Vs gas induced porosity [8]	10
1.8	Example of Balling Effect [8],[16]	11
1.9	Example of Delamination [8],[16]	11
1.10	Example of Surface Defects [8]	12
1.11	Example of Warping [8]	12
1.12	Smoking effect of one powder layer [4],[8]	13
1.13	Two possible camera arrangements: First one at the top [17], the second at front [20]	14
1.14	Detected defect in thermal image [5]	16
1.15	Metallographic images Vs IR images [17]	17
1.16	Temperature profile in hatch melting [19]	18
1.17	Average temperature profiles at different build heights [19]	18
2.1	Description of Machine Learning types, taken from <a href="https://cleanpng.com/Rusbert">https://cleanpng.com/Rusbert</a>	22
2.2	A simple NN	23
2.3	Architecture of Convolution Neural Network [59]	24
2.4	Involvement of ML in different AM domains [54]	25
2.5	Additive manufacturing data Vs Machine learning (Baumann et al [40])	26
2.6	Additive manufacturing monitoring system (Xinbo Qi et al [45])	28
2.7	SVM-prediction of macro properties of EBM built parts [53]. (i) For 12 different process-parameters, top-surface conditioning the printed samples. (ii) Micrograph of cross section of each sample. (iii) Construction of the process map for optimization of process parameters to obtain good surface finish and low porosity.	30
2.8	Development of ANN model for the framework proposed by Mallikharjun et al [30]	31
2.9	The employed Neural Network Model by Mallikharjun et al [31]	32
2.10	Algorithm of selection process parameters by Mallikharjun et al [31]	32
3.1	Viewing of graphs in Log Studio, example 1 (Arcam Log Studio)	35

3.2	Viewing of graphs in Log Studio example 2 (Arcam Log Studio) . . . . .	35
3.3	Graph of Beam current (Arcam Log Studio) . . . . .	37
3.4	Graph of Bottom Temperature (Arcam Log Studio) . . . . .	37
3.5	Graph of Column Temperature (Arcam Log Studio) . . . . .	38
3.6	Graph of Filament Current (Arcam Log Studio) . . . . .	38
3.7	Graph of Rake Current Feedback (Arcam Log Studio) . . . . .	39
3.8	Graph of Left/Right Regulator Pulse Length (Arcam Log Studio) . . . . .	39
3.9	Graph of Current Height (Arcam Log Studio) . . . . .	40
3.10	Graph of Backing Vacuum Gauge Feedback (Arcam Log Studio) . . . . .	40
3.11	Graph of Chamber Vacuum Gauge Feedback (Arcam Log Studio) . . . . .	41
3.12	Graph of Column Vacuum Gauge Feedback (Arcam Log Studio) . . . . .	41
3.13	SVM classifier separating hyper-plane ( <a href="https://developer.xilinx.com/en/articles/exploring-support-vector-machine-acceleration-with-vitis.html">https://developer.xilinx.com/en/articles/exploring-support-vector-machine-acceleration-with-vitis.html</a> ) . . . . .	42
3.14	Process flow of artificial neural network . . . . .	44
4.1	Results of Correlation analysis of build done case I, Part-1 . . . . .	48
4.2	Results of Correlation analysis of build done case I, Part-2 . . . . .	49
4.3	Results of Correlation analysis of build done case II, Part-1 . . . . .	50
4.4	Results of Correlation analysis of build done case II, Part-2 . . . . .	50
4.5	Results of Correlation analysis of build done case III, Part-1 . . . . .	51
4.6	Results of Correlation analysis of build done case III, Part-2 . . . . .	52
4.7	Results of Correlation analysis of build failed case I, Part-1 . . . . .	53
4.8	Results of Correlation analysis of build failed case I, Part-2 . . . . .	53
4.9	Results of Correlation analysis of build failed case II, Part-1 . . . . .	54
4.10	Results of Correlation analysis of build failed case II, Part-2 . . . . .	55
4.11	Results of Correlation analysis of build failed case III, Part-1 . . . . .	56
4.12	Results of Correlation analysis of build failed case III, Part-2 . . . . .	56
4.13	Results of Correlation analysis of arc trip error case, Part-1 . . . . .	57
4.14	Results of Correlation analysis of arc trip error case, Part-2 . . . . .	58

---

# List of Tables

1.1	Some EBM Parameters . . . . .	6
1.2	EBM Vs SLM . . . . .	7
1.3	EBM: Benefits and Drawbacks . . . . .	8
1.4	SLM: Benefits and Drawbacks . . . . .	8
1.5	Review of Process Monitoring in EBM . . . . .	16
2.1	Real world application of ML techniques (MathWorks, 2016) . . . . .	24
3.1	Most important categories of Log Studio (Arcam Log Studio) . . . . .	34
4.1	Summary of Correlation analysis . . . . .	59
4.2	Shape of SVM data set . . . . .	60
4.3	Results of SVM model . . . . .	60
4.4	Shape of ANN data set . . . . .	61
4.5	Results of ANN model . . . . .	61

# List of Acronyms

<b>AM</b>	Additive Manufacturing
<b>ANN</b>	Artificial Neural Networks
<b>AI</b>	Artificial Intelligence
<b>CNN</b>	Convolutional Neural Networks
<b>NN</b>	Neural Networks
<b>ML</b>	Machine Learning
<b>PBF</b>	Powder Bed Fusion
<b>EBM</b>	Electron Beam Melting
<b>DED</b>	Direct Energy Deposition
<b>FDM</b>	Fused Deposition Modeling
<b>SLS</b>	Selective Laser Sintering
<b>LOM</b>	Laminated Object Manufacturing
<b>ASTM</b>	American Society for Testing and Materials
<b>PID</b>	Proportional - Integral - Derivative
<b>MLP</b>	Multi Layer Perceptron
<b>ANFIS</b>	Adaptive Network Based Fuzzy Inference System
<b>MSE</b>	Mean Squared Error
<b>RMSE</b>	Root Mean Squared Error
<b>PPMCC</b>	Pearson Product Moment Correlation Coefficient

---

---

## CHAPTER 1

---

# INTRODUCTION

### 1.1 OVERVIEW

Additive manufacturing AM represents a novel manufacturing paradigm capable of completely revolutionizing conventional technologies, thanks to the ability of producing complex shapes, innovative lightweight structures, internal features and functional surface patterns that can not be produced with traditional approaches. Its origins move from Austin, TX, where Deckard obtained in 1986 the first SLS (Selective Laser Sintering) patent. AM technologies allows the manufacturing industry to go beyond the limits of conventional processes providing the so-called “complexity for free” but also a completely new approach for the management of the overall value chain. Additive Manufacturing uses produces the part by adding many layers of a material. As per ASTM F42 standard [1] Additive manufacturing has seven types: Binder jetting, Direct Energy Deposition, FDM, Material Jetting, Powder Bed Fusion (SLS/SLM/EBM), Sheet Lamination (LOM) and Vat Photopolymerization. The first application of AM was in Rapid Prototyping applications on polymers. Thanks to continuous technological development, AM passed from prototyping to industrial production, by expanding the range of materials. Recently, industrial discrete-part manufacturers focused their interest onto metal additive manufacturing. According to the ASTM standard above mentioned [1], only four processes of the seven listed pertain to metal additive manufacturing: binder jetting, direct energy deposition, sheet lamination and powder bed fusion. All these processes bond together the feedstock into a final 3D object. Binder jetting produces 3D objects through the iterative deposition of a liquid binder over powder material (spread over a build platform) layer by layer [27]. Direct energy deposition encompasses different processes, similar to that of material extrusion, where the feedstock (powder or wire) is deposited directly into a melt pool generated by a focused energy. Sheet lamination process uses sheets of metal to form parts. Metal sheets are bond together through ultrasonic welding. Finally, powder bed fusion processes use a focused energy (laser beam or electron beam) in order to selectively melt a layer of powder. Powder is spread and selectively melted layer by layer until the part is complete. Selective Laser Melting (SLM) and Electron Beam Melting (EBM) can be differentiated on the basis of the power source. Figure 1 shows AM processes for metals on the basis of classification done by ASTM [2].

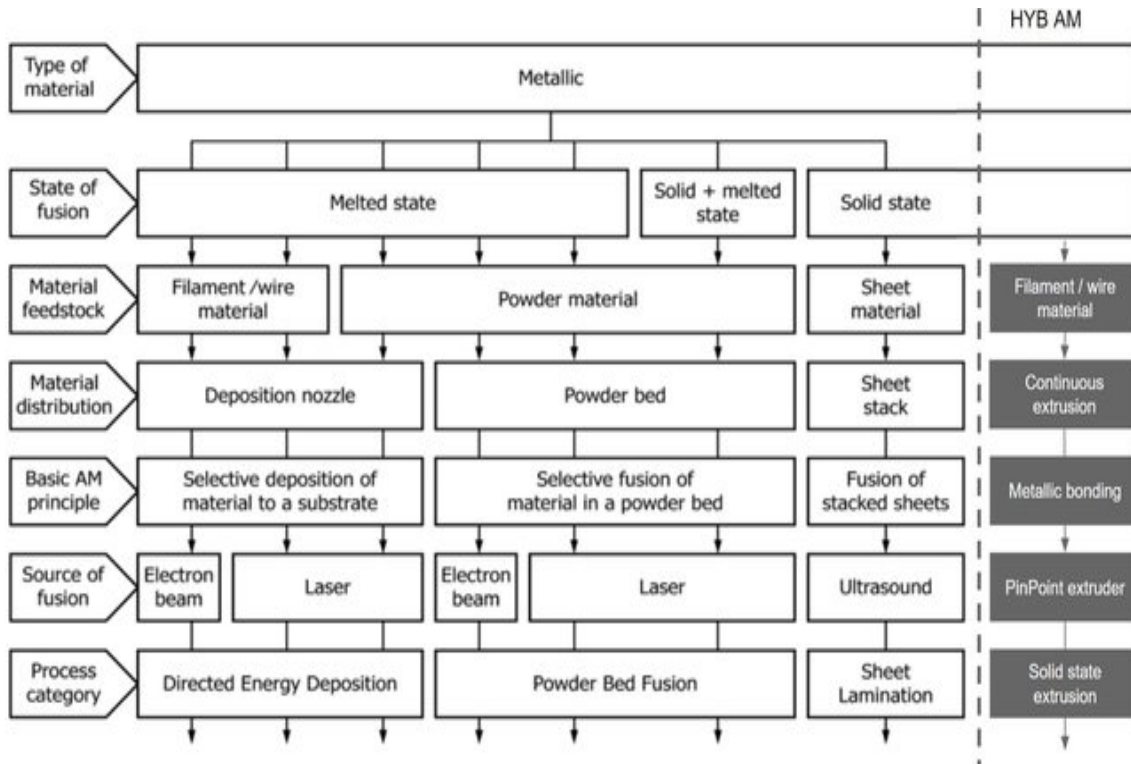


Figure 1.1: Metal Additive Manufacturing processes: ISO-ASTM 52900 [2]

Generally speaking, powder bed fusion processes are able to produce parts with a minimum feature size smaller than other AM processes. In particular this thesis work will focus on Electron Beam Melting, which has the peculiarity to exploit an electron beam as source of power. With respect to other processes, EBM presents the advantage of being hot, enabling the processing of materials that require extremely high temperature to be worked. A remarkable rapid development has to be noticed for EBM, which was first patented in 2000 by Larsson Anderson and now is becoming a standard process in the aeronautic sector, e.g., for turbine blade production. EBM finds many other applications in the medical sector (in the production of medical prosthesis) and in the automotive sector as well. Despite its potentialities, the process presents many issues. The interaction of the electron beam with the metal is regulated by complicated physical principles that are connected with the emission of many relevant by-products (like charged particles and different kind of radiations). Very few materials have been developed for the production in EBM due to the difficulties in defining optimum process parameters. Furthermore one of the most important process issues is related to the capability of achieving high quality and repeatability performances. In this sense, some very recent papers related to in-situ process monitoring have been published. This thesis provides a state of the art analysis for EBM that encompassed all the above-mentioned issues.

The work starts with a detailed analysis of system properties and performances, in the perspective of providing a comparison with SLM, considering technical parameters, pros and cons. A physical description of the electron beam interaction with the part is provided, with the aim to point out the nature of the signal emitted during the process: process by-products are potential process information for future in-situ process monitoring strategies. A state of the art concerning major defects and EBM process

monitoring is provided.

The thesis is organised as follows. The first section presents a description of the technology and a comparison with SLM. The second section discusses the physical issues related to electron beam and matter interactions, going on with an analysis of the materials developed for EBM manufacturing. In section three, reported is the review of state the of the art of EBM process monitoring. Section three expands the analysis of the previous section. Section four the application of Neural Networks to optimize the process parameters.

## 1.2 EBM THE PROCESS

A generic description of Electron Beam Melting technology is provided in this section. Electron Beam Melting technology along with system configuration is reviewed in the sub-section 1.1. Finally, advantages and drawbacks of EBM with respect to SLS based PBF are discussed in sub-section 1.2.

### 1.2.1 EBM TECHNOLOGY

Fig. 1.2 shows a generic EBM based additive manufacturing hardware setup.

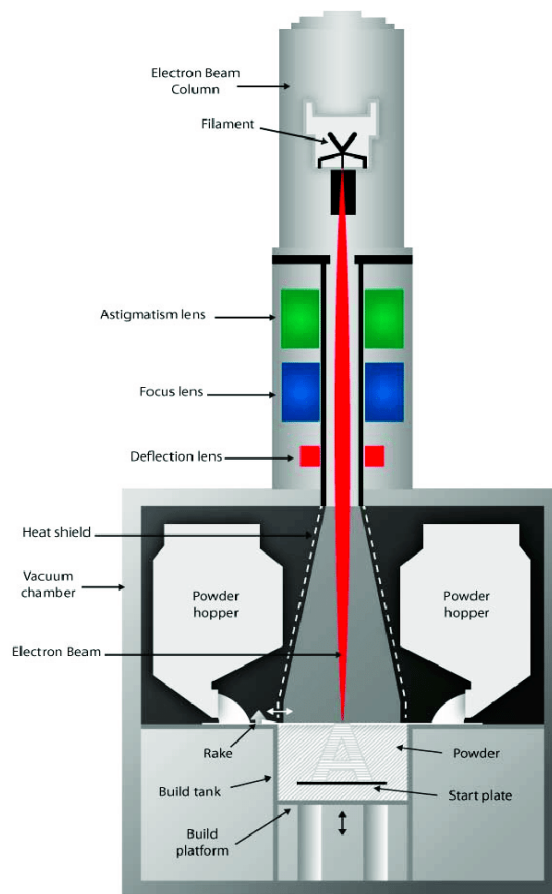


Figure 1.2: Schematic of an EBM apparatus (Source: Arcam)

The hardware consists of many parts. The most important part is the power source that is the electron gun in our case. Electron beam is generated by the electron gun that is further directed towards the build platform with the help of a setup of electromagnetic lens. A start plate is housed in the build platform which is moved down after each scanning cycle in order to add the layers. Powder hoppers setup is responsible of storing the needed powder for manufacturing of the part. A powder handling system joins hands with the powder hoppers and it takes the required amount of powder to be laid as a layer. A powerful vacuum is generated with the help of a pump. To protect the internal assembly of the machine from high temperature machine is done with a shielding internally. Moreover, to protect the human around the machine from the toxic radiations, an x-ray shielding is also constructed [3]. Figure 1.3 shows the important parts of build chamber.

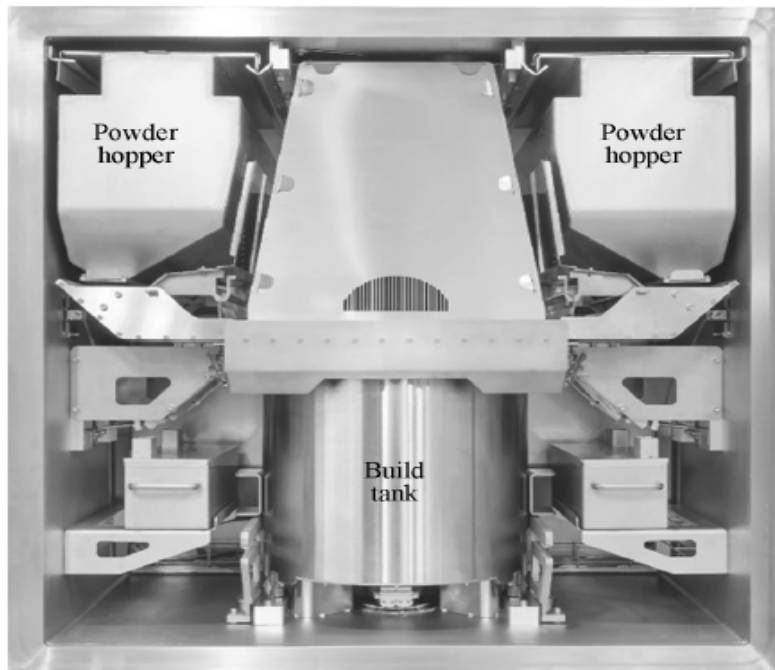


Figure 1.3: Schematic of important parts of EBM build chamber (Source: Arcam)

To start with the process, a design of the required part is created in the CAD. Advantage of this technology is that the required part can be directly build after the cade process without any need of complicated planning of process. There is no need of different tooling and complex fixtures. Therefore additive manufacturing is cheaper than the conventional manufacturing techniques in many ways. A generic overview of the additive manufacturing production cycle is shown in figure 1.4.

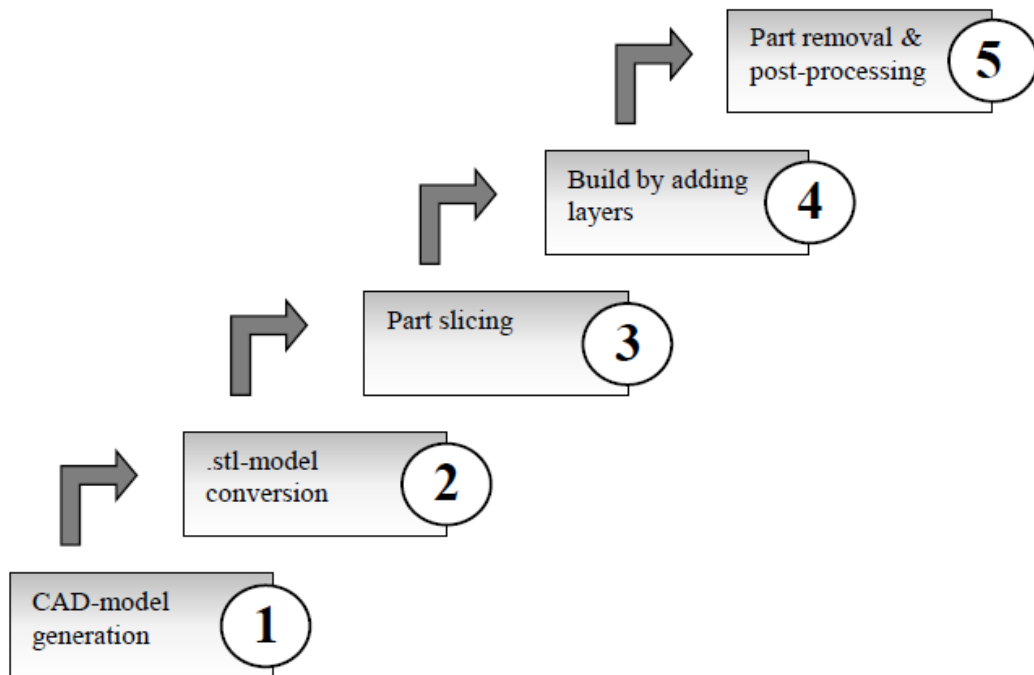


Figure 1.4: Flow chart of a general AM production cycle

The CAD file is converted to a STL file before manufacturing the part in the machine. To facilitate the acceleration of the electrons, the system consists of a hot cathode which is a tungsten filament most of the time and one or more anodes. Underneath the anode cathode system there exists two levels of electromagnetic focusing lenses. The purpose of first level of focusing lenses is to focus the electron beam into a concentrated spot. The required beam pattern is deflected by the second level of lenses. In the build platform a layer of metallic powder is laid on a table, the layer thickness used to be from 0.1 mm to 0.01. Thermionic effect is responsible to produce the free electrons in the cathode. The electrons generated by the electric field are deflected by the deflection lenses after being focused into a beam by the first level of lenses and directed towards the table carrying the metallic powder. After initiation of the process the first phase comes is the pre-heating where the electron beam heats the powder to a desired temperature level [4]. As per the work done of [5] the target temperature during this phase is usually half of fusion point. The residual stresses are greatly reduced as the powder up to the pre-heating phase is only partially melted and the gradient in-between the lower layer and the pool of melt is lowered. The melting phase is followed by pre-heating. In this phase the scanning speed is reduced and the power of electron beam is increased. The powder is melted during the scan and converted to solid form in a quick time. After the completion of the scan the height of platform is adjusted in such a way that it moved down equal the thickness of the layer that is added. In a same way many layers are added until the final product is achieved. This cycle repeats layer by layer until the final product. Also some helium pressure is present in the vacuum chamber [6]. The phases involved in the EBM process are shown in the figure figure 1.5.

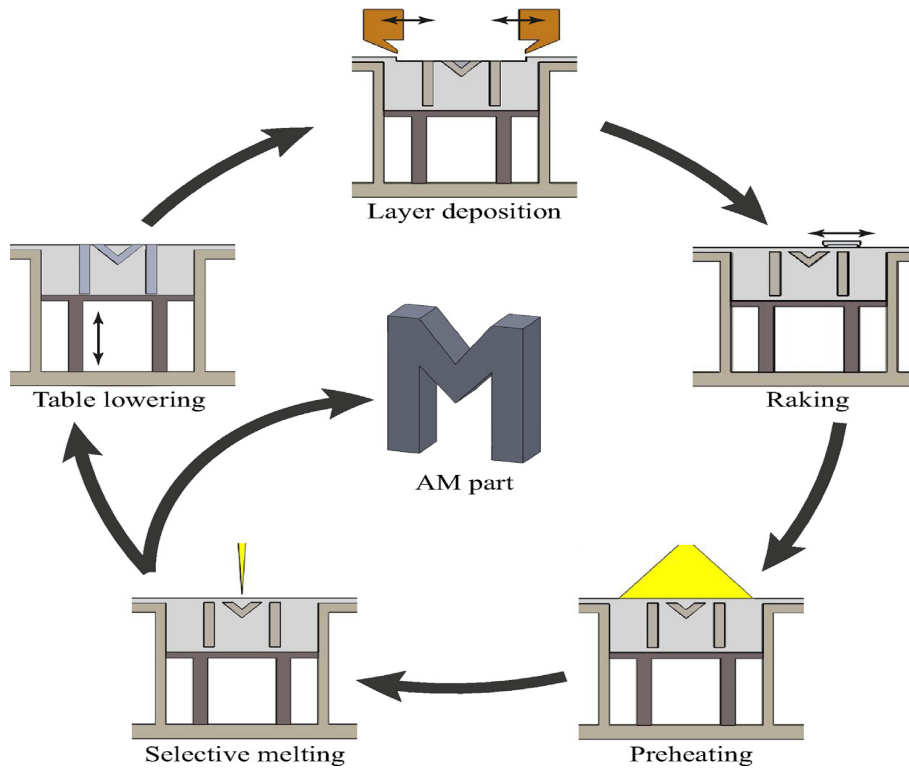


Figure 1.5: Phases of EBM process (Galati and Iuliano, [57])

### 1.2.2 ELECTRON BEAM PARAMETERS

There are many process parameters that can effect the quality of the finished product, some relevant parameters are given by [7].

Sr. Nr.	EBM PARAMETERS
1	Current to generate the beam
2	The current that is used to focus the position by the lens
3	The scanning speed
4	The current that is used to deflect the beam
5	The pulsing of the beam
6	No. of repetition cycles of the scan
7	Offset present in.between the lines of scan
8	The sequence of line in order to generate hatch pattern

Table 1.1: Some EBM Parameters

The total beam power can be evaluated by the multiplication of beam current and accelerating voltage. Considering that the phenomenon of electron back scattering causes the repulsion of a pre-determined percentage of electrons according to specific material, in order to increase the heat transfer it results more effective to manage the current intensity than voltage. Scanning parameters influence also an important quantity: Andrews's number, a.k.a. applied energy density (simplified model):

$$E_A = \frac{P}{V * SP}$$

P = beam power V = scan velocity SP = scan distance between parallel lines [20]

According to above expression, the supplied energy density increases by decreasing the scanning velocity and scan spacing. Scan velocity can be optimized considering this formula and the optimal energy quantity estimated through experiments considering also that the scan velocity influences the probability of balling effect and smoking effect occurrence.

COMPARISON BETWEEN EBM AND SLM After having an insight of the process description it is important to describe the key difference between both the PBF technologies, i.e; EBM and SLM. Table 1.2 provides this comparison on the basis of some major technical parameters [3].

DRIVER	EBM	SLM
Thermal source	Electron beam	Laser
Atmosphere	Vacuum	Inert gas
Scanning	Deflection coils	Galvanometer
Energy absorption	Conductivity limited	Absorptivity Limited
Power pre-heating	Uses electron beam	Uses infrared heaters
Scan Speeds	Very fast ->magnetically driven	Limited by galvanometer inertia
Energy costs	Moderate	High
Surface finish	Moderate to poor	Excellent to moderate
Feature resolution	Moderate	Excellent
Materials	Metals (conductors)	Polymers, metals and ceramics
Layer thickness (um)	50 um	10-50 um
Min wall thickness (mm)	0.6	0.2
Accuracy (mm)	+_-0.3	+_-0.1
Build rate (cm <sup>3</sup> /h)	80	5.20
Surface roughness	20-30	5.15

Table 1.2: EBM Vs SLM

The most basic difference between the two is the power source, that is laser beam for SLM and electron beam for EBM. It is the power source that determines the overall environment of carrying out the process. For EBM scanning system is electro-magnetic lens while SLM utilizes the galvanometer. This causes the EBM to be at an advantage as building speed in EBM is way higher than the SLM. As for as the power consumption is concerned, both the techniques are at par to each other standing at 5 kW/h. The finished quality of the product greatly relies on the powder parameters that include composition, size, porosity, shape and the morphology of the surface [8]. EBM uses powder particles of larger dimensions as compared to the SLM. It is pertinent to mention here that the smaller the size of powder grains, better the final finish of surface, therefore, SLM is better as far as surface finish is concerned of the obtained part from the machine. However the smaller is the powder particle size, higher is the cost. Therefore, the powder dimensions of size that is in-between the two sizes is preferable. The most significant property of EBM is that it's a hotter process that makes us enable to work with the materials that are very difficult

to process with the common conventional technologies and the SLM. Due to preheating and then the high temperature the chance to develop residual stresses in EBM is lower as compared to SLM. Generic benefits and drawbacks for both EBM and SLM are summarized in the tables 1.3 and 1.4.

EBM	
BENEFITS	DRAWBACKS
High productivity	The choice of material is very limited as only those materials can be processed which are conductive in nature
Stacking of parts is possible which enables the mass production	Powder sintered cake makes the powder removal tricky (specially from the inner chambers)
Residual internal stress is avoided due to the constant high build temperature (680-720 Degree Celsius)	Eight hours are required to cool the machine in between two productions (its long time)
Parts are embedded in a powder cake that is sintered before. Therefore gives a better thermal conductivity and the supports required are less	Powders finer than 40 micro meter are difficult to work with
As the build chamber remains in a vacuum therefore, the powder do not catch any sort of contamination	The maintenance of the machine is relatively expensive
It gives mechanical and microstructure properties at par or greater than the traditional manufacturing processes	If the machine goes to breakdown for maintenance, the under process part can not be processed further, hence it becomes useless

Table 1.3: EBM: Benefits and Drawbacks

SLM	
BENEFITS	DRAWBACKS
It provides flexibility in case a new material is to be introduced	SLM is not for bigger parts as it purely depends on the thickness of the walls
In SLM it is possible to use finer powder like 10 micro meter	The finished parts has the internal stresses and it required further heat treatment like annealing
Parts are not embedded in a sintered powder cake. Therefore to remove the powder is easy	For proper fastening of the part, SLM needs very powerful supports
The dead time is very short as compared to EBM as SLM needs only 2 hours to cool down in between two manufacturing cycles	Build plates should be made of the same material
It is possible the start the process again if it was stop due to any reason	Cutting tools are required in order to remove the manufactured part from the build plate

Table 1.4: SLM: Benefits and Drawbacks

### 1.3 ELECTRON BEAM-MATTER INTERACTION

The comprehension of EBM process dynamics and by-products emission requires a comprehension of the material-electron beam interaction. In the EBM literature, a few thermal models of the process were discussed [9] but there is a limited literature devoted to the physical principles that drive such interaction. The interaction in-between electrons and matter occurs at an atomic level, involving energy interactions described by the quantum physics laws. This chapter reports a general description of the physics behind the process. Sub-section 2.1.1 provides a general discussion about electrons.

#### 1.3.1 ELECTRONS AND MATTER

According to Shultz [10], even though the physical description of electron beams is known since the sixties, the microscopic processes are so complex that they still do not have a full quantitative description. The basic electron beam principles are discussed in various EBM papers [9] whereas a deeper analysis of the beam interaction, from a physical point of view, is provided in the electron-microscopy literature [11]. The electron beam is focused against the target in a small spot and the electrons impact the surface at a speed near the speed of light. The electrons transfer their kinetic energy to the part, but the mechanism is quite complex as it involves several phenomena at different levels. According to Shultz [10], since electrons mass is very small ( $9.109382 \times 10^{-31}$ ), they cannot transfer momentum directly to the heavier nuclei in the lattice's atoms. The collisions, more likely, involve the electrons of the crystal lattice in the outermost atomic shells, in particular the free conduction electrons. The conduction electrons transfer the energy gained after the impact with the lattice by subsequent collisions, interacting with the lattice phonons (quantised lattice vibration), leading to an energy increase of the lattice atoms. Phonons are "quasi-particles" (or equivalently, waves, according to the dualism wave-particle of the quantum mechanics) associated to the vibration motion of atoms in the crystal lattice. In other words, atoms oscillate around their equilibrium point and this vibration, according to classic mechanics, is associated to a wave with specific wavelength and frequency. This particular wave is defined as phonon and the transfer of energy occur due to an interaction between the electron beam and the phonons [12]. As a result, the solid material starts warming reaching extremely high temperatures [13]. Moreover, the process is accompanied by emission of by-products as illustrated in Fig 1.6: scattered and backscattered electrons, second charged particles (electrons and ions).

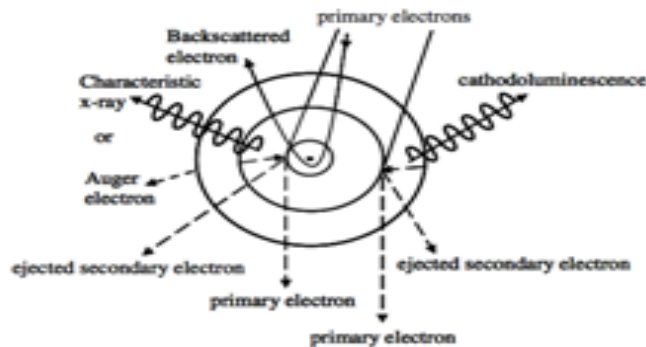


Figure 1.6: By products of electron beam – matter interaction

These by-products are considered un-desirable by an efficiency perspective. Actually, they correspond to energy losses, which do not contribute to the melting process. However, they can be considered signals of interest, considering the fact that they are potential information carrier of the on-going process. In the following sections a deeper analysis of all these aspects is carried out.

## 1.4 REVIEW OF PROCESS DEFECTS IN EBM

Most of defects that may occur during the EBM process are typical defects of metal powder bed fusion processes, regardless of the nature of the energy source (laser or electron beam) [27]. They include: pores and un-fused powder within the part, balling phenomenon, surface defects, geometric defects, residual stresses, cracking and delamination [14], [15]. Material inclusions and contaminations, which are largely discussed in the SLM literature, are poorly discussed in the EBM literature. A specific EBM problem, source of defects, consist in the “smoking” effect. Understanding how defects arise, which are their characteristics and how they impact the mechanical properties of the final part, may help to improve the process reliability and the final part quality. Beyond the defects listed and discussed in the following paragraphs, it is important to point out that instability in the final micro structure is a criticality of particular interest for the industry. In-situ monitoring of the micro structure would be one of the major goal that would definitely boost the industrial breakthrough of the technology. The following sub-sections describe in more detail each type of defect.

### 1.4.1 POROSITY AND LACK OF FUSION

Porosity is a major defect in additive manufacturing including EBM also. The main causes of are powder quality or poorly optimized parameters [8]. Types of porosity are shown in Fig 1.7 During the process of quick solidification the gas remains trap in the form of bubbles or spherical voids.

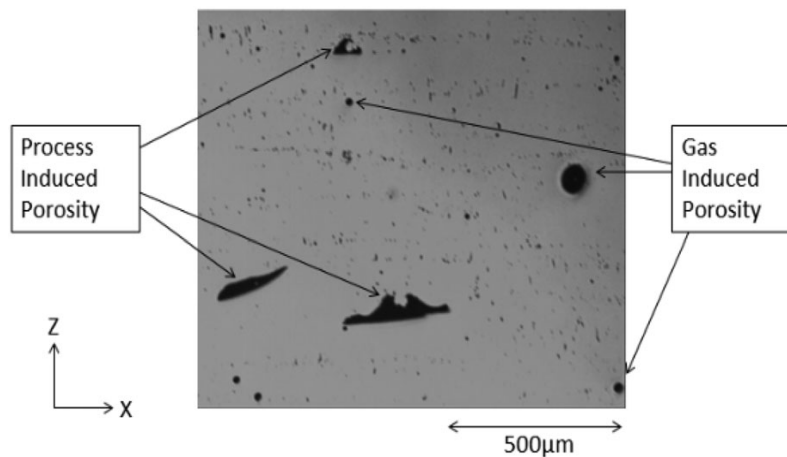


Figure 1.7: Process induced Vs gas induced porosity [8]

### 1.4.2 BALLING

Balling effect that is sometimes called Melt ball formation, takes place when molten powder do not solidifies into solid layers instead it solidifies in spheres melted metal solidifies into spheres as shown in

Fig 1.8 ([8],[16]).

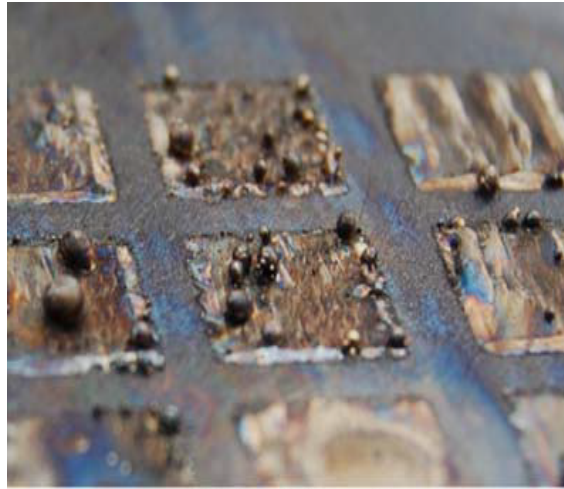


Figure 1.8: Example of Balling Effect [8],[16]

### 1.4.3 RESIDUAL STRESS, DELAMINATION AND CRACKING

Residual stress is very natural in additive manufacturing process. It mainly occurs because the material undergoes through different temperature levels hence the change temperature gradient induced the residual stresses in the manufactured parts. Although residual stresses are linked to all AM process, but its level of intensity is quite low in EBM when we compare it with SLM, mainly due to the fact that the EBM undergoes from a very high temperature being a hot process as compared to SLM [8].

The defect of delamination is associated with residual stresses [8],[16]. The residual stresses are induced during the heating of the powder mainly because of difference in thermal gradient. Basically delamination is caused when the tensile stress in-between the two layers become more than their capacity of binding. Another cause of delamination is improper fusion of the metal powder and the partial melting of the layer underneath. This phenomena is depicted in figure 1.9.



Figure 1.9: Example of Delamination [8],[16]

Cracking mainly depends on the material and there may be many causes of its occurrence. One type of cracking is known as solidification cracking and it is caused by the residual stresses. The main cause of this type of cracking is the application of excess energy creating the forces in-between the liquid area of the pool and the areas that have been solidified.

#### 1.4.4 SURFACE DEFECTS

The two major indicators of the roughness of the finished part are the powder size and the diameter of the heating spot. There are two main phenomena that are responsible for the roughness of the surface, that are: Irregular edges of layers and the material surface roughness [8]. This phenomena is shown in the figure 1.10.

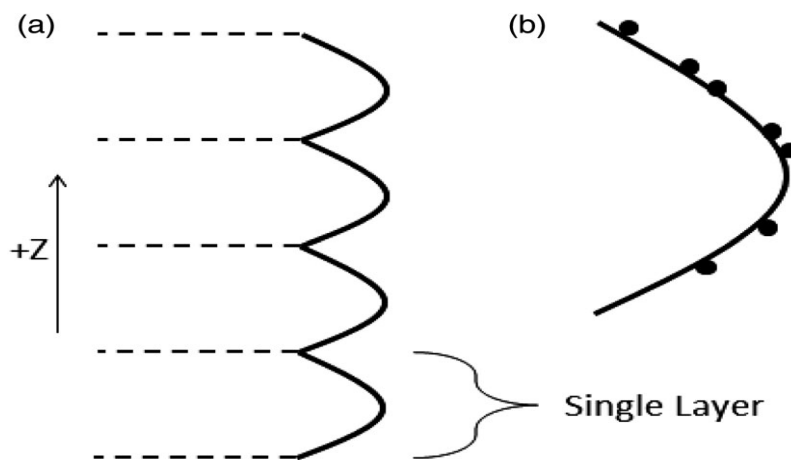


Figure 1.10: Example of Surface Defects [8]

#### 1.4.5 GEOMETRICAL DEFECTS

The excess application of heat may cause the material to deform from its shape. The important geometries are manufactured by using the supports either thermal or mechanical. Swelling effect may also occur that is mainly responsible for solidification of the melt pool over the surface of the part. Warping is another type of geometrical defects. This is because the heating effect warps the substrate during the process, as shown in figure 1.11.

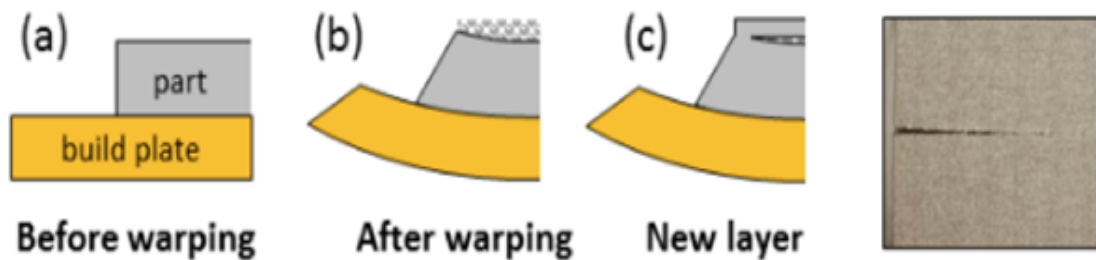


Figure 1.11: Example of Warping [8]

### 1.4.6 SMOKING

As in EBM the beam consists of electrons therefore, upon striking with the powder, it not only produces the heat but also the electric charge. Therefore, it is utmost important to optimize the electron beam before the start of the process because it is so crucial to avoid the static charge. When the electrostatic force exceeds the binding force in power, it causes the powder particles to disperse from the bed [7], [8] causing the smoking effect as shown in the figure 1.12.

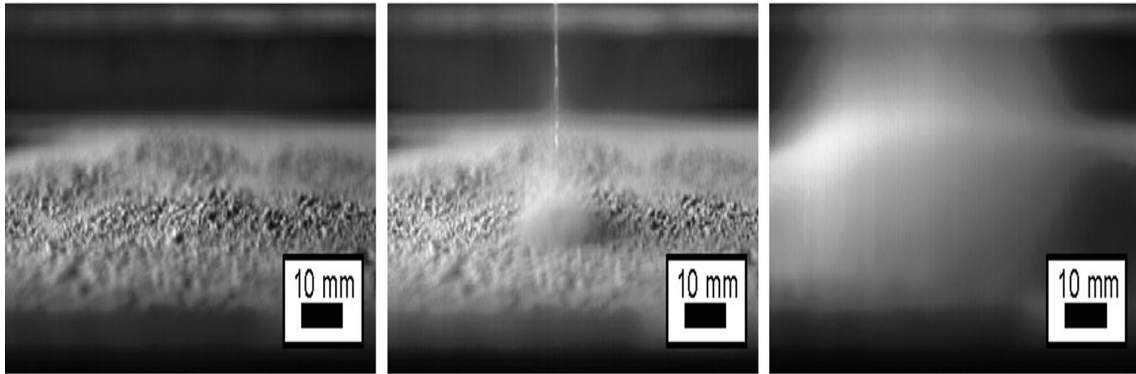


Figure 1.12: Smoking effect of one powder layer [4],[8]

To avoid the smoking effect the pre-heating is applied in the EBM, that elevates the temperature of the powder making it to partially sinter. The helium gas that is present in the chamber also helps dissipation of the electrical charge.

## 1.5 REVIEW OF PROCESS MONITORING IN EBM

The main problem that hinders the major industrial breakthrough of Additive manufacturing specially EBM is the lack of stability, repeat ability and precision. [14], [15]. Considerable research efforts are expected in order to develop new strategies for in-situ process monitoring and data gathering to enable quick detection of material discontinuities and process defects. Despite continuous RD efforts of major SLM and EBM system developers, there is still a lack of both automated defect detection capabilities and for defect prevention or repair strategies. In this section the literature related to the in-process monitoring of EBM process will be discussed.

### 1.5.1 IN-PROCESS MONITORING METHODS IN EBM

The literature of in process monitoring for EBM is comparability less than SLM. This is also due to the fact that EBM is still a proprietary technology, with one single system developer on the market. Moreover, EBM process characteristics make the process monitoring more challenging than SLM. Inside the electron gun are housed the electron magnetic coils due to which co-axial sensor installation is not possible in the EBM machine [17]. In the method of co-axial sensing the main concept is to exploit the source of power and consequently the powder melt pool on the working table can be measured along with the thermal intensity of the melt area. As the EBM process doesn't consist of optical path as the beam is made of electrons, hence, the co-axial sensing is not possible in the case of EBM. Therefore,

the only way of monitoring in the EBM process is the off-axial methods. In off-axial monitoring the basic concept is the mounting of sensors off the path of the beam at an angular position so that the targeted area can be monitored. EBM machine has a window at the front face and another window at the bottom side. Therefore, off-axial monitoring is possible EBM. However one of the major problem in off-axial monitoring in the EBM is the metallization of the window that is caused by the vaporization and condensation of the byproduct coming from the melt pool [18]. Monitoring sensor integration on EBM machines is made more difficult also by the vacuum environment in which the process takes place and X-ray emissions. Infrared (IR) cameras are the most studied technology for in-situ monitoring of EBM. As a matter of fact, the possibility of measuring the temperature map during the process provides much information about the process stability and quality [19]. Two different setups of the IR camera are made possible thanks to the two windows just described. Fig. 1.10 shows the possible IR camera set up on Arcam machines. These two set up enable the monitoring of the entire power bed. Set up monitoring by the window on the top of the chamber, close to the beam vertical, allows a quasi-coaxial monitoring of the powder bed, thanks to the small mounting angle respect the beam column.

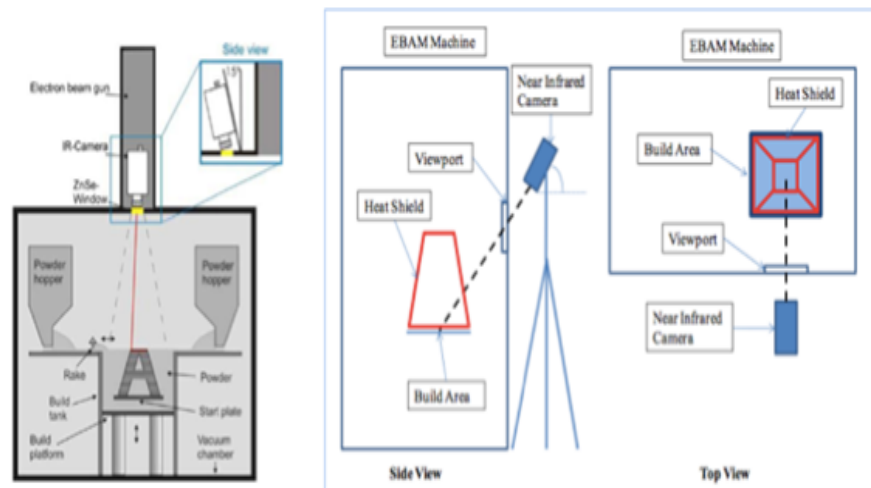


Figure 1.13: Two possible camera arrangements: First one at the top [17], the second at front [20]

A detailed classification of the literature is reported in the table 1.5.

SENSOR TYPE AND SPECIFICATIONS	SPATIAL RESOLUTION AND WAVELENGTH	SENSOR SETUP	ARCAM MACHINE	RESEARCH OBJECTIVE	REFERENCE
FLIR SC 645 IR CAMERA. (60 Hz) 640x480 (resolution)	350 $\mu\text{m}/\text{pixel}$ 780-1080 nm	Top window (330 mm from powder bed) 274x206 mm (field of view)	Arcam A2	Acquiring temperature distribution on the surface bed to find correlation with surface defects	Rodriguez et al (2012) [5]
LumaSense MSC640 NIR CAMERA. (60 Hz)	48 $\mu\text{m}/\text{pixel}$ (lens A) 8,3 $\mu\text{m}/\text{pixel}$ (lens B) 780.1080 nm	Front window (31x23 mm (A), 5,3x4 mm (B) field of view)	Arcam S12	Acquiring temperature measurement with NIR camera for process model validation and, process monitoring and process parameter effects on thermal characteristic	Price et al (2012) [20]
FLIR A320 IR CAMERA 320x240 (resolution)	0,83 mm/pixel	Top window (all build filed view)	Arcam A2	Demonstrate correspondence between flaws detected in IR images and flaws recorded by traditional metallographic images	Schwerdtfeger et al (2012) [17]
FLIR SC 8200 IR CAMERA	-	Front window (all build area field of view)	Arcam system (model not specified)	Porosity and over melting during preheating detection via thermal images. Determining the effect of focus offset in overhang regions	Dinwiddie et al (2013) [21]
LumaSense MSC 640 NIR CAMERA (60 Hz)	-	Front window (31x23 mm field of view)	Arcam S12	Thermal characterization of Ti6Al4V sintered powder.3D thermal model application to investigate process parameters effects on part temperature and melt pool size.	Gong et al (2013) [19]
FLIR SC 645 IR CAMERA 350 $\mu\text{m}/\text{pixel}$ (Resolution)	-	Top window	Arcam A2	Step by step procedure development to obtain emissivity measurement for Ti6Al4V pre melting and post melting	Rodriguez et al (2014) [5]
LumaSense MCS640 NIR (60 Hz) 640x480	-	Front window (31x23 mm field of view)	Arcam S12	Developing a comprehensive thermal model using FE method capable to predict temperature distribution and temperature history	Cheng et al (2014) [22]

(resolution)				for EBM process	
FLIR SC645 IR CAMERA	-	Top window (all build area field of view)	Arcam system (model not specified)	Developing a method for detecting size shape and surface area of fabricated object. Additionally an algorithm for thermal data and CAD layer comparison is developed in order to identify any excessive surface porosity	Ridwan et al (2015) [23]
FLIR SC645 IR CAMERA	--	Top window (all build area field view)	Arcam A2	Developing of an automatic feedback control system to acquire thermal data from the powder bed communicated to a software interface capable to change necessary parameters on demand.	Mireles et al (2015) [24]
FLIR 7600 IR CAMERA	-	Front window (all build field view)	Arcam S12	Developing a method for camera calibration in order to gain temperature data to approximate thermal gradient and solid liquid interface speed to monitor effect of thermal gradient on grain structure development	Raplee et al (2017) [25]
FLIR SC645 IR CAMERA (25 measurements/s) Multi wavelength pyrometer	-	Top window (all build field view)	Arcam S12	Developing a method for thermal data acquisition based on the combined use of IR camera and multi wavelength pyrometer in order to detect thermal anomalies relate to porosity warping and delamination.	Cordero et al (2016) [26]

Table 1.5: Review of Process Monitoring in EBM

Rodriguez et al [5] used an IR camera to study the temperature distribution over the entire build area. A Flir SC645 at high resolution was chosen for the installation in an Arcam A2, not without many machine modifications to make the installation itself feasible. The angle between the camera and the surface normal is 25°. A specific system was also installed to automate the image acquisition process. The main problems addressed are the IR camera calibration for an accurate temperature measurement and image analysis in order to find correlation between thermal images and metallographic images for defect detecting. The camera allows the in-process detection of over melting, temperature distribution, temperature gradient control and internal flaws detection. Fig. 1.14 show the image obtained.

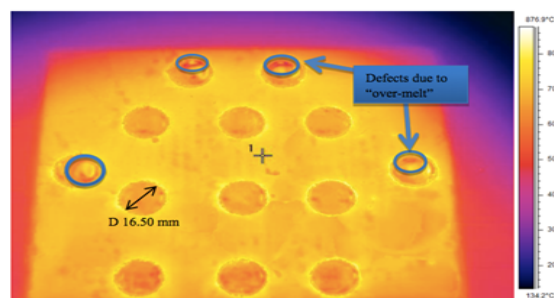


Figure 1.14: Detected defect in thermal image [5]

Shwerdtfeger et al [17] installed at the top of an Arcam A2 a Flir A320 IR camera with a resolution of 320 x 240 pixels, at a 15° angle to the bed. IR images of the powder bed surface, after the completion of each layer, were collected together with the corresponding metallographic images, in order to provide a comparison. In IR images colder regions appear with darker colour. Comparing IR images with the corresponding metallographic is possible to see a clear pattern correlation as shown in Fig. 1.15.

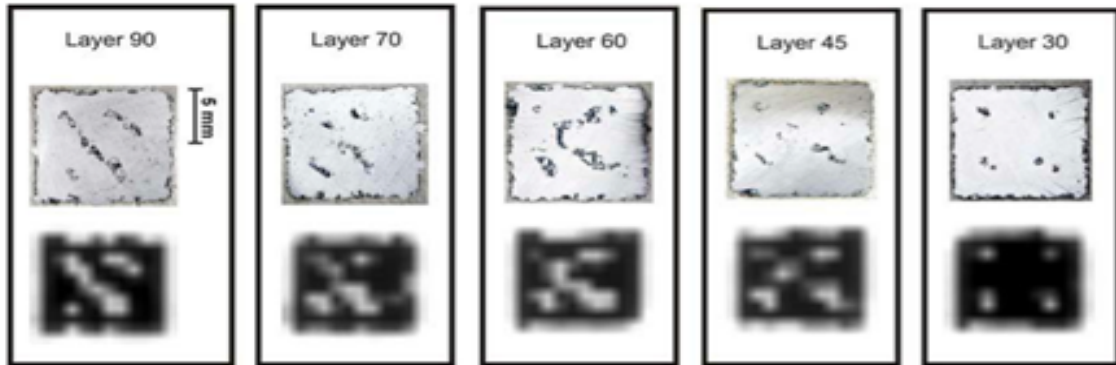


Figure 1.15: Metallographic images Vs IR images [17]

The image shows a clear correlation between areas of higher heat radiation and material flaws. Automating image processing and flaw detection gives the possibility to move from the online flaw detection to the online healing. In [5] Rodriguez et al addressed in detail the problem of IR camera calibration. They produced a step-by-step procedure to obtain precise emissivity data of Ti6Al4V pre melting and post melting. An original analytical model is presented for view factors associated with the Arcam A2's thermal enclosure. Such theory is claimed by the authors to potentially contribute to future works in establishing correlation among process parameters, IR surface temperature measurements and micro structure properties of EBM fabricated parts.

Price et al [20] carried out similar experiments in order to evaluate the feasibility and capability of a NIR camera for thermal analysis of EBM process. They installed a NIR MCS 640 from LumaSense onto an Arcam S12. The thermal camera was placed on a sturdy tripod, close to the glass window at a vertical tilt angle of 55°. The camera has a spectral range between 780 and 1080 nm, with a detectable temperature from 600 °C up to 3000 °C. The researches demonstrated the possibility to employ a NIR camera to capture 2D images of the temperature profile over the melt pool and along the scan path.

Dinwiddie et al [21] used a Flir SC-8200 IR camera aiming it through the front window of Arcam system discussing the possibility to obtain thermal images capable to provide information about EBM focus, porosity detection and over-melted regions. They also illustrated two shutters less systems able to avoid window metallisation, which allow a continuous infrared monitoring of the process. Details are provided regarding the possibility to detect over melting regions during the preheating via thermal images.

Gong et al [19] carried out similar experiments to those reported in [20]. The camera is a LumaSense MCS640 NIR IR vertically inclined at 35° ahead the front window of the machine. Camera parameters are the same as those disclosed in [20]. In the paper is presented a Ti6Al4V characterization regarding thermal conductivity of partial sintered powder. They came up to a similar results of [20] producing a 2 dimensional temperature profile of the scan path for each hatch melting frame, result is shown in Fig.

1.16 and Fig. 1.17.

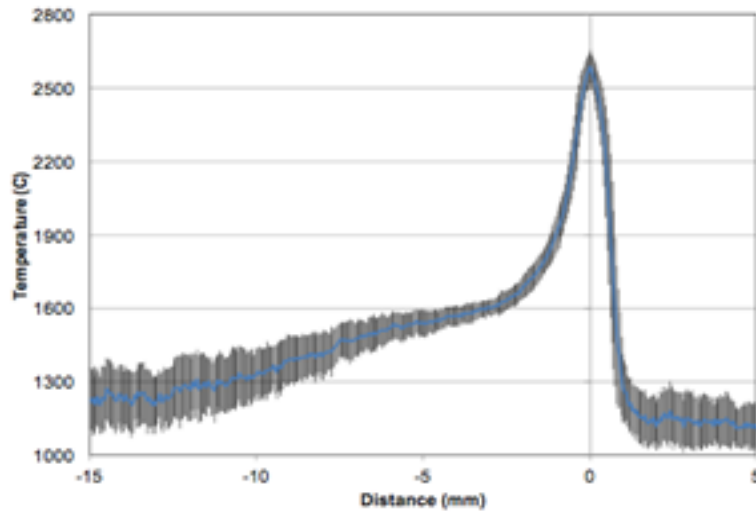


Figure 1.16: Temperature profile in hatch melting [19]

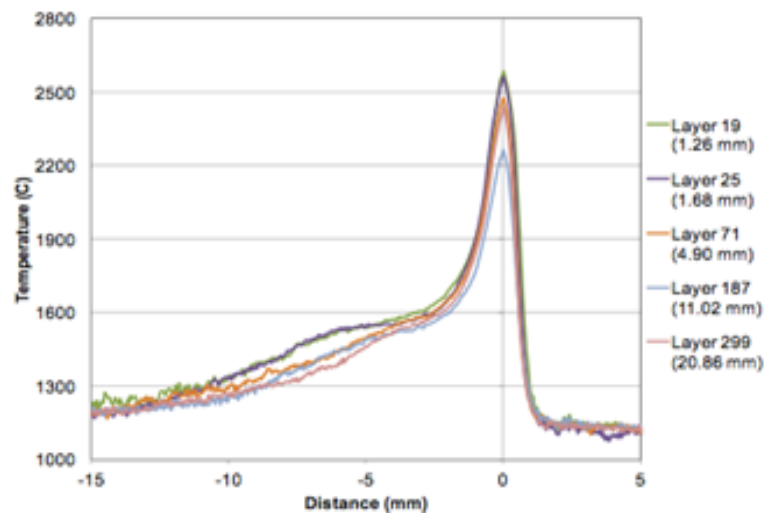


Figure 1.17: Average temperature profiles at different build heights [19]

The main information given by this data is that the cooling rate is greater at higher build heights. Other relevant results have been obtained in defining thermal properties of metal powder; in particular it has a much lower thermal conductivity; more over, it is highly thermal dependent ( $0.63 \text{ W/m}\cdot\text{K}$  at room temperature but less than  $2.44 \text{ W/m}\cdot\text{K}$  at  $750 \text{ }^\circ\text{C}$ ).

Cheng et al [22] developed a comprehensive thermal model of EBM process using finite element software (Abaqus). They used a NIR camera with the same parameter above discussed to acquire temperature measures for model validation. The model is applied also to obtain information about the correlation between powder porosity and temperature profile and melt pool size. Experimental data were collected in order to validate the model built. Ridwan et al [23], used a FLIR SC645 (IR) camera (same set up parameter described in[24]) installed at the top window of an Arcam machine (model not

specified), developed an algorithm to compare the thermal data gathered from the operation chamber with an input layer derived from CAD. The algorithm was coded in Matlab and it provides an analysis on the basis of colours and on the basis of edge detection technique. The output of the method employed provides information about porosity together with geometrical data, which give a rough approximation of the process precision.

Mireles et al [24] developed an automatic feedback control system to monitor and control the build temperature. The aim of this control system is to address the problem of microstructure differences throughout the part due to thermal gradient inside the chamber during the building process. In order to guarantee the production of mechanical isotropic parts, the automatic feedback control loop monitors the part, layer by layer, adjusting the process parameters (relevant for grain size control) to attempt temperature optimization. The system is also able to detect porosity during a build.

Raplee et al [25] settled a Flir 7200 by the front window of an Arcam s12. They developed a method to calibrate the temperature data in order to monitor how the thermal conditions affect the grain structure.

Cordero et al [26] introduced beside IR camera the use of a pyrometer in order to gain more information about the thermal situation in the build chamber. A multi wavelength pyrometer was mounted inside the Arcam S12 to record surface temperature during the process. Respect IR camera, pyrometers have the advantage that do not depend by emissivity. Nevertheless, the disadvantage is that it is able to measure a fixed spot size. Both the instruments at the end of the study were found able to identify thermal differences related to process parameters modifications, capable to influence the final microstructure.

---

---

## CHAPTER 2

---

# MACHINE LEARNING IN ADDITIVE MANUFACTURING: STATE OF THE ART

In this modern time of Industry 4.0 also called FIR (the Fourth Industrial revolution), the overall sector of manufacturing is producing piles of data for production and assembly lines. Also the 3-D printing or additive manufacturing is equally contributing to this data. According to Alabi et al [35] Additive manufacturing technologies and ML are an important sub set of the industry 4.0.

In recent times many research activities has been carried out to implement the machine learning techniques in the additive manufacturing in order to manufacture the simple as well as complex parts. State of the art of machine learning in additive manufacturing is described in the following sections.

Machine learning is a technique of artificial intelligence (AI). ML makes a system able to automatically learn from a given data and accordingly take the decisions or predictions without being programmed again and again. Recently the research in the field of machine learning is gaining pace in the fields of smart manufacturing [36], object recognition, medical, processing of natural language, prediction of material properties and auto driving.

## 2.1 MACHINE LEARNING TECHNIQUES

There are three categories of machine learning techniques that are supervised learning, unsupervised learning and reinforced learning. These three techniques have their own specific algorithms. For example clustering is the most common algorithm for unsupervised machine learning technique and its purpose is to search for the hidden pattern [37].

In the subsections below some details of categories of ML are described.

### 2.1.1 SUPERVISED LEARNING

In this method, data has a described relation between ground truth output and input. This means data is labeled: for example if we have several text-documents and we know their genre we can predict the similar document relation for others. This approach is widely used in sentiment analysis, text

classification and spam filtering. Some most common algorithms are Support Vector Machine, Naïve-Based and Nearest Neighbor for classification and Linear Regression, Decision Trees, Neural Networks for Regression [38].

### **2.1.2 UNSUPERVISED LEARNING**

Contrary to supervised learning, data is unlabelled here which defines the main objective of arranging data in structures and identify patterns. Unsupervised Machine Learning has three basic objectives, dimensional reduction, Clustering, and Association. This technique is simply used in Sentence segmentation, Machine Translation, and Dependency Parsing. Some common algorithms are fuzzy logic, Bayesian Clustering, Hidden Markov Model, PCA (Principal Component Analysis and LDA (Linear Discriminant Analysis) [38].

Semi-supervised learning techniques are a blend of the previous two exhibited above. This approach address problem where majority samples of the training are unlabeled, even though only limited data points with label are available. Advantage of this is that in several areas a huge amount of unlabeled data points is willingly available. Applications, where semi-supervised learning is used, are nearly the same as supervised learning [38]. This type of learning is most beneficial when the labeled data points we have are not too common or so exclusive to get then using that unlabeled available data points can raise the performance. It has a common application of speech analysis and web-content classification.

### **2.1.3 REINFORCEMENT LEARNING**

This approach is widely used in robotics, record management, and finance where the prime goal is to develop a policy. For instance: in games where a correct step gives some rewards and wrong movement penalize the score. The Reinforcement Learning helps agents to learn by witnessing the available behaviors and their conduct by using only an evaluative response, called the return. The policy's ultimate goal is to increase its long-term success. Few well-known algorithms are Q-learning, SARSA, Deep-QNetwork [39].

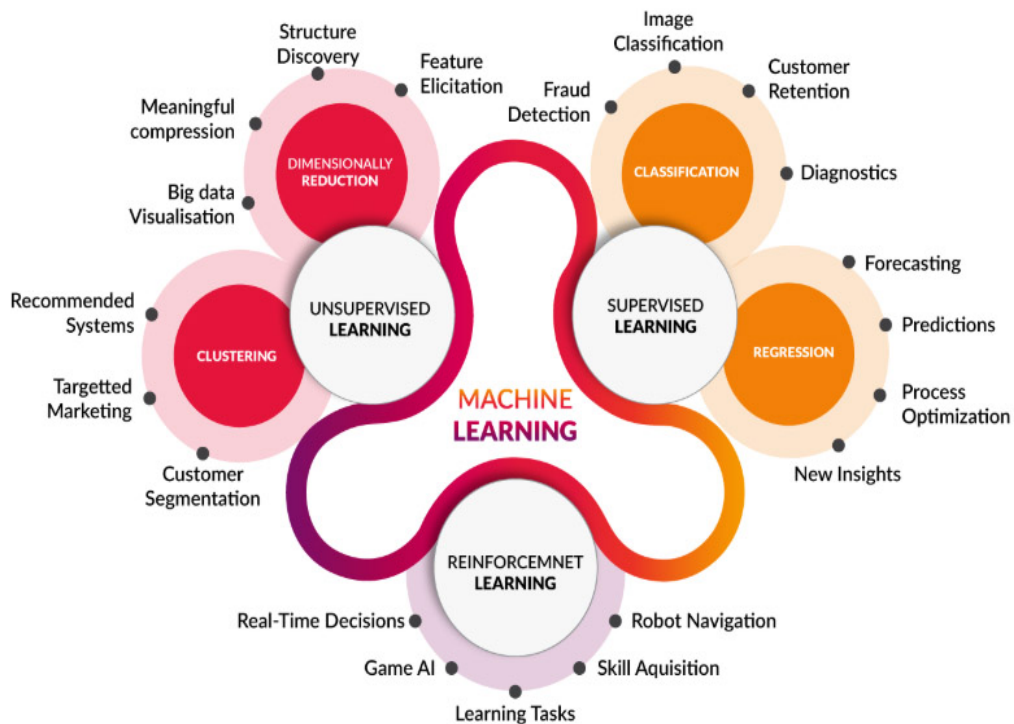


Figure 2.1: Description of Machine Learning types, taken from <https://cleanpng.com/Rusbert>

## 2.2 NEURAL NETWORKS

Neural networks are the algorithms that are inspired by the brain of human. When we see something or touch anything the data is sent to the brain, where it is processed by the neurons. Neural Networks are commonly known as Artificial Neural networks (ANN), because of their artificial capacity to mimic brain were primarily used in computer vision tasks. Neural networks is a type of supervised machine learning, while other all forms of machine learning are un-supervised learning. In a neural network algorithm the data is pre-labeled i.e; the system has been trained about to what answer should be given to the inputs. The NN is ideal for additive manufacturing because we have the clear targets and qualification criteria before hand in this techniques.

Neural networks algorithm has the strongest decision capability having the complex relationship between inputs and the outputs. There are three type of layers in a neural network, i.e; input layer, hidden layer, and output layer. Each layer consists of nodes or neurons, so as to copy the human mind. Weights are the coefficients of the NN and connection magnitude in-between neuron and adjacent layer is represented by the weights as illustrated in figure 2.2.

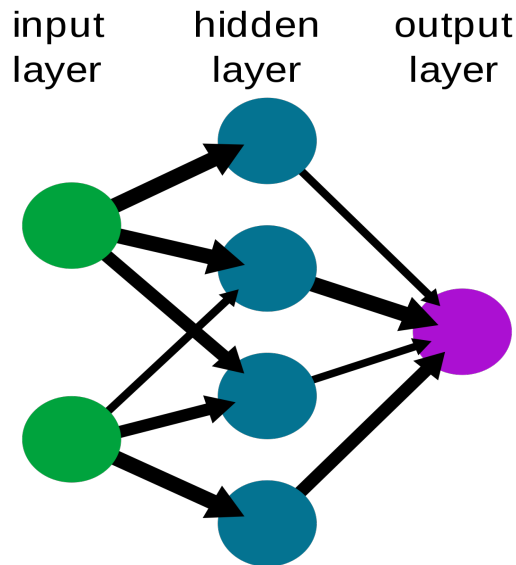


Figure 2.2: A simple NN

The values of weights are determined by training the NN iteratively, the most famous method for updating weights is called back propagation, which uses the mathematical chain rule to iteratively compute gradients for each layer. Once training is achieved, the NN will have the capacity to infer the outputs based on previously unseen inputs.

### 2.2.1 CONVOLUTION NEURAL NETWORKS

Neural networks are composed of human brain-inspired algorithms. Generally, when you open your eyes, what you see is called data and is processed in your brain by the Neurons (data processing cells) and knows what's around you. Alex Waibel et al (1987) [59] introduced convolution networks inspired by the visual cortex of the human brain . Applicative CNN by Yan LeCun et al (1998) were class of deep, feed-forward artificial neural networks used for banking systems to recognize numbers on cheques [58]. Neural Networks are commonly known as Artificial Neural networks (ANN), because of their artificial capacity to mimic brain were primarily used in computer vision tasks. Artificial Neural Networks are universal approximators which means they can form any function. Nevertheless, most recently, Convolutional Neural Networks have found prominence in addressing NLP-related issues such as Sentence Classification, Text Identification, Sentiment Analysis, Text Summarization, Machine Translation, and Answer Relations. This is because CNN has the capability of dealing with data parallelly. CNN among its other variants like RNN is preferred on account of fast response and possible implementation on GPU units.

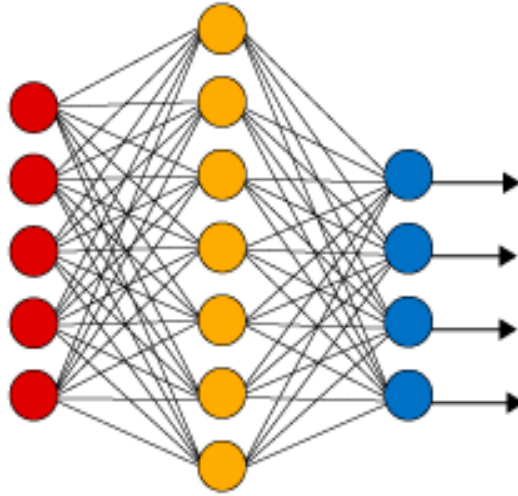


Figure 2.3: Architecture of Convolution Neural Network [59]

## 2.3 ML APPLICATIONS IN REAL WORLD

Due to the rapid growth of machine learning it is now possible to resolve small or complex problems from data set of whatever size coming from different sensors, or from a data base. In the table 2.1, some real world applications of machine learning are described.

S/N	ML Applications in the Real World	Description of the Application
1	Computer Vision and Image Processing	ML used for facial recognition, signal processing, object detection, speed detection.
2	Computational Biology and Health Care	ML applied to data collected from the health care sector, i.e; sequencing of DNA, detection of tumor etc.
3	Aerospace, Manufacturing and Automotive	In manufacturing it is being used in real time detection, predictive maintenance, in situ monitoring etc.
4	Energy	Used for price and load forecasting etc.
5	Natural Language Processing	To process the text and speech data exactly according to human writing or speech.
6	Computational Finance	Used for algorithmic trading and to score credit etc.
7	3D Printing Additive Manufacturing	ML is being used in ML such as detection of malicious defects, sensor data analysis and classification, cyber attacks etc.

Table 2.1: Real world application of ML techniques (MathWorks, 2016)

## 2.4 APPLICATION OF MACHINE LEARNING IN AM

The involvement of machine learning into additive manufacturing can be broadly divided into three categories, i.e; Additive Manufacturing Process, Design for Additive Manufacturing (DfAM) and Additive Manufacturing Production. The schematic representation of this classification is shown in the figure 2.3 ([54]).

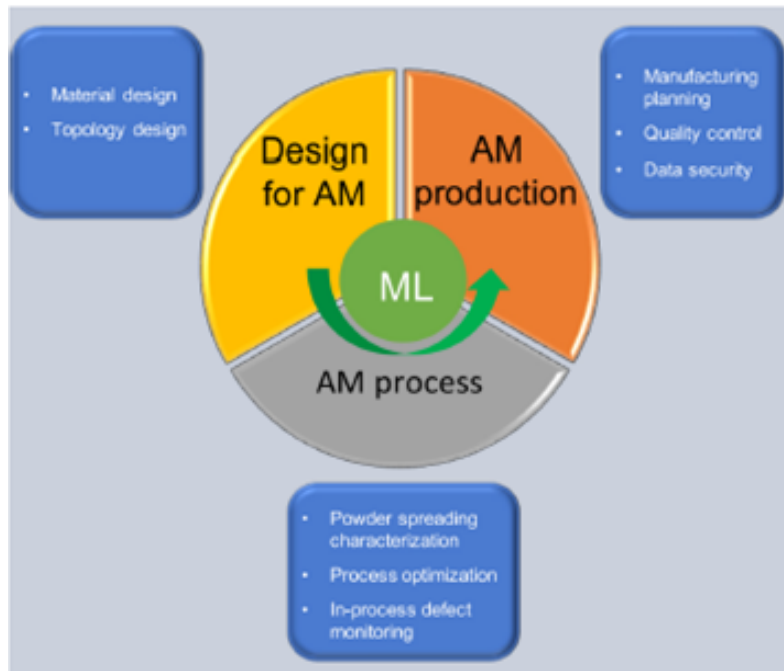


Figure 2.4: Involvement of ML in different AM domains [54]

Application of machine learning in AM has become an active research area both in industry and in education sector [40]. In this section three additive manufacturing techniques are discussed because in these three AM techniques the machine learning has been widely applied. These techniques are Powder Bed Fusion (PBF), Material extrusion and Direct energy deposition (DED). These are the most important AM techniques and are greatly used in the industry and academia. However, the PBF processes will be discussed more specifically in this section.

A graphical representation correlation between additive manufacturing data and machine learning is shown in the figure. It presents the data collection process, the data feeding process into machine learning algorithm, based on the prediction and the classification the resultant data from the input and lastly the optimization of data to be used as a fresh parameter for the further manufacturing through the additive manufacturing process [40].

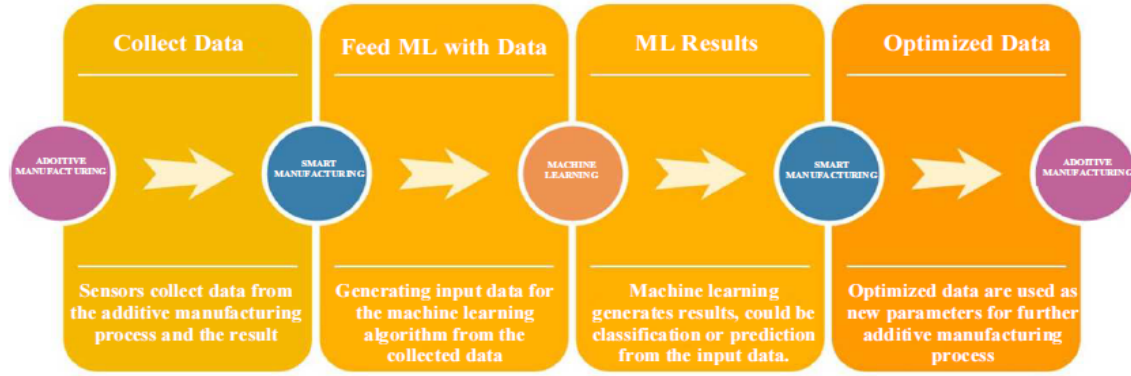


Figure 2.5: Additive manufacturing data Vs Machine learning (Baumann et al [40])

In the following subsections the application of machine learning in AM processes is described, specially for In- process defect monitoring, powder spread characteristics and process parameters optimization.

### 2.4.1 APPLICATION OF ML IN THE IN-PROCESS DEFECT MONITORING

In process monitoring and control is the most worked on area in AM where the machine learning techniques have been applied. In situ monitoring is growing day by day; it includes different sensors like pyrometers, photo-detectors, thermocouples, high speed optical cameras and many more [14]. But perfectly achieving the control in real time is still in early stages. This is because yet it is not fully clear that the data coming from a specific sensor is the exactly required data for that specific parameter control. Also, data-fusion strategies must also take into account the data that is not coming from the sensors. Furthermore, the fused data must be incorporated in the machine learning techniques, though recently it has been incorporated in the ML techniques.

A research was carried out by Roberson III [41] on the real time quality monitoring of additive manufacturing process in FDM. In his research, a desktop 3D AM machine was attached with sensors while the data was continuously gathered during the build process. The main objective of his research was to specify the causes that can impact on the quality of the finished product and cause the printing failure. Roberson III [41] used the machine learning for the classification to detect the failure of printing. The initial modeling showed that the surface roughness was below 8 percent. Roberson III [41] identified two machine learning algorithms that were most suitable and these algorithms are random forest and support vector machine (SVM). His study is important to understand the future possible endeavors on using machine learning in the AM processes.

Wu et al [42] applied image classification and machine learning for the detecting malicious defects during the build process in additive manufacturing. The high resolution cameras were used at the left, top and front side of a desktop printing machine. Images were gathered for each layer from the top view. The images with defects and images with no defects were used for the further process to check the defects. After getting the data from the captured images, they applied two machine learning algorithms namely J48 decision tree and the Naïve Bayes classifier.

Gobert et al [43] used high resolution images to detect the defects in the PBF process using the supervised learning technique of ML. Process monitoring was mainly focused in their study. By using a high resolution digital camera many images were collected layer by layer during the PBF build process. The most relevant information was extracted from the images with the help of machine learning. SVM (support vector machine) algorithm was used. In situ detection of defect accuracies they obtained was more than 80 percent. A demonstration of it was also carried out by [43] for verification.

Scime and Beuth [44] used a trained computer vision technique to detect the defect in the laser powder bed fusion process. At this point of time most of the laser bed fusion machine do not provide the real time feedback during the build process as they are single loop machines. There are some laser PBF machine that provide the real time feed back but still they can not monitor the process automatically. Scime and Beuth [44] focused on this problem and they carried out the analysis of laser PBF for the in situ monitoring and finally to fabricate on the laser PBF machine a real time controller. Their technique used was the unsupervised machine learning technique and a reasonable set of data was used that was collected from the patches of images.

Liu et al. [33] realized a real time feedback control system for Fused Deposition Modeling. Their proposed methodology included a system that was able to capture the images in real time, a technique that was able to analyze the images and a PID controller that was responsible for feedback control. Two types non conformances were found by them firstly the under fill secondly the over fill. They used the technique of SVM in order to divide the features in two groups i.e.; defective features and normal features after getting the texture features of the images. After that the defect severity was identified again by an SVM for the second time. Finally the PID controller was responsible to provide a feedback to the system in order to remove the defects.

Yao et al. [34] worked on an optimal feedback control system for the laser based PBF. The multiracial analysis was used on each layer to find the defect condition. After that the upcoming defects were predicted in the layers to come. Finally, in order to derive the policy of optimal control, they used a Markov decision process for the modeling of stochastic dynamics of different layers.

Grasso et al. [32] worked on the technique of data fusion to manipulate the data coming from many sensors in EBM. In order to classify the the process signals that are out of control and the process signals that are under control, they used SVDD that is the Support Vector Data Description strategy in ML. They used this technique in order to stabilize the process signal as this technique is able to detect autonomously the errors and unwanted data form the data coming from the sensor. However, their proposed methodology is suitable where only one part is being produced in bulk quantity.

Xinbo Qi et al [45] used acoustic emission and neural networks for the quality monitoring of in situ SLM process. The schemed used is shown in the figure. A fiber based bragg gratin sensor was used to record the acoustic emission signals. The neural network algorithm used was a SCNN (Spectral convolution neural networks. SCNN is an extension of the convolutional neural networks (CNN). The packet transform of the wavelet and narrow frequency band's relative energies were the inut features used. The output of the system was the information that either the quality is poor, high or medium of the printed layer. Xinbo Qi et al [45] reported that the accuracy of the CNN was 83 percent, 85 percent for medium and 89 out of hundred for poor part quality.

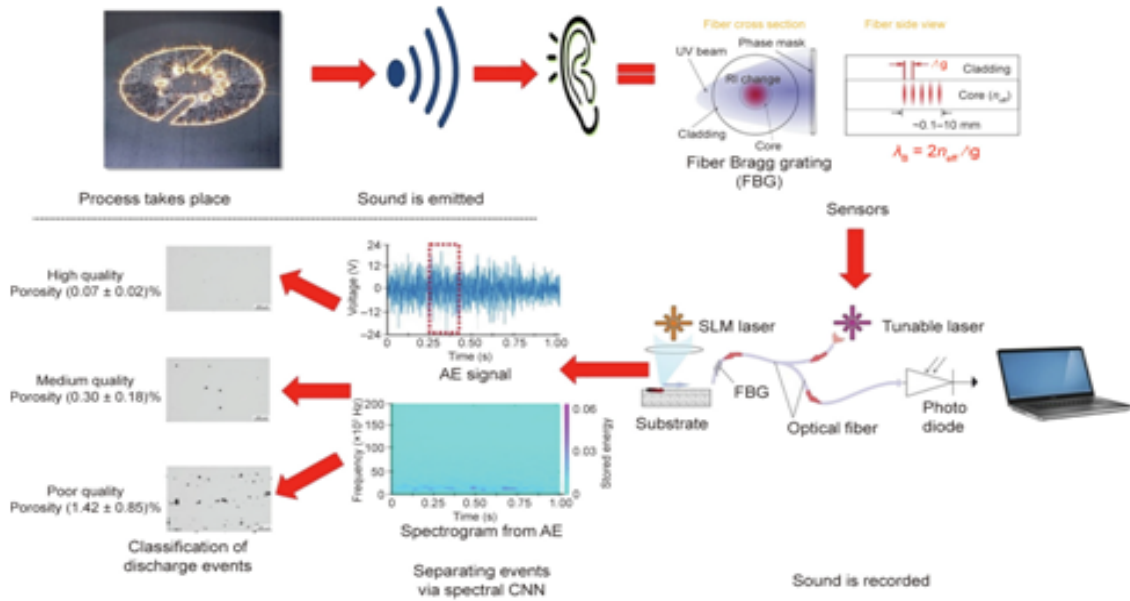


Figure 2.6: Additive manufacturing monitoring system (Xinbo Qi et al [45])

Because of the potential major breakthrough of additive manufacturing technologies by implementation of machine learning into AM, two of the world's most known companies, Autodesk and the General Electric (GE) has worked on the application of ML to additive manufacturing technologies. Netfabb 2018 is a software that was launched by the Autodesk. With this software it is possible to put the designs into a software that is design regenerative. Digital models are being evaluated by Autodesk with the use of ML for advance level additive manufacturing. Autodesk has worked on the generative design software for AM part manufacturing for some giant engineering firms like the Under Armour and the AirBus [46].

#### 2.4.2 APPLICATION OF ML IN POWDER SPREADING CHARACTERIZATION

In the powder based fusion processes it is an equally important factor that the uniformity of the powder that is spread layer wise should be uniform and as per already defined amount. It plays a very important role in maintain the quality of the manufactured part. Some major defects like swelling and warping may occur if the powder is not spread properly. It is very important not to use any physical anomaly detectors on the machine. Therefore, an automatic system is very important to realize that can control the powder spread mechanism and is able to control the in process defects that may occur due to improper powder spread during the build process. Scime and Beuth [44], [47] used the computer vision technique of AI and used multi scale convolutional neural networks [47] and k mean clustering [44] for the training of the system in order to classify the patches of powder bed fusion process images. The research of [44] and [47] also provided a way forward to implement a feedback controller for the in situ rectification of the anomalies.

W. Zhang et al [56] performed the experiments, simulation and a Back Propagation Neural Network (BP-NN) ML approach to correlate the quality of the spread-layer, characterized by its roller (spreader) rotational and translational speed to roughness.

### 2.4.3 APPLICATION OF ML IN PROCESS PARAMETER OPTIMIZATION

In the past many simulations and experiments were carried out to optimize the parameters of additive manufacturing processes. These traditional methods were solely based on the trial and error; as a consequence these methods were so expensive and also so time consuming [48]. These physical simulation processes can provide the info about the some feature like micro structure, geometry of the melt pool, keyhole. Without any doubt the simulation that is carried out on a macro scale like FEM undergoes from discrepancies in the results of experiments because of the assumption that are very simple. Thus there has been so much research by different researchers in order to implement the machine learning techniques to solve the problems encountered during the parameters optimization in the additive manufacturing processes.

There have be applications of ML in every process of Additive manufacture, however the PBF process is focused here.

The machine learning techniques in the additive manufacturing processes were basically used to interlink the main process parameters and the indicators concerned to the ultimate quality of the part at two distinct levels i.e; macro-scale level that is for example mechanical properties and the meoscale level that is related to geometry of the meltpool and relative density or porosity. Furthermore, process maps were also constructed by some researchers. The process maps can provide in depth visualization of the process windows.

While the single track meoscale provide the basic building blocks for the high energy additive manufacturing processes. The properties of the meltpool like the continuity, uniformity and geometry are of major importance in the finished part quality. Keeping in view this fact, in order to make a prediction of geometry of the meltpool like height, depth and width for PBF, the MLP technique that is the multi layer perception technique was used by [49]. Here a strong linkage was created between the in-between the meltpool geometry and the process-parameters. In a reverse way it can be said that by controlling the process-parameters a required morphology of the meltpool can be obtained. To further carryout this research Tapia et al. [50] worked on the Gaussian process (GP) based surrogated model in order to map the process parameter against the depth of meltpool in order to make a response map in 3D. To avoid the unwanted melting mode of the keyhole the process widow can be pre-determined. After using some filters the obtained prediction error was around 6.023 micro meters that was acceptable when it was compared to the error that occurred during the collection process of data. In some cases open porosity is a demand, for example for energy absorption auxetic structures are needed and for implants in medical science porous structure are needed. A. Garg and Jasmine Siu Lee Lam [51] explored the support vector machine (SVM) and the multilayer perceptron (MLP) technique for the prediction of the open porosity during the selective laser sintering PLA material.

The machine learning approach can also be employed in the macro-scale properties of AM-built parts. ANFIS system (adaptive network based fuzzy inference system) has the capability to handle the relative truths only. Therefore, keeping in view the uncertainties that are faced in the fatigue process , thus ANFIS is a good tool to assess the properties of the fatigue process. Zhang et al. [52] used the same selective laser sintering machine and they gathered 139 data of fatigue from SS316-L-parts and they got

this data by varying the conditions of processing 18 times. ANFIS was successfully applied for the prediction of high-cycle fatigue-life with the RMS (root-mean-squared) error between 11 to 16 percent by employing two models, i.e; the process-based-model that includes the temperatures for heat treatment and the process parameters of printing, and the property-based model that includes the elongation and the uts-ultimate tensile strength. According to Wang et al. [48], as described before, for EBM process process window can be narrowed down by observing the surface condition of the top build. Its advantage is that the SVM is good when there is a clear margin between the classes. But its disadvantage is being prone to over-fit. Aoyagi et al. [53] suggested a relatively easy way by using only 11 samples for constructing the process maps for electron beam melting EBM process. Process parameters; the speed of the scan and the current of the electron-beam, were correlating with surface conditions, as shown in the figure. In this work the sole purpose of SVM was to only do the fitting of the data for plotting of the boundaries of decision. As the chosen set of data was very small, therefore, it was very difficult that a test set could be allocated for the purpose of evaluation of the model.

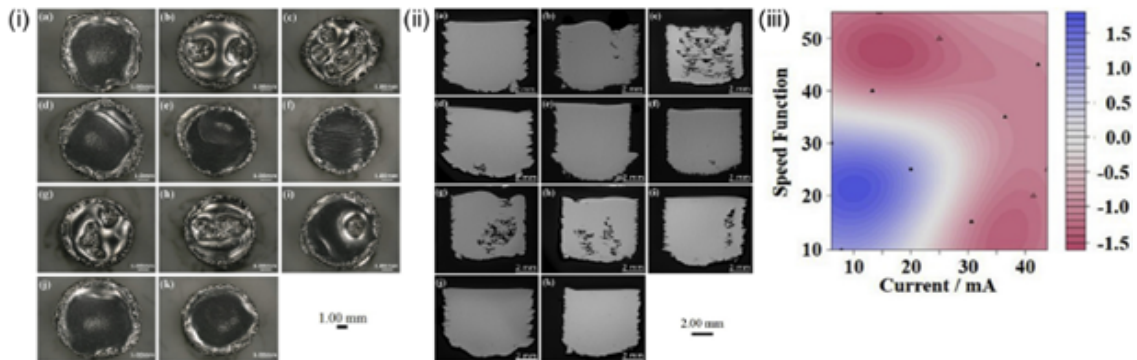


Figure 2.7: SVM-prediction of macro properties of EBM built parts [53]. (i) For 12 different process-parameters, top-surface conditioning the printed samples. (ii) Micrograph of cross section of each sample. (iii) Construction of the process map for optimization of process parameters to obtain good surface finish and low porosity.

B. Kappes et al. [55] worked on the optimization of the process parameters of powder bed fusion process using the INCONEL 718 by applying a Random-Forecast-Network Machine learning algorithm. 3600 samples were printed in their experiments and they correlated the porosity of the part to the orientation of the part to the location of the part and usage of powder that was recycled.

Imani et al. [31] proposed system where the real time data was used from different sensors in order to observe the conditions of the process causing the porosity with the help of a machine learning technique. This was sort of a 'qualify as you build model'. Imani et al. [31] analyzed correlation between the location and the frequency of the produced parts and the process parameters in a laser PBF process like hatch spacing, power of laser and the velocity. Layer by layer images in this in situ process were used to extract the statistical features. Afterwards, classification of these features was done by the machine learning techniques i.e; k-NN, SVM and feed forward neural networks in order to find the conditions of the process that were mainly responsible for producing the pores.

Mallikharjun et al [30] proposed a framework by using the ANN (Artificial Neural Networks) in the

powder bed fusion process for the purpose of optimization of the process parameters. To different sets of the experimentation was employed in this framework. The first set of experiments was mainly for narrowing down the inputs (the process parameters) to push them to their optimum ranges. The second set of experiments employs on the findings that how a specific set of parameters effect the outputs (ultimate properties). Then, they tested the final properties of manufactured part after performing the two sets of DOE (Design of Experiments) in the next step. The authors at the end proposed a framework to for the optimization of the process parameters in order to get the best final quality by using the acquired resultant data in the previous step and training an intelligent system on the basis of this data. Figure 2,8 shows the schematic of the process.

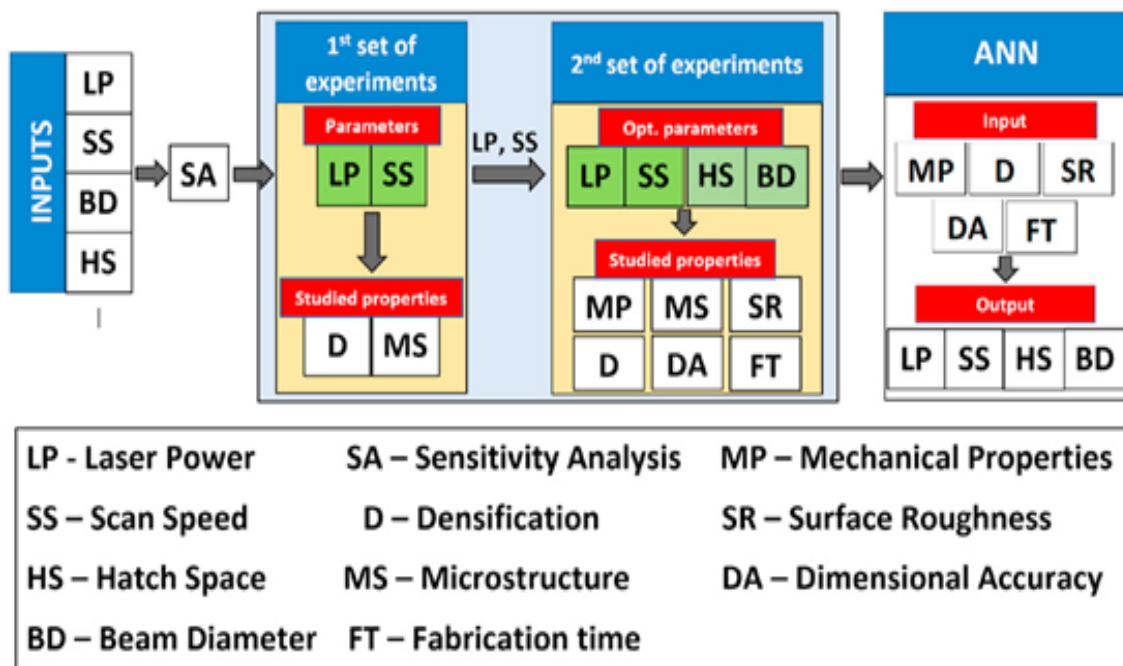


Figure 2.8: Development of ANN model for the framework proposed by Mallikharjun et al [30]

The feed forward neural network model has been proposed in this study. In feed forward neural network an multi in, out optimization is developed by using the back propagation algorithm. Scan speed, beam diameter, laser power and hatch space are the inputs. The final properties of a manufactured part like mechanical strength, dimensional accuracy, Porosity, surface roughness, and process time). Figure 2.8 and 2.9 show the Neural network model and algorithm for selection of process parameters.

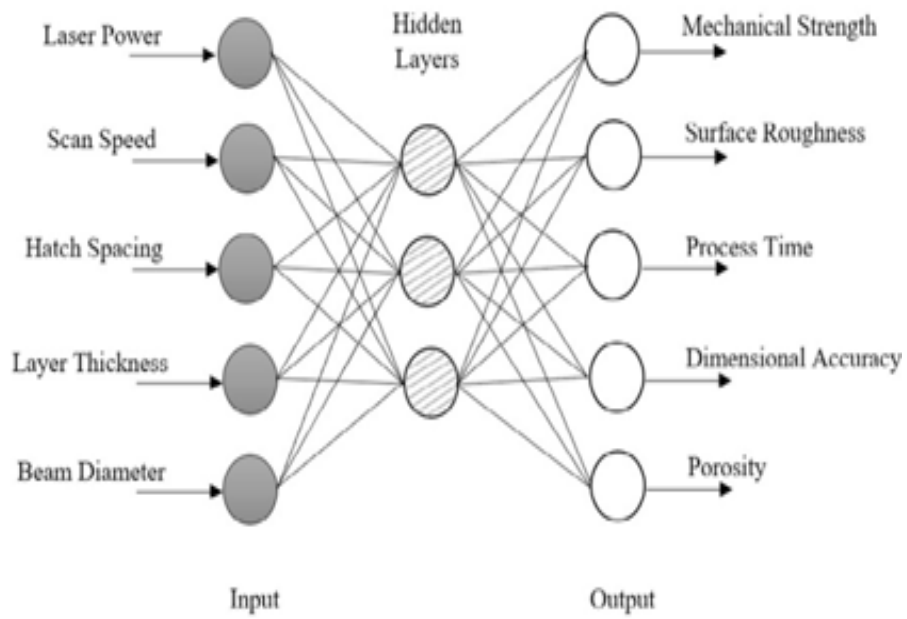


Figure 2.9: The employed Neural Network Model by Mallikharjun et al [31]

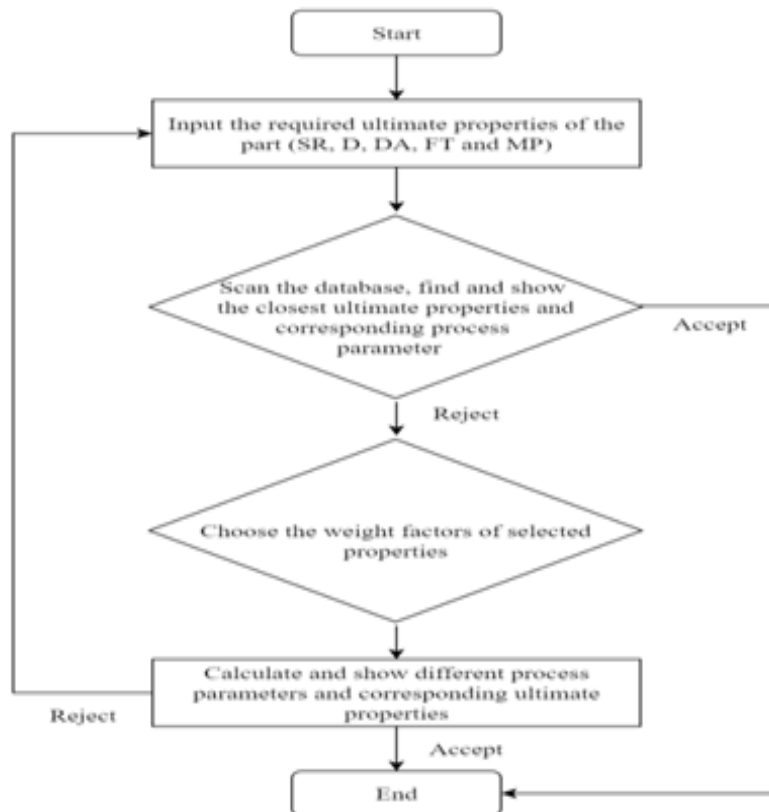


Figure 2.10: Algorithm of selection process parameters by Mallikharjun et al [31]

---

---

## CHAPTER 3

---

# MATERIALS AND METHODOLOGY

Despite so much research, the quality improvement of EBM parts continues to be an open problem that poses challenges in its major industrial breakthrough. Hundreds of parameters are involved in the EBM process. The main problem of EBM process being sub-optimal is the lack of proper analysis and understanding of the co-relation of major parameters impacting on the quality of the part.

Therefore, in this thesis the parameter analysis and co-relation was carried out in the first phase and some important parameters were selected out of so many parameters by using different analytical techniques both by physically observing the process behavior and parameter variation on the Arcam LogStudio software that comes inbuilt in the Arcam machines and then by applying some software statistical analysis techniques.

In the second phase the machine learning algorithms like Support Vector Machine (SVM) and Artificial Neural Networks (ANN) were developed and compared in order to get the most precise prediction of the final product quality qualification based on these selected parameters.

Below in section 3.1 the material used during the experiments to build all the parts of build passed and failed categories is discussed. In section 3.2 the parameter analysis and correlation is discussed. In the section 3.3 Pearson Correlation Coefficient and in section 3.4 the machine learning algorithms developed for the prediction and validation purposes are discussed.

### 3.1 Material

A total of six parts were selected. Three of them were corresponding to successfully build done category and three of them were corresponding to build failed category. The material used for manufacturing of these parts was Ti-6Al-4V.

Ti-6Al-4V is sometimes also named as ASTM Grade 5 and Ti64 or TC4. It is an alpha-beta titanium alloy. Ti-6Al-4V has the quality of high strength to weight ratio and also has an excellent corrosion resistance.

Ti-6Al-4V is a very commonly used titanium alloy. As it provide low density and great corrosion resistance, therefore, it is very largely used in the aerospace industry and in the biomedical applications.

## 3.2 Parameter Analysis and Co-relation

Poor control of the EBM process parameters can lead to unacceptable variation in product quality, leading to the manufacturing of large amounts of out of specification production. This results in an increase in both re-work and give-away and hence a significant increase in energy consumption and raw material usage. The development of an industrially reliable manufacturing performance prediction scheme for such processes, that is capable of detecting process changes and disturbances and providing relevant diagnostic information, would be a major step towards improving manufacturing effectiveness in the EBM process. The first step towards this accomplishment is the proper understanding, selection and co-relation of the parameters. In this part, first the most important parameters were found by analysis and then correlation techniques were applied on the dataset and finally results were plotted using the Pearson's Correlation Coefficient technique.

### 3.2.1 Arcam EBM® Log Studio

The Arcam EBM® Log Studio is a program used for analyzing and viewing the results from a build done by the Arcam EBM® system.

Log Studio consists of three different parts: Report, Graph and Reader. The Report part generates a Build Report that checks different pre-set values to see if the build is within limits. In the Graph part it can be studied how selected parameters have changed during the build in an easy and simple way. The Reader shows the selected parameters as numerical values and can be used for the parameters that are not suitable to show on a graph, for example logical values. During the build the machine logs values to log files and after the build is done and the machine is ventilated the log files are automatically zipped. A log file cannot be viewed in Log Studio at the machine during build process, but it can be viewed on another computer if the folders with the generating log files are shared.

<b>Analyse</b>	contains calculated value for each layer of the process
<b>Builds</b>	contains information about the loaded job, like; current height, max layer time and serial number
<b>Machine</b>	contains machine specific values, like; rake method, rake calibration, maximum column temperature, information about the focus and the astigmatism
<b>OPC</b>	contains signals sent by various hardware to EBM® Control, like; the rake motor, turbo pumps and thermo elements
<b>Process</b>	contains signals that was sent from the software to the hardware, like; power supply, rake- and temperature control
<b>Themes</b>	contains all the values for the different themes, like; process themes, filament themes and material themes

Table 3.1: Most important categories of Log Studio (Arcam Log Studio)

There is a lot of information in every categories, but the most helpful to check is the OPC and the Process categories. Under OPC we can find hardware values like vacuum, temperature and current for

different things. Under Process the rake pulses and positions can be found together with the process manager. The Graph tool is used to visualize the data stored in the log files as graphs. When the Graph pane is selected, a number of predefined graph pages are displayed (see figure 3.1-2):

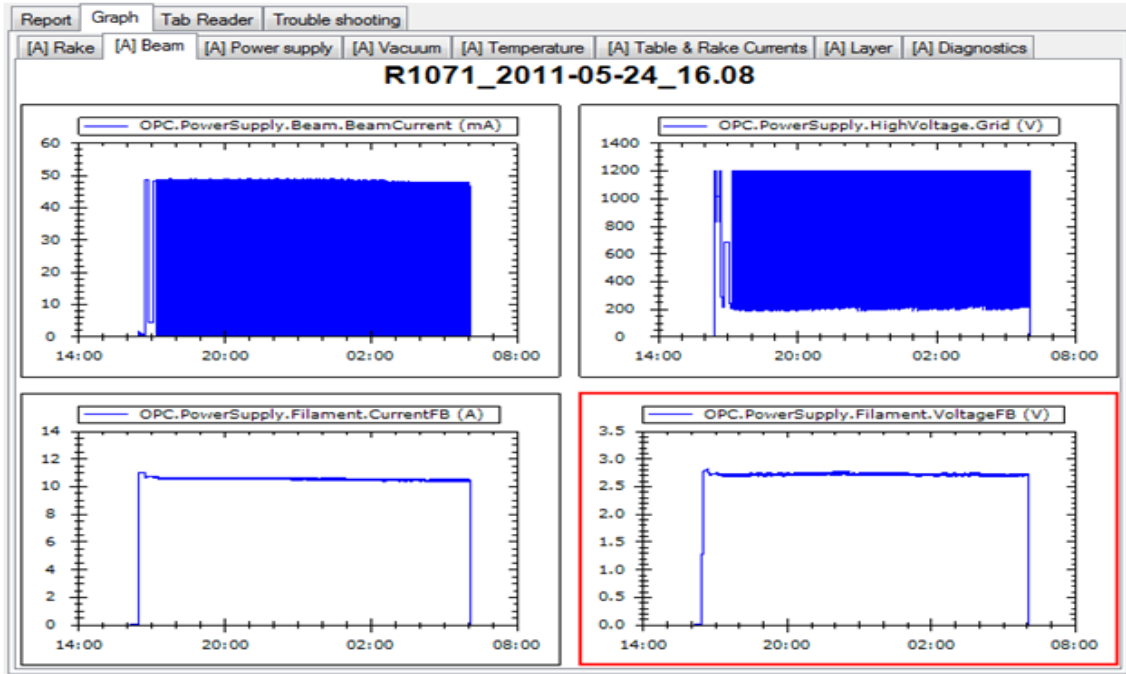


Figure 3.1: Viewing of graphs in Log Studio, example 1 (Arcam Log Studio)

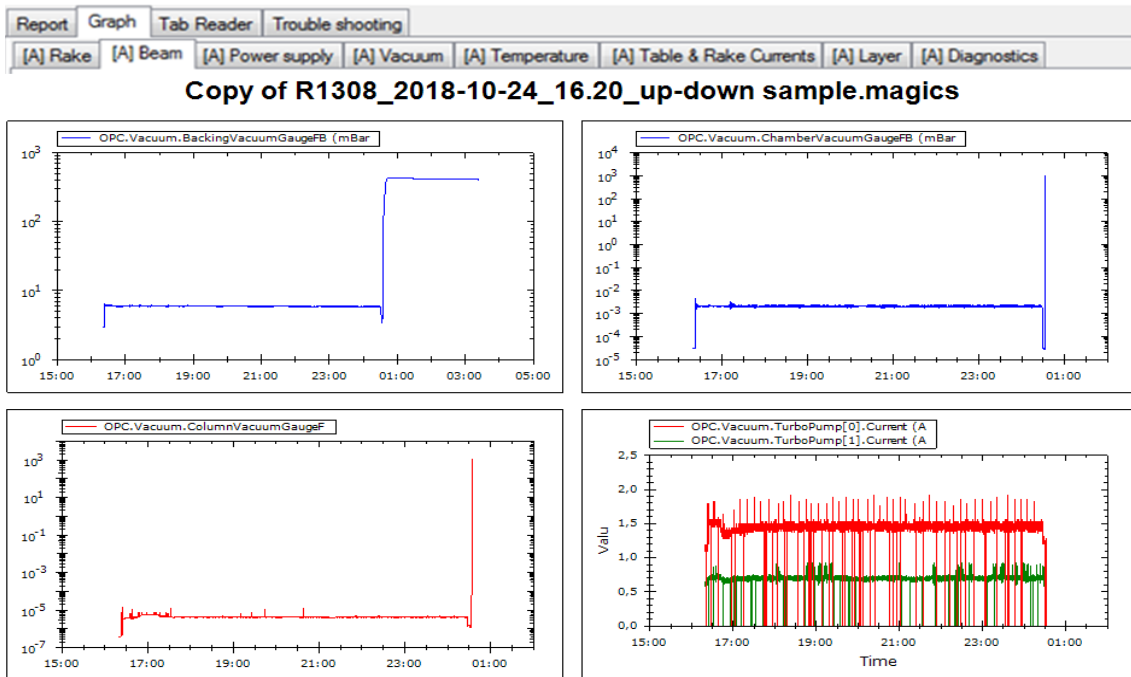


Figure 3.2: Viewing of graphs in Log Studio example 2 (Arcam Log Studio)

Below is a short explanation of the interface:

Rake: Displays pulse length and next position values of the left and right rake regulator.

Beam: Shows beam current, grid voltage, number of registered arc trips and filament current.

power Supply: Shows diagnostics about the power supply such as High Voltage , Arc trips, Remaining Buffer and Focus value.

Vacuum: Displays the backing gauge pressure, the chamber pressure and the gun pressure.

Temperature: Displays the gun temperature and the temperature (registered by the thermo-couple) under the start plate.

Table Rake Currents: Display rake and table current.

Layer: Shows the build height.

Diagnostics: Shows the performance and response time of the computer. The predefined pages are all marked with in the header and cannot be deleted.

Parameters Selection for the data-set

The Comma Separated Values (CSV) files of many parameters were obtained from the LogStudio software against each build category. In the CSV file of LogStudio against each parameter, its value is stored with respect to mili second of time. Therefore, each CSV file contains thousands of rows indicating value of that parameter captured at each point of time. All the parameters were combined in such a way that they are arranged with respect to the time.

After many experimental trials and analysis of the processes for both quality wise passed and rejected parts, the most significant parameters were selected for the data set and correlation was carried out with different statistical techniques. The final correlation was calculated using Pearson's Correlation technique. The parameters selected to constitute the data set are described below:

### **3.2.2 Beam Current**

Beam current is the most important parameter of the EBM process. The electron beam is generated by the potential difference between the negatively-charged cathode and the positively-charged anode. The beam current is the current of the electrons released in the electron beam. The beam current and the focus offset jointly control the spot size. In order to improve the surface roughness, it's needed to decrease the beam current. The beam power is calculated as the product of the acceleration voltage and the beam current, while the section of the beam depends on the spot size. The graph of beam current from log studio is shown in the figure 3.3.

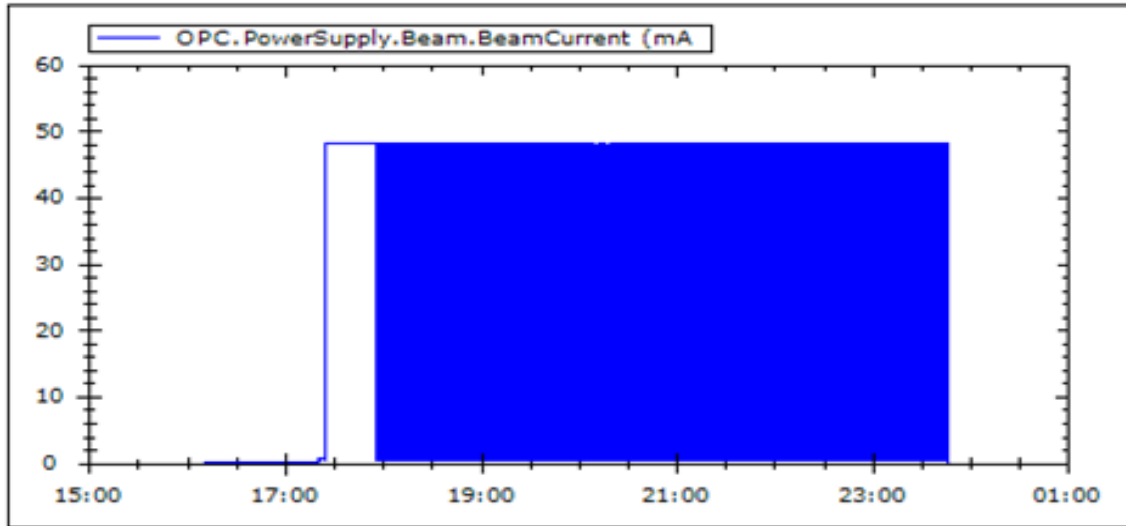


Figure 3.3: Graph of Beam current (Arcam Log Studio)

### 3.2.3 Bottom Temperature

This is the temperature measured at the bottom of the build chamber. The graph of Bottom temperature obtained from Log Studio is shown in figure 3.4.

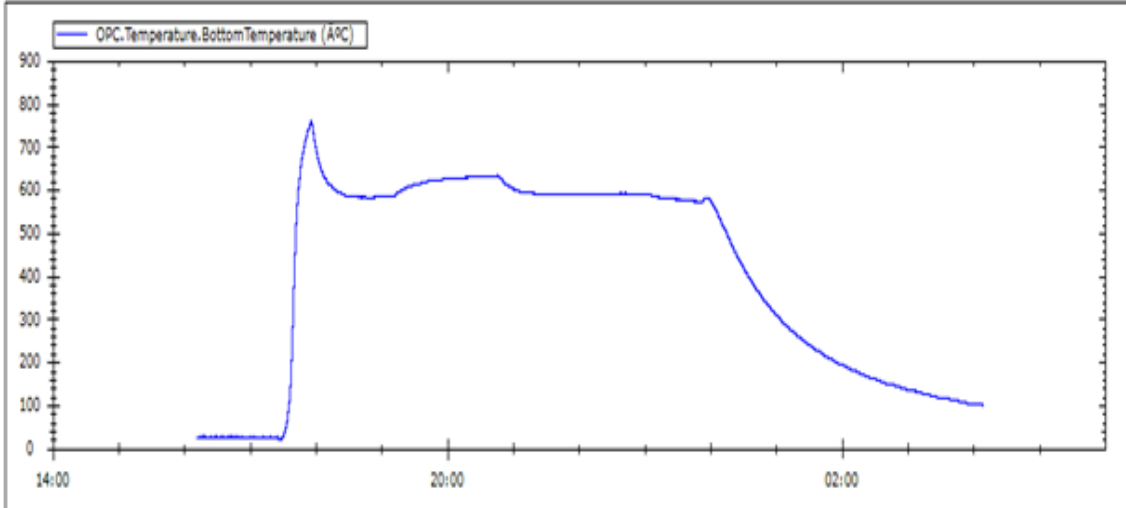


Figure 3.4: Graph of Bottom Temperature (Arcam Log Studio)

### 3.2.4 Column Temperature

This is the temperature measured along the EBM machine column. The graph of Bottom temperature obtained from Log Studio is shown in figure 3.5.

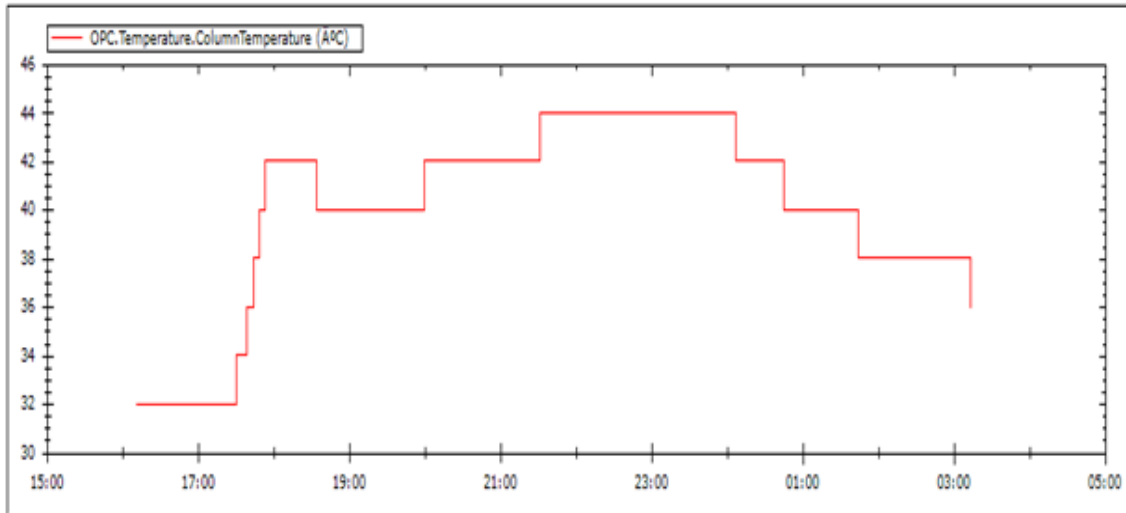


Figure 3.5: Graph of Column Temperature (Arcam Log Studio)

### 3.2.5 Filament Current

It denotes the current intensity required to heat the tungsten filament. The graph of Filament current obtained from Log Studio is shown in figure 3.6.

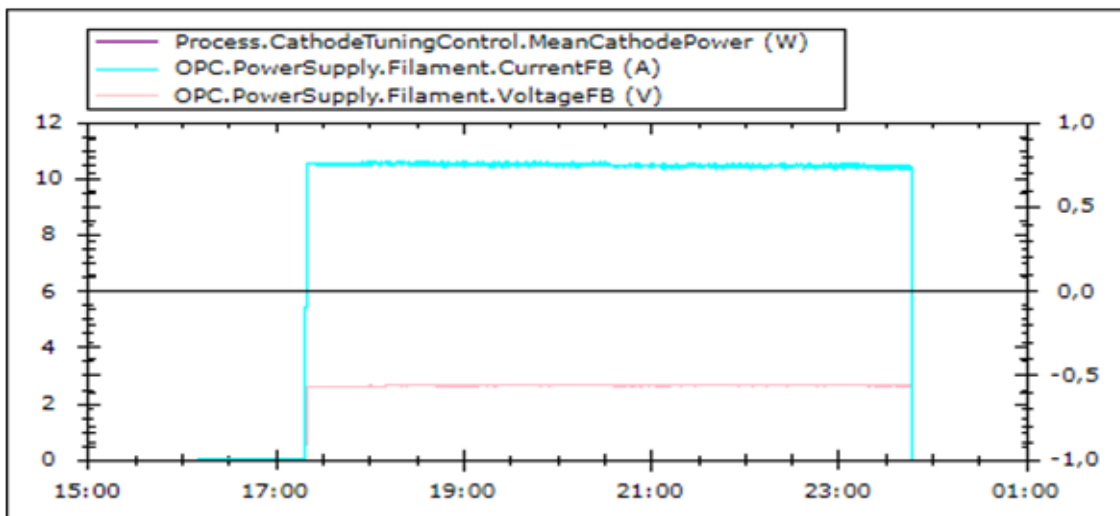


Figure 3.6: Graph of Filament Current (Arcam Log Studio)

### 3.2.6 Rake Current Feedback

The rake fetches powder from the powder slopes, which are formed by openings at the bottom of the hoppers, and distributes the powder across the build table. The build platform moves vertically along the z-axis, with each layer moving the component being built, the surrounding powder, and the start plate downwards along with it. The graph of Rake current feedback obtained from Log Studio is shown in figure 3.7.

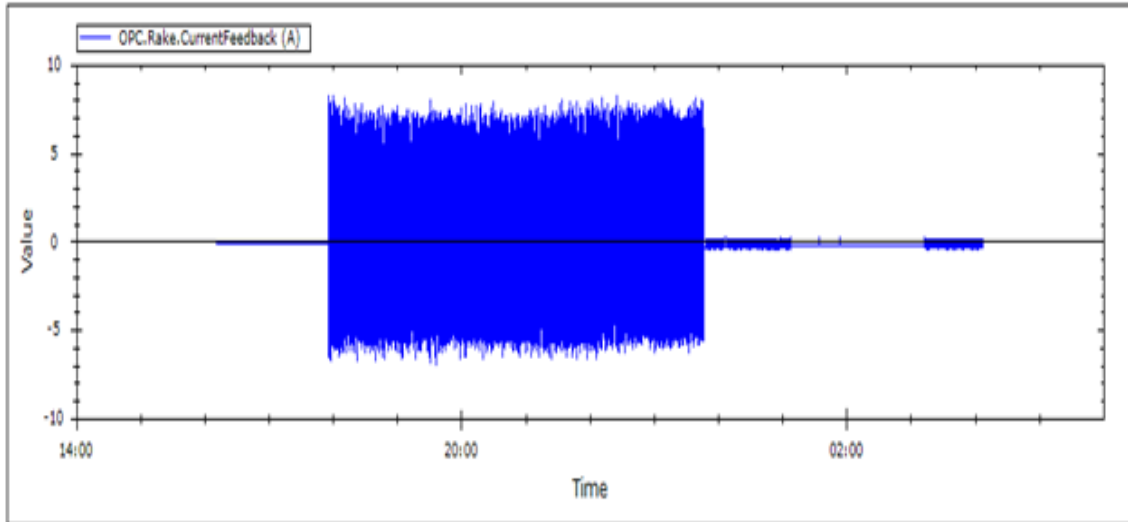


Figure 3.7: Graph of Rake Current Feedback (Arcam Log Studio)

### 3.2.7 Left/Right Regulator Pulse Length

The output pulse of two sensors located near the initial and the final position of the rake, with respect to its zero position, are used to control the powder spreading. The reference pulse is 180 ms.

The graph of left and right regulator pulse length obtained from Log Studio is shown in figure 3.9.

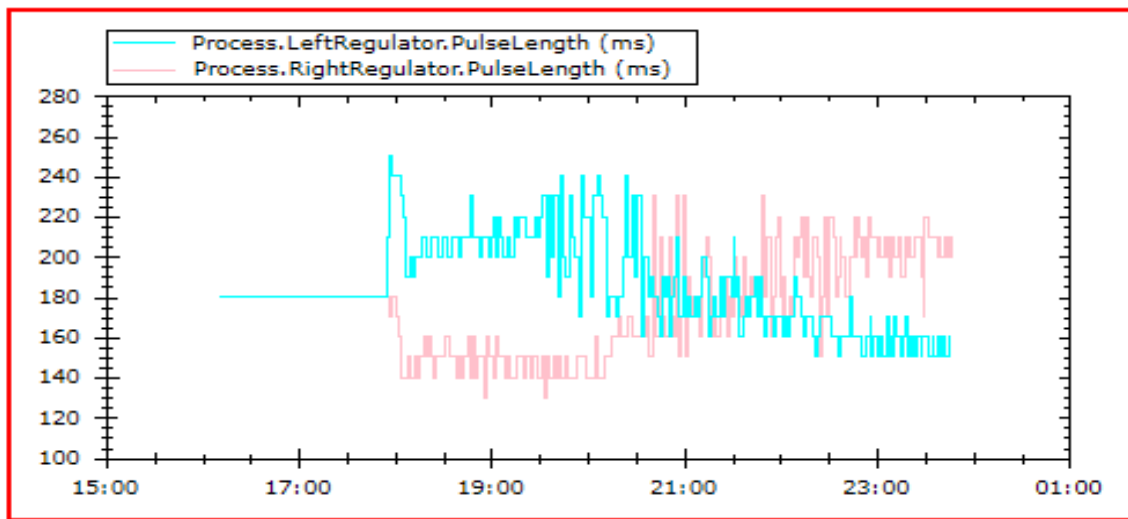


Figure 3.8: Graph of Left/Right Regulator Pulse Length (Arcam Log Studio)

### 3.2.8 Current Height

Current Height indicates at which layer a particular problem occurs. This parameter is actually the history of the height of the job that increases over time.

The graph of Current height obtained from Log Studio is shown in figure 3.9.

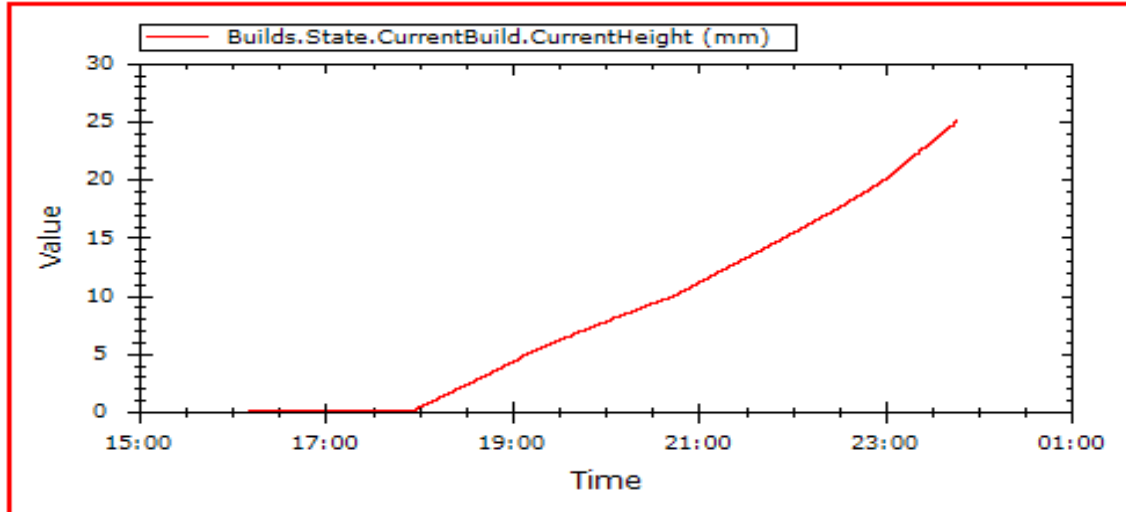


Figure 3.9: Graph of Current Height (Arcam Log Studio)

### 3.2.9 Backing Vacuum Gauge Feedback

The parameter is the measure of feedback of the backing up vacuum. The graph of Backing Vacuum Gauge Feedback obtained from Log Studio is shown in figure 3.10.

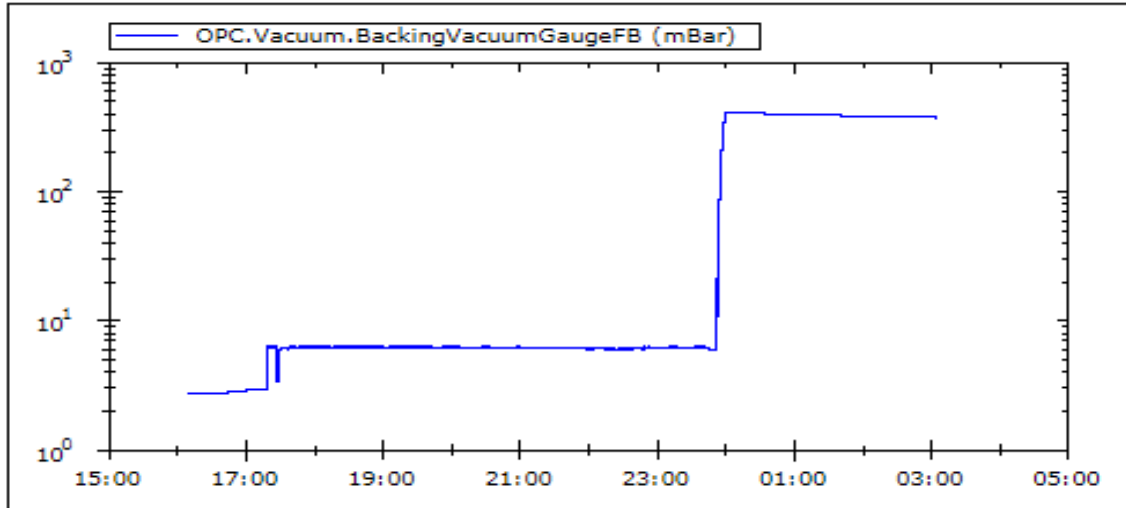


Figure 3.10: Graph of Backing Vacuum Gauge Feedback (Arcam Log Studio)

### 3.2.10 Chamber Vacuum Gauge Feedback

This parameter is the measure of the feedback of the vacuum created in the chamber. The graph of Chamber Vacuum Gauge Feedback obtained from Log Studio is shown in figure 3.11.

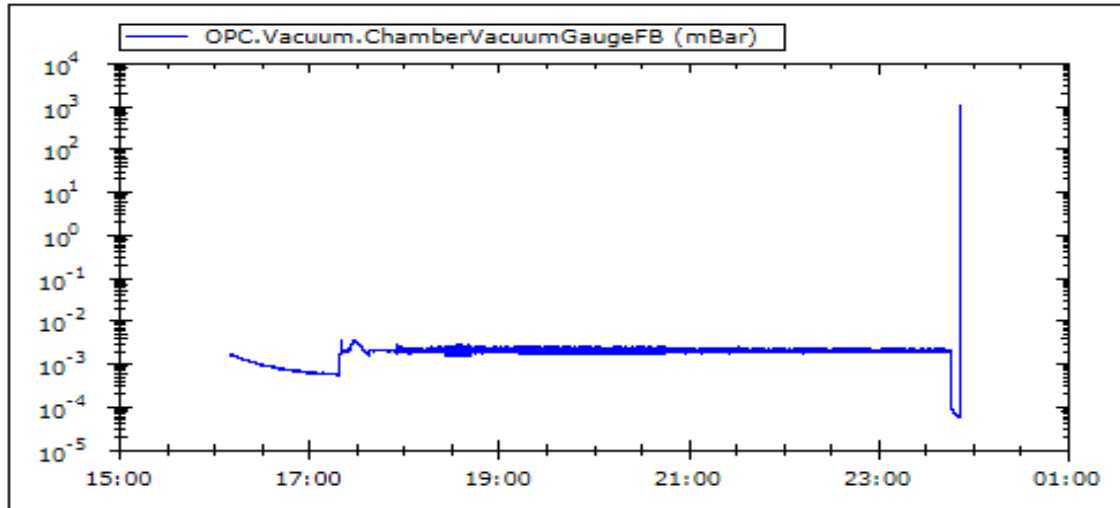


Figure 3.11: Graph of Chamber Vacuum Gauge Feedback (Arcam Log Studio)

### 3.2.11 Column Vacuum Gauge Feedback

Column Vacuum Gauge Feedback is the measure of vacuum feedback created in the column of the EBM machine. The graph of Column Vacuum Gauge Feedback obtained from Log Studio is shown in figure 3.12.

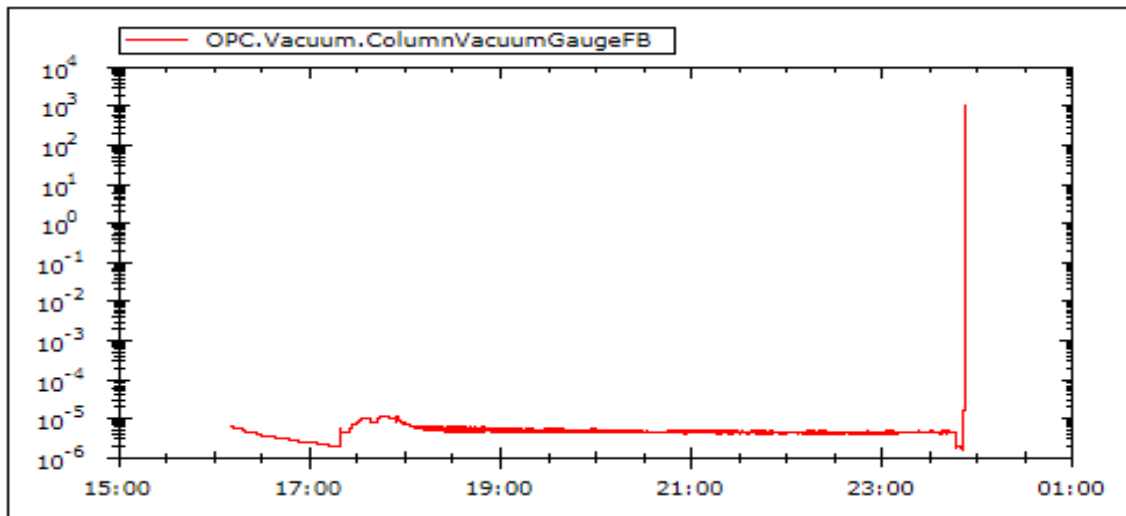


Figure 3.12: Graph of Column Vacuum Gauge Feedback (Arcam Log Studio)

## 3.3 Pearson Correlation Coefficient

Prior to going towards networks the correlation between the parameters was calculated. This was done in the Python environment using the Pearson correlation coefficient method.

Pearson Correlation coefficient is also called Pearson product moment correlation coefficient (PPMCC)

or sometimes bi variate correlation and it determines the statistical relationship between the two variables. It calculates the value of relationship between +1 and -1. Plus or minus signs refer to either the correlation is directly proportional or inversely proportional, while the value refers to the magnitude of the relationship.

### 3.4 Prediction Models/Classifiers

The prediction was calculated with the help of two techniques. The Support Vector Machine (SVM) and the Artificial Neural Networks (ANN).

A Support Vector Machine (SVM) is a discriminate classifier defined by a separating hyper-plane. This technique belongs to supervised learning. Given training data, the algorithm gives us an optimal hyper-plane which categorizes new examples. In 2-dimensional space this hyper-plane is basically a line dividing the plane in 2 parts where, each class lay in each side side.

Basic concept of separation through SVM classifier hyper-plane is shown in figure 3.13.

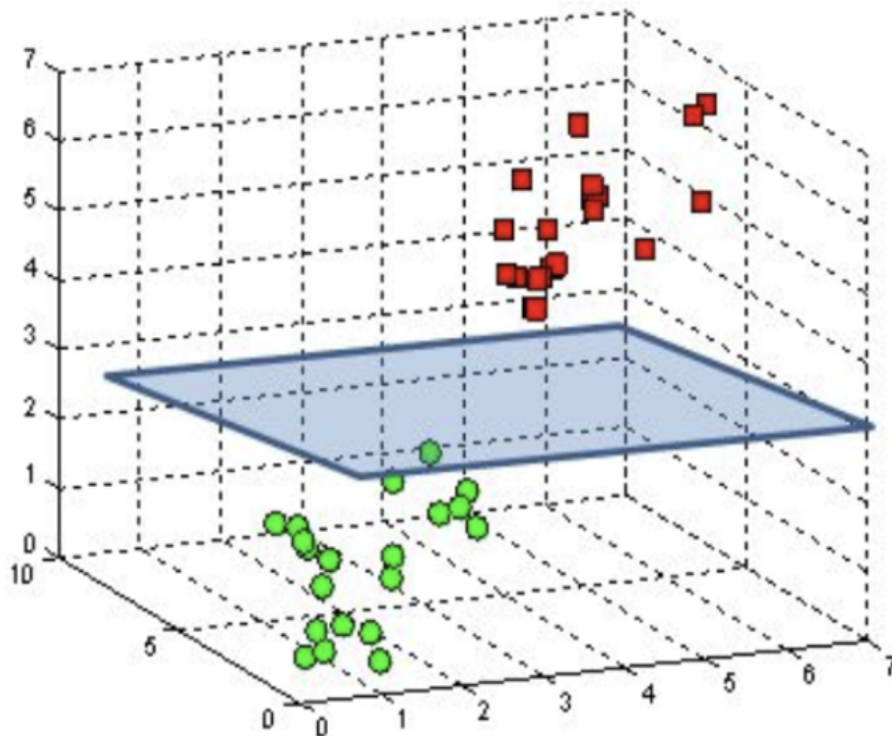


Figure 3.13: SVM classifier separating hyper-plane (<https://developer.xilinx.com/en/articles/exploring-support-vector-machine-acceleration-with-vitis.html>)

Algebraic techniques are basically used for the transformation of the problem for the purpose of learning of the hyper-plane in the SVM. The basic role of the Kernel is to perform this separation task.

For linear-kernel the new output is predicted by using the dot-product in between each support vector  $x_i$  and each input  $x$ . The equation is given below.

$$f(x) = B(0) + \sum (a_i * (x, x_i))$$

In the equation above, the inner products of all the support vectors with a new vector  $x$  in the training data are calculated. With the help of the learning algorithm, the coefficients represented by  $a_i$  and  $B(0)$  are predicted against each input from the training data.

Polynomial and exponential kernels calculate separation line in higher dimension. This is called kernel trick. The polynomial kernel can be represented as:

$$K(x, x_i) = 1 + \sum (x * x_i)^d$$

The exponential kernel can be represented as

$$K(x, x_i) = \exp(-\gamma * \sum (x - x_i)^2)$$

The gamma tells us that how far is the influence of a training example. When gamma has a low value, it means the influence has reached so far. Alternately if gamma is high, it means the influence is close. To put it in another way, we can say that when the value of gamma is low, it means that the points that lie too much away from the line of plausible separation become in the calculation range of the line of separation. In other words the higher the gamma the more closer points are taken into the circulation.

Margin is very important characteristic of SVM classifier. This helps SVM to achieve good margins. Separation of the line from the class points lying very close is called the margin. Larger this separation the better the margin. When the margin is good, it helps the points to stay in their own class instead of lying to other classes.

Artificial Neural Networks:

A block diagram of the development of artificial neural networks carried out in this thesis is shown in figure 3.14.

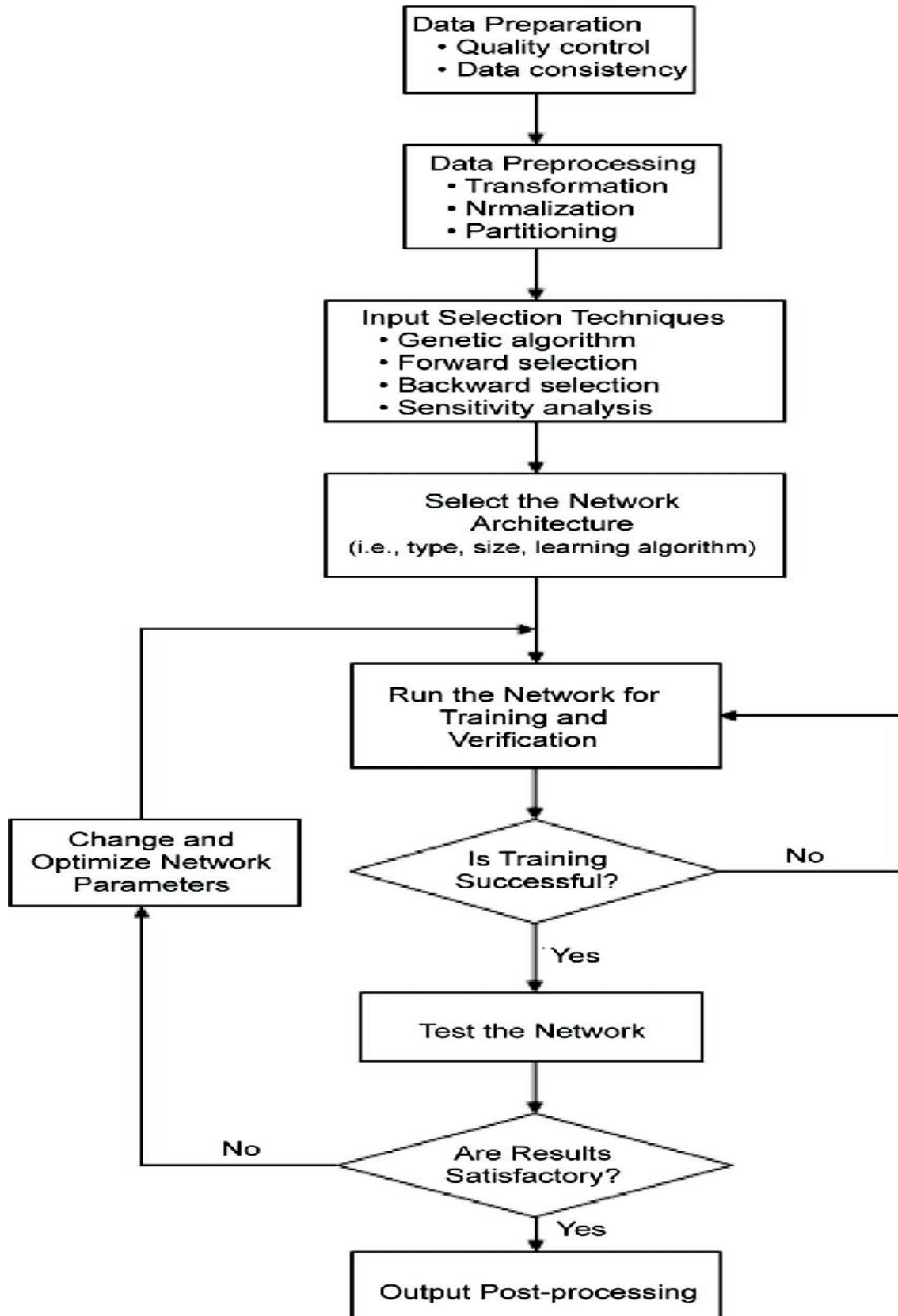


Figure 3.14: Process flow of artificial neural network

**Training Data set:** Training data set is the sample of the data that is used to fit the model or classifier. This is provided by the actual data set that we use to train the model. The model sees and learns from this data through a repetitive process.

**Validation Data set:** Validation data set is the sample of the data that helps to provide realistic evaluation of a model fitted on the data set used for training while tuning model hyper-parameters. The evaluation goes to be more biased because the skill on the validation data set is implemented on the configuration of the model .

**Test Data set:** This is the collection of the data used to provide an realistic evaluation of a final model fit over the data set of training.

**Number of hidden layers:** The model that is developed in this thesis contains four hidden layers: the input layer has eleven neurons that is the equal to the number of input features, first hidden layer contains 28 neurons, second hidden layer contains 17, the third one contains 12, the fourth one contains 5 neurons, while the output layer contains one neuron as we are predicting the binary classification problem.

**Activation function:** This is a function that is nonlinear in nature and its purpose is to transform over the input signal ( $x$ ). The decision about the firing of neuron is carried out by the activation function. Activation function holds very important place in the artificial neural network structure, this is because if a network don't has the activation function than its nothing more than a regression model that is linear in nature thus it is unable to perform any task that is complex in nature. Some famous activation functions are described below:

$$\textit{Sigmoid} : f(x) = \frac{1}{(1 + e^{-x})}$$

$$\textit{ReLU} : f(x) = \max(0, x)$$

In practical applications, sigmoid gradient that is present on both sides of it and the ReLU negative axis tends to approach to zero becoming smaller and smaller. Due to this reason the learning problem occurs as weights become unable to learn because they cant be adjusted. Therefore, the it gives rise to the disappearing gradient issue. To overcome this problem a function that keeps the input to a specific range is used and that function is called Max-min normalization.

**Loss function:** The loss function can be interpreted like a real life problem. The exact problem is used to find the the loss function. For instance the distance that persists between two vectors, vector corresponding to target values and the vector of prediction is measured by two errors, i,e; mean absolute error and the root mean square error. The mathematical expressions of mean absolute error and the root mean square error are given here:

$$RMSE : f(x) = \sqrt{\frac{\sum_{i=1}^n (y_i - y_t)^2}{n}}$$

$$MAE : f(x) = \frac{\sum_{i=1}^n (y_i - y_t)}{n}$$

In the above equations,  $i$  is index value,  $y_i$  is the number that represents the predicted value, and  $y_t$  represents the predicted value. Also there exist some small differences between the mean absolute error and the root mean square error: for example root mean square error corresponds to the L2 norm (the Euclidean norm) that represents a common familiar distance, while mean square error belongs to the L1 norm where the distance is calculated in the shape of a regular grid that is started from the target origin.

---

---

## CHAPTER 4

---

# Experiments and Results

The parametric data of three build done and three build failed parts was selected for the experiments. All the parameters of data set were gathered against these parts from the log files of Arcam LogStudio. In the section 4.1 the results of parametric analysis and co-relation are discussed, in section 4.2 the result of SVM and in the section 4.3 the results of artificial neural networks are discussed. In section 4.4, the python script is describe.

## 4.1 Results of Parameter Analysis and Correlation

### 4.1.1 Build Done Case I

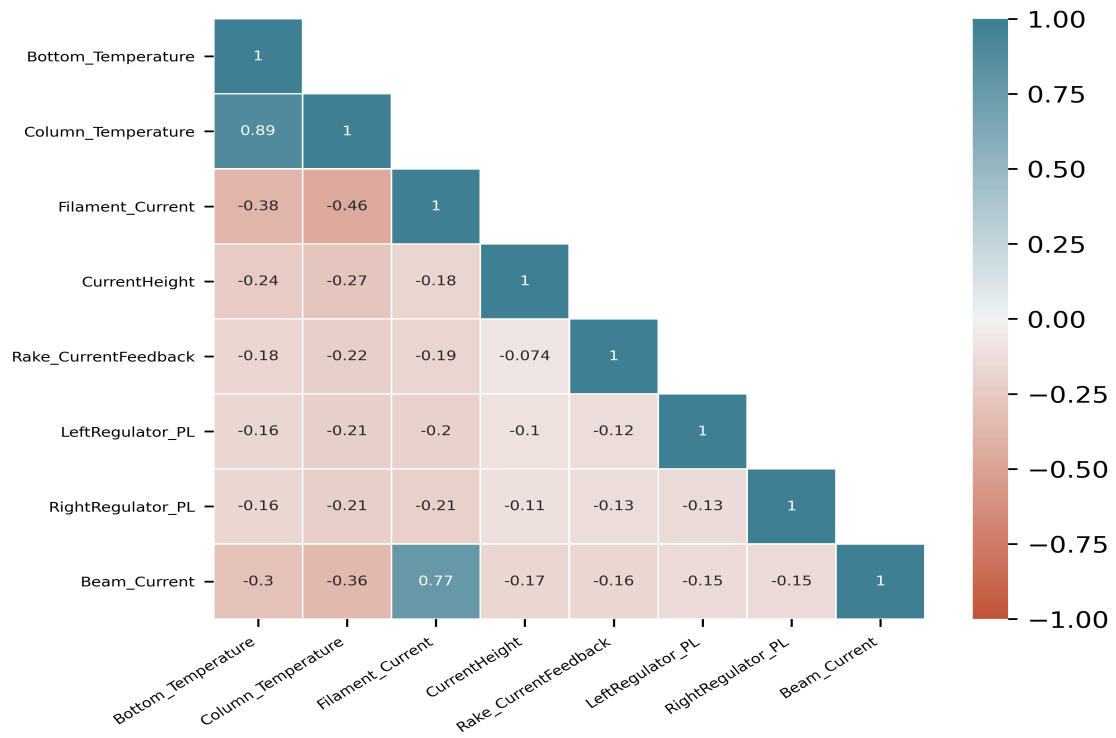


Figure 4.1: Results of Correlation analysis of build done case I, Part-1

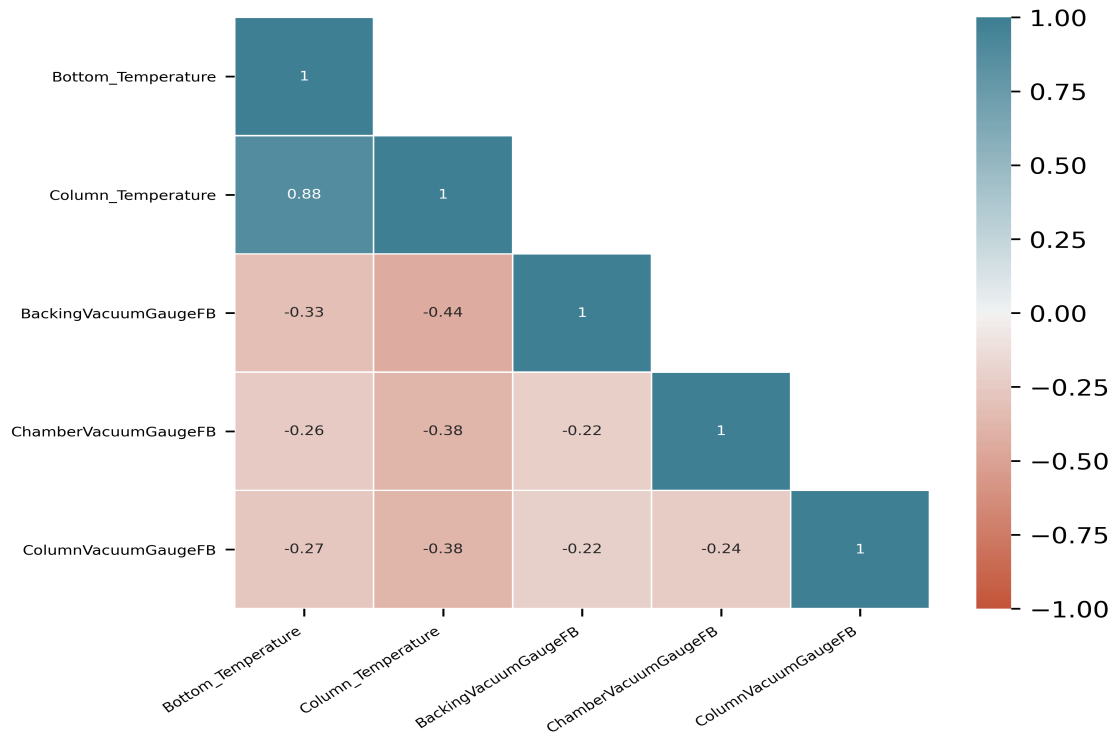


Figure 4.2: Results of Correlation analysis of build done case I, Part-2

The vacuum Backing vacuum gauge feedback, Chamber Vacuum gauge feedback and Column Vacuum gauge feedback are co-related separately against Bottom and Column temperatures because realistically no such relation exist between these vacuum feed-backs and currents.

It is quite logical and also visible from the result that the beam current and the filament current have a very strong positive correlation between them. Its value is +0.77 which indicates a very good co-relation.

Bottom temperature and column temperature were also very strongly co-related with each other and their value comes out to be +0.89.

The correlation among the beam current, the bottom temperature and the column temperature is also very significant and comes out to be -0.36 and -0.30. The negative sign indicates an inverse correlation between the parameters. Same is the case with the filament current and these temperatures.

Right and left regulator pulse lengths, which are responsible for controlling the amount of powder spread in each layer is a little inversely correlated with filament current and column.

Current height of the build part has also very strong inverse co-relationship with the bottom and the column temperature, that stands at -0.24 and -0.27 respectively. Figure 4.2 also indicates significant co-relationships among the bottom and column temperatures and the vacuum feed-backs.

4.1.2 Build Done Case II

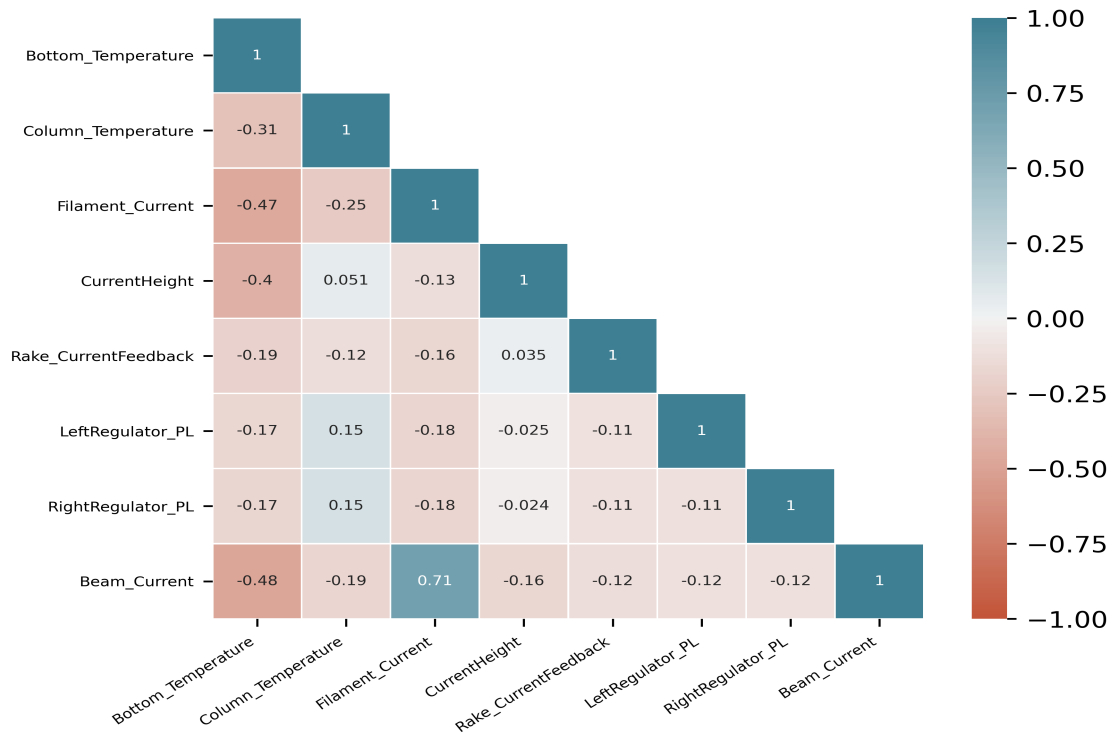


Figure 4.3: Results of Correlation analysis of build done case II, Part-1

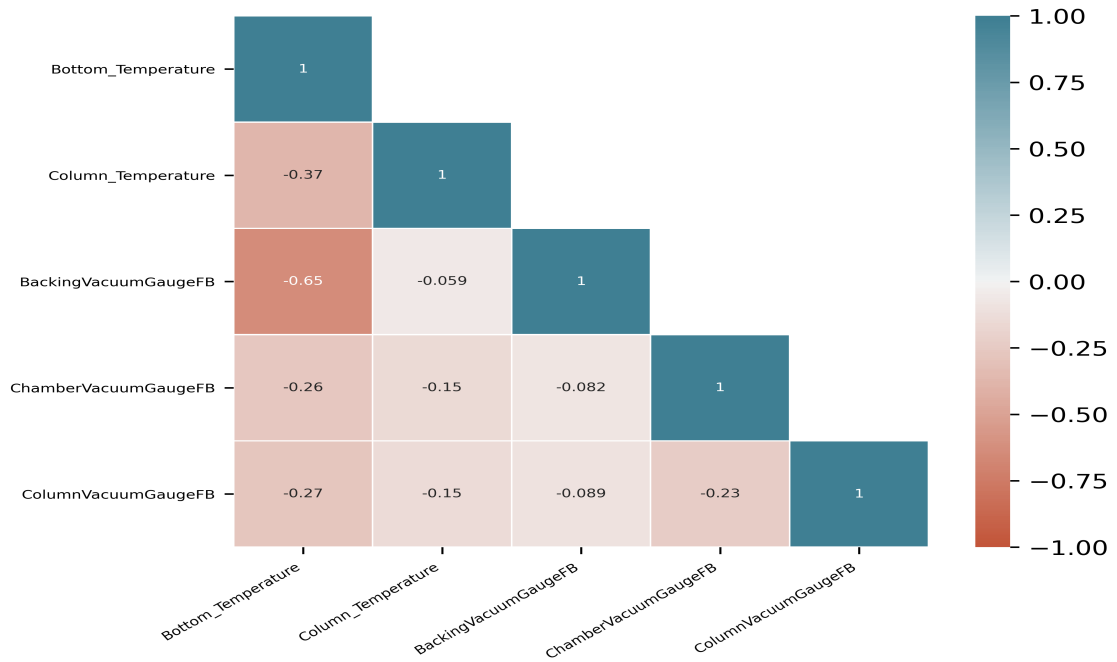


Figure 4.4: Results of Correlation analysis of build done case II, Part-2

Again, in this case strong positive co-relationship exists between the beam current and the filament current. Bottom temperature is very strongly correlated with the filament current, beam current and current height. Beam current is inversely co-related with the Bottom temperature and Column temperature. In this case Bottom temperature and column temperature are inversely co-related with each other. Also bottom temperature and Backing vacuum feedback have a very strong inverse correlation.

### 4.1.3 Build Done Case III

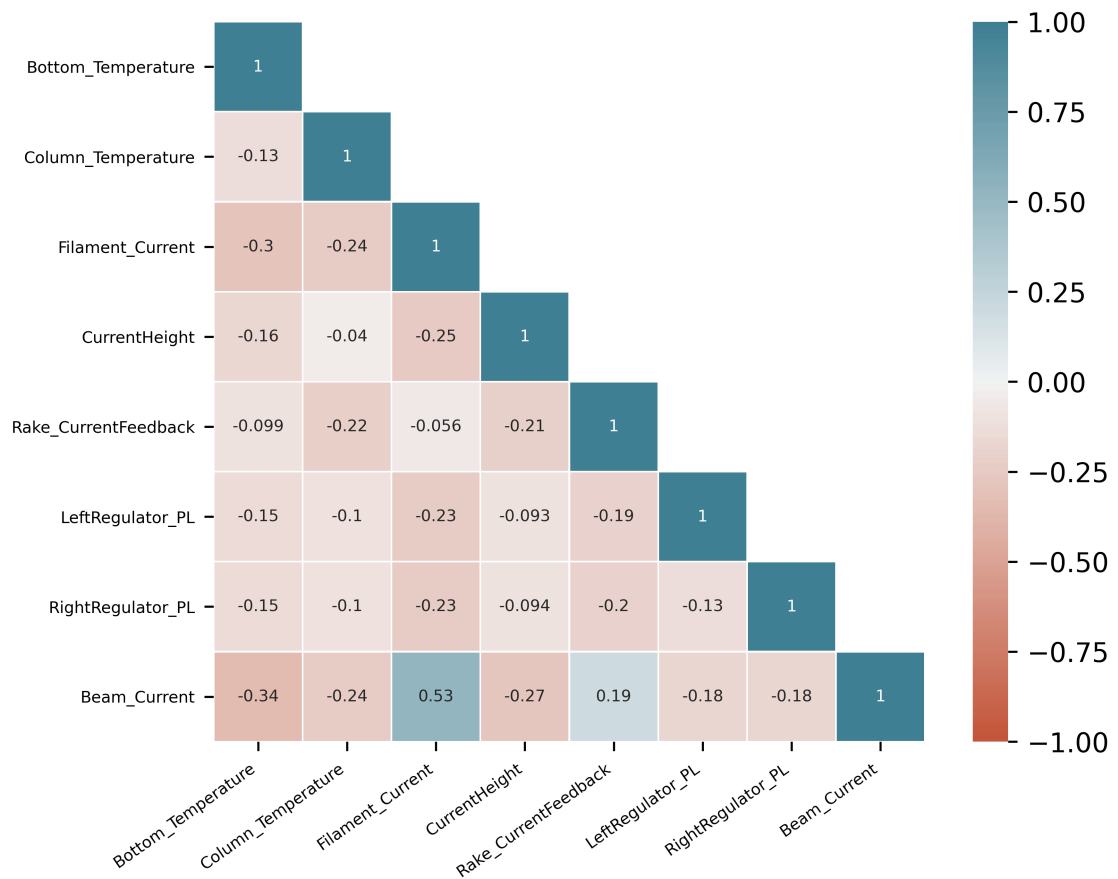


Figure 4.5: Results of Correlation analysis of build done case III, Part-1

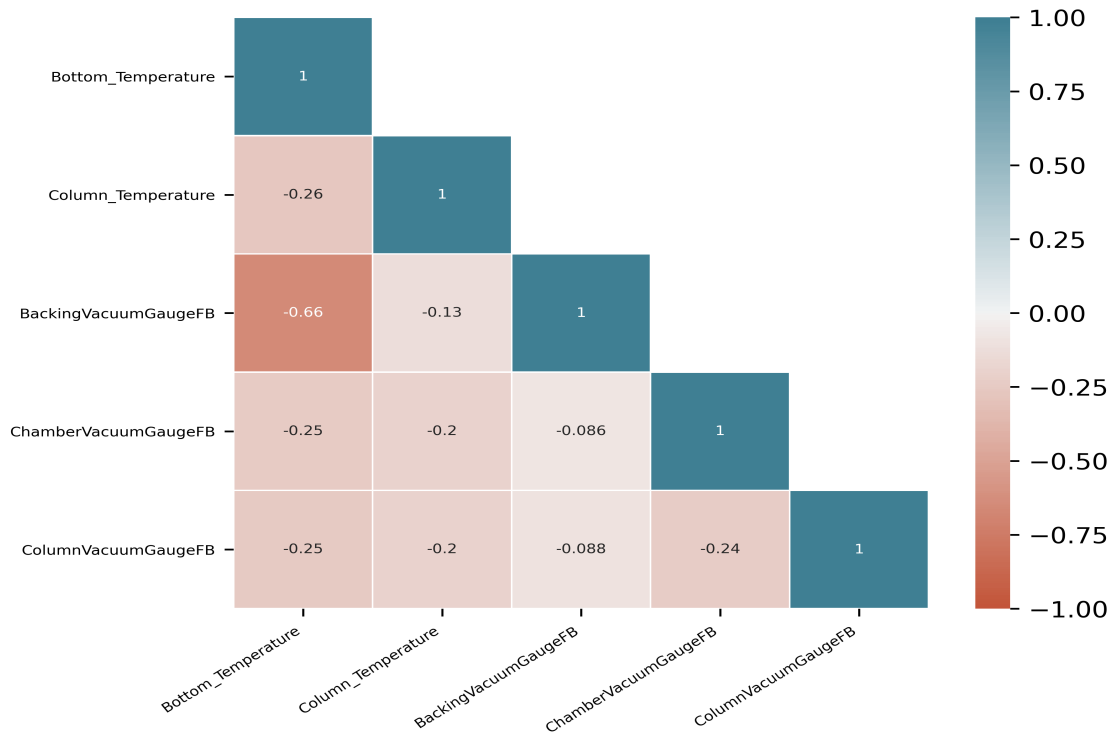


Figure 4.6: Results of Correlation analysis of build done case III, Part-2

In this case a strong positive correlation was observed among the beam current and filament current as well as beam current and the Rake current feedback. Moreover, there exist strong negative correlation between beam current and bottom temperature and beam current and column temperature, valued at -0.34 and -0.24. Apart from that a significant negative correlation was also observed between beam current and current height. As far as the correlations between Vacuum feed-backs and temperatures are concerned, there is a very strong negative relationship between Bottom temperature and backing vacuum gauge and its value is -0.66.

4.1.4 Build Failed Case I

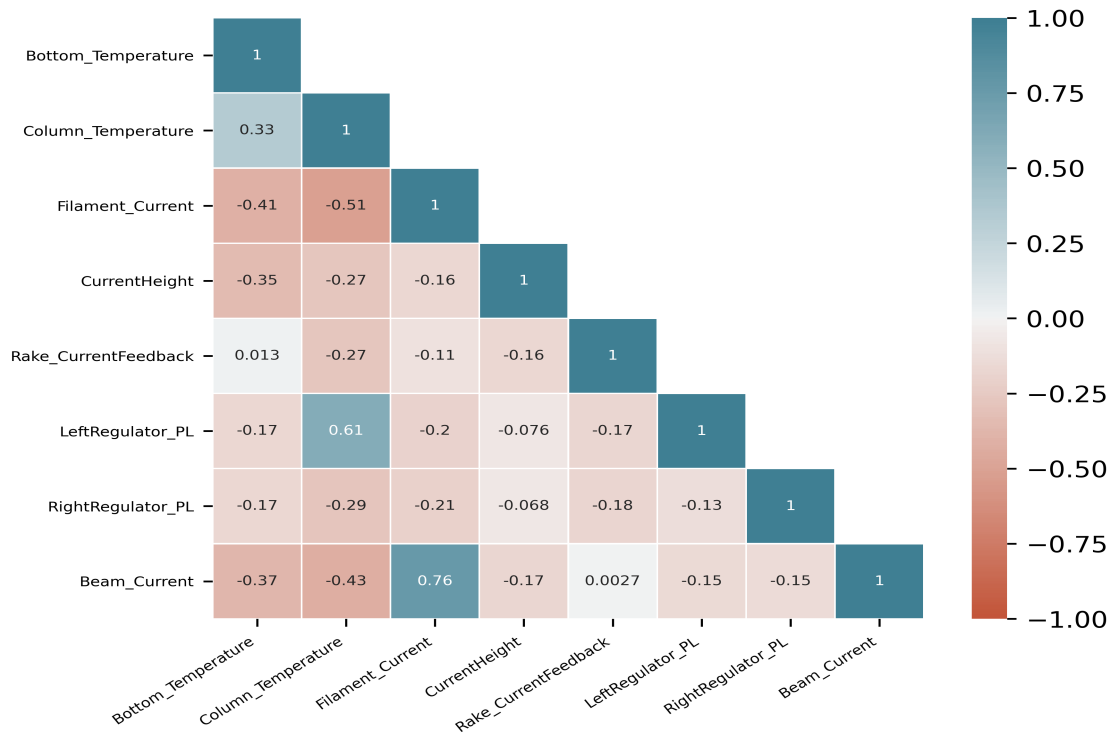


Figure 4.7: Results of Correlation analysis of build failed case I, Part-1

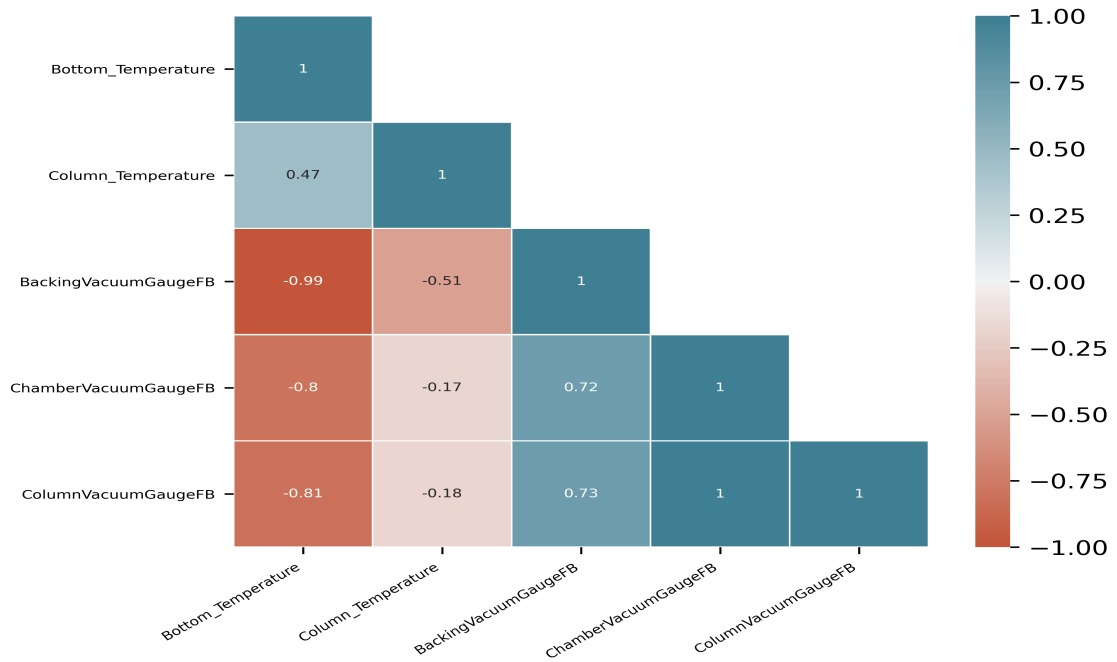


Figure 4.8: Results of Correlation analysis of build failed case I, Part-2

In this case, apart from very strong correlation between beam current and the filament current, another very strong correlation was observed that is between column temperature and left regulator pulse length. Also in this case there is an unusual scenario to observe that was not present in the build done cases, that is the correlations between temperatures and vacuum feed-backs. For example, there are very strong positive correlations between backing vacuum gauge feed-back and column vacuum gauge feed-back, also between backing vacuum gauge feed-back and chamber vacuum gauge feed-back, standing at +0.73 and +0.72 respectively. While Column vacuum gauge feed-back and Chamber vacuum gauge feed-back enjoy a correlation of exactly 1. Talking about the negative correlations, there is a correlation of -0.99 between Bottom temperature and Backing vacuum feedback. While the correlation of bottom temperature with column vacuum gauge feed-back and chamber vacuum gauge feedback stands at -0.81 and -0.80 respectively. Column temperature and backing vacuum feedback are correlated as -0.51. Furthermore, the correlation of Filament current and Bottom and Column temperature came out to be -0.41 and .051 respectively.

#### 4.1.5 Build Failed Case II

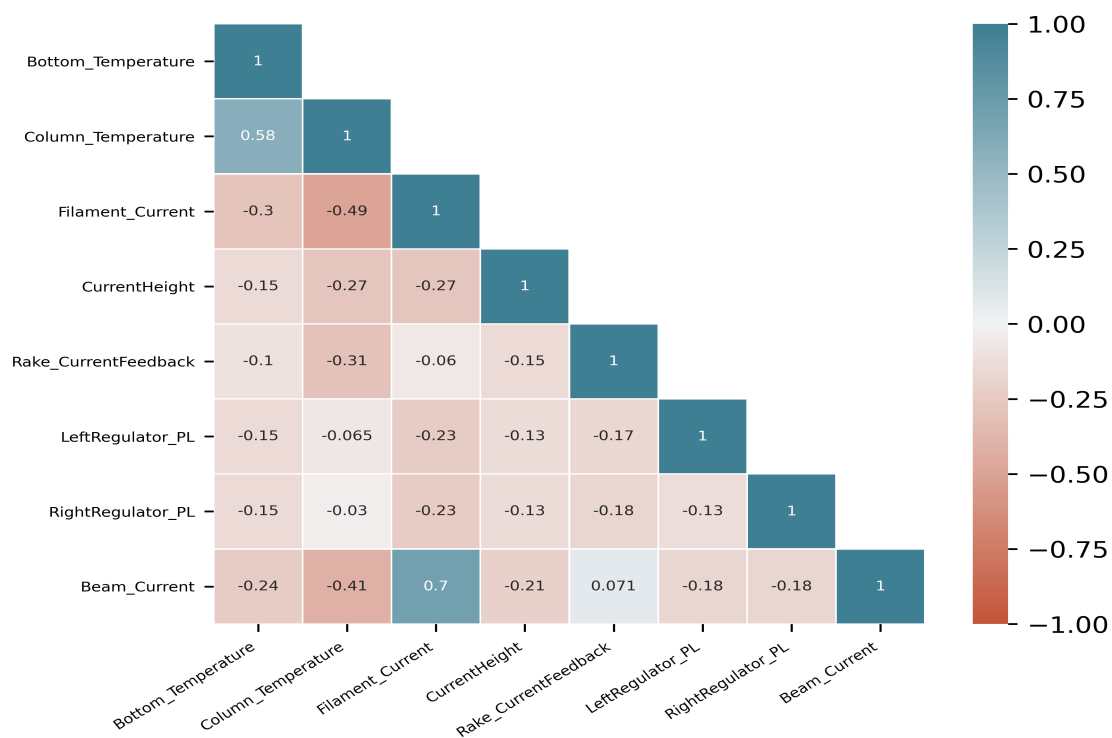


Figure 4.9: Results of Correlation analysis of build failed case II, Part-1

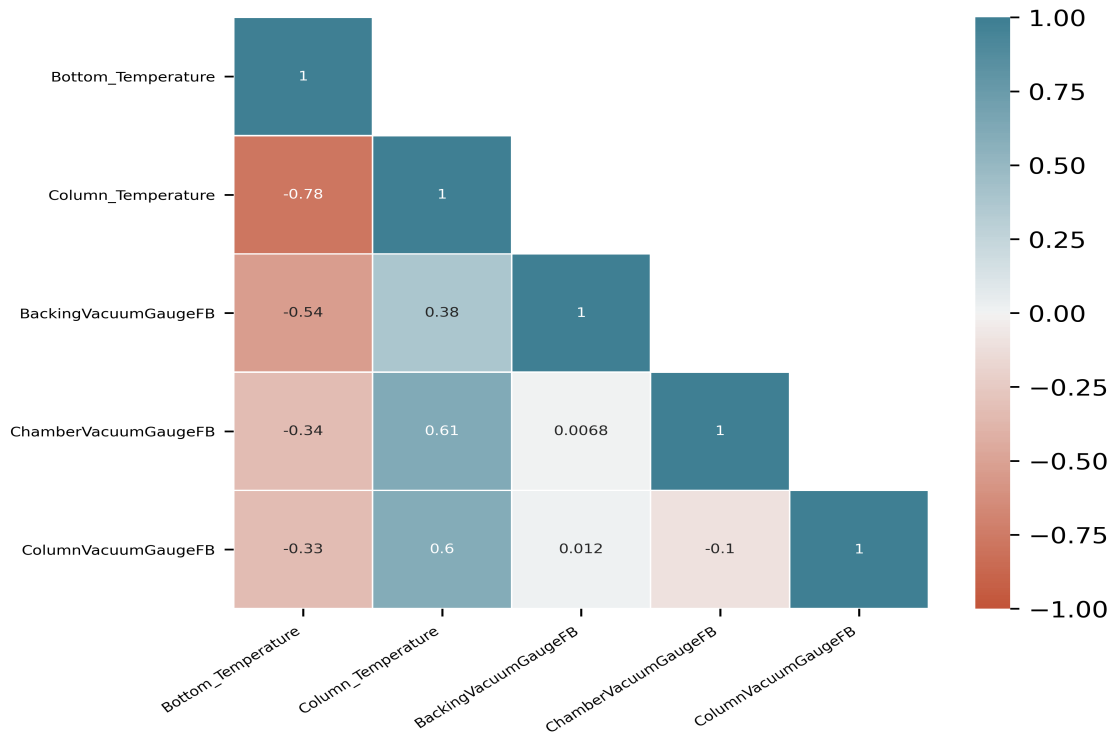


Figure 4.10: Results of Correlation analysis of build failed case II, Part-2

In this case long with a positive correlation between the bean current and the filament current, there is also a strongly positive correlation between column temperature and bottom temperature, that is +0.58. Among other positive relationships are the correlations of column temperature with chamber vacuum feedback and column vacuum feedback, standing at +0.61 and + 0.60 respectively. While column temperature and backing vacuum feedback are correlated as +0.38. As far as the inverse correlations are concerned, the correlation of column temperature with filament current and beam current stands at -0.49 and -0.41. There is a very unusual scenario observed in this case that is between column and bottom temperatures. Value of this correlation in figure (a) is +0.58 and in figure (b) is -0.78. This result is very strange and may be the cause of the failure of the part.

4.1.6 Build Failed Case III

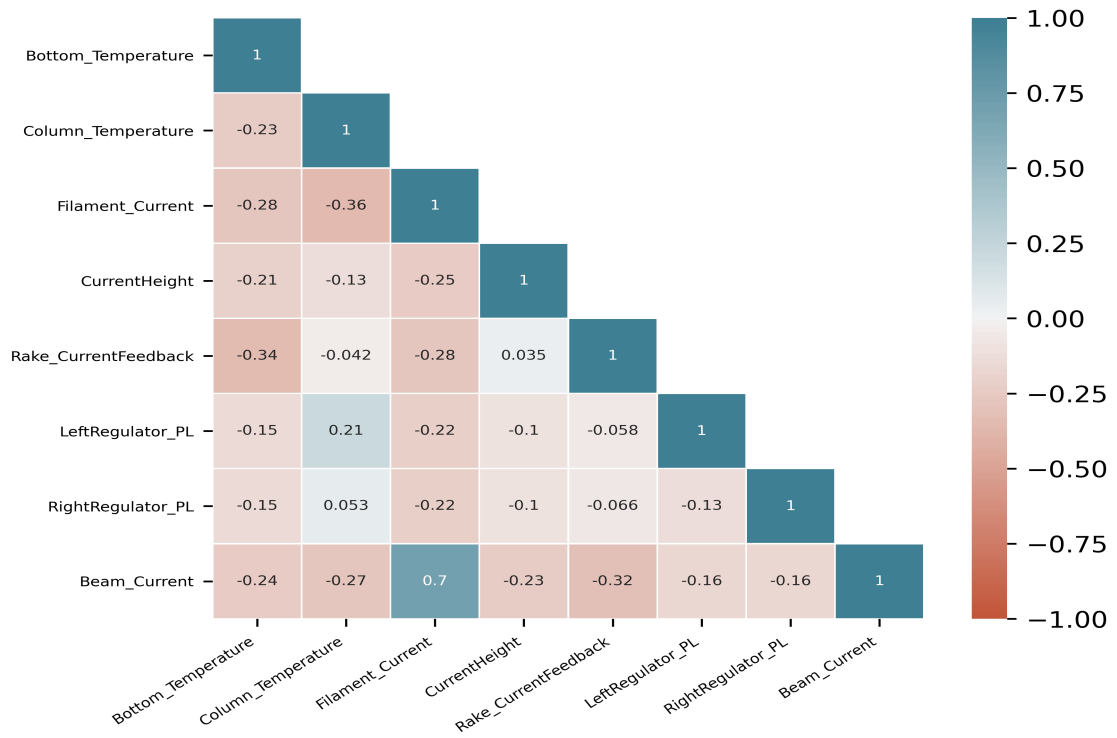


Figure 4.11: Results of Correlation analysis of build failed case III, Part-1

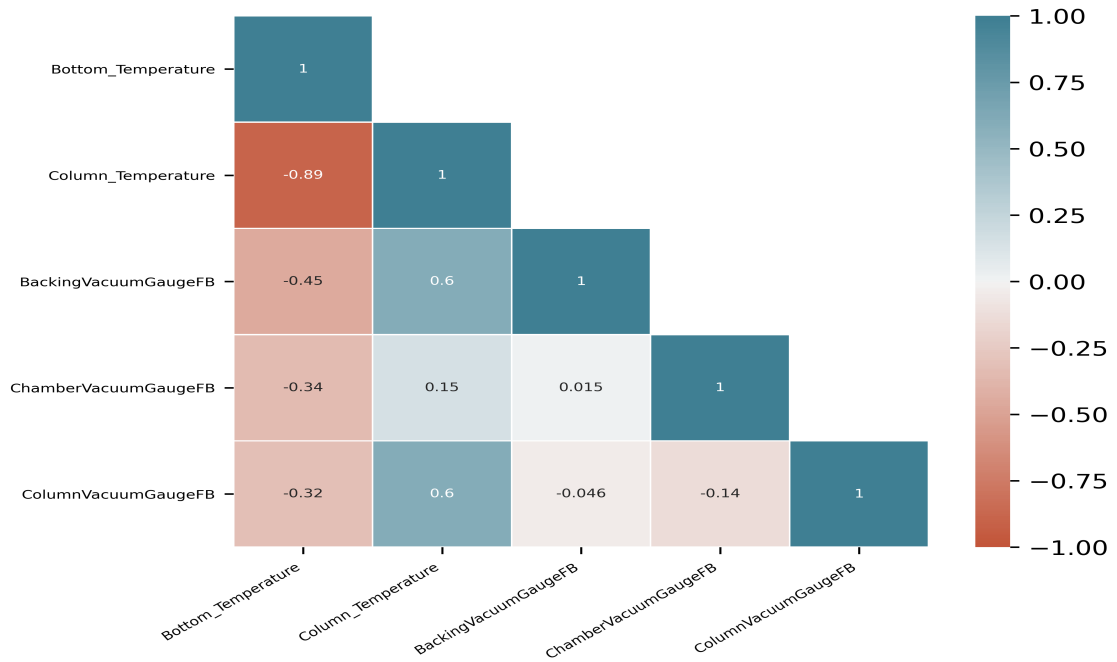


Figure 4.12: Results of Correlation analysis of build failed case III, Part-2

If we talk about the positive correlations as usual there is one between beam current and the filament current. Second positive relationship is between column temperature and left regulator pulse length and its value is +0.21. The column temperature is also positively correlated with the column vacuum feedback and the backing vacuum feedback having the same value as +0.60. However filament current and column temperature are negatively correlated with each other as -0.36. Rack current feedback and bottom temperature as -0.34. Beam current is also negatively correlate with bottom temperature and column temperature as -0.24 and -0.27 respectively. It is worth noting here the difference of correlation between bottom temperature and column temperature between the two figures. It's a huge difference one at -0.23 and other stands at -0.89. May be something happened to these parameters to cause a failure of the part.

### 4.1.7 Arc Trip Error Case

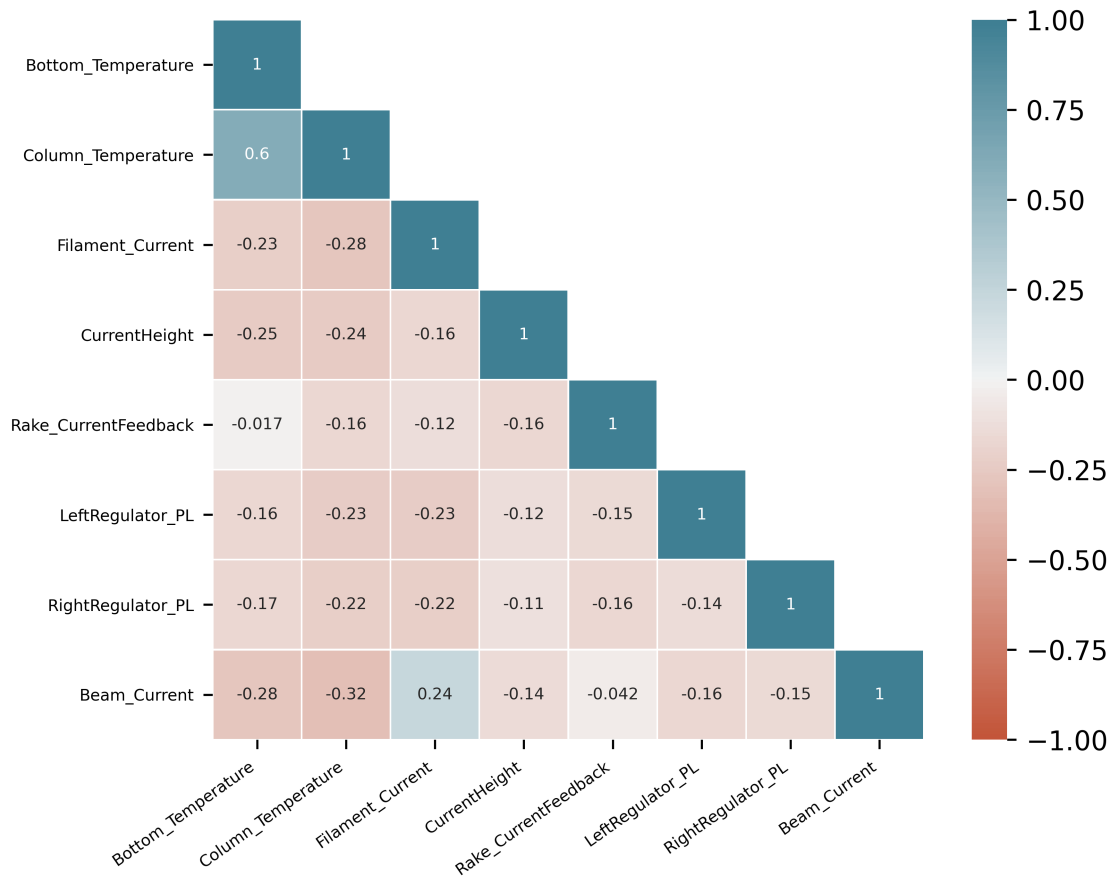


Figure 4.13: Results of Correlation analysis of arc trip error case, Part-1

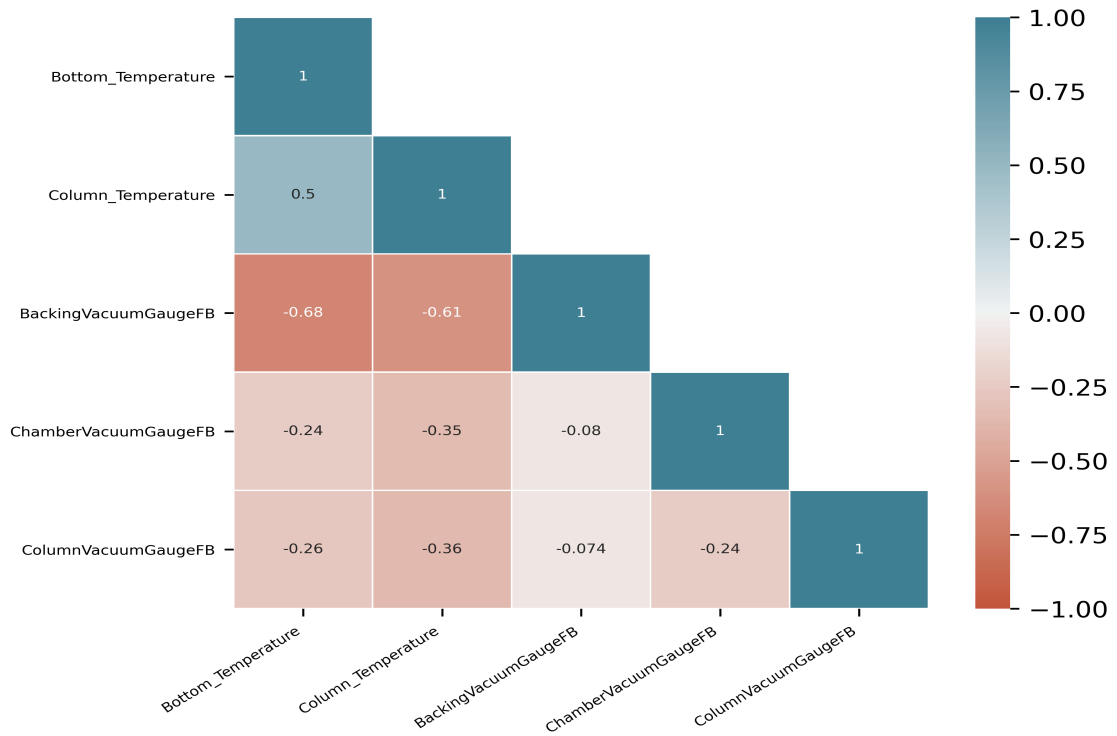


Figure 4.14: Results of Correlation analysis of arc trip error case, Part-2

In this case there is positive relationship in both the figures between the bottom temperature and the column temperature, and its value stands at +0.6 and +0.5. While the thing to be noted is that the beam current and the filament current are not as strongly positively correlated to each other as they were in previous cases, as in this case its value turned out to be only +0.24. Among negative relationships, there are two strongly inverse correlations. One is between backing vacuum gauge feedback and bottom temperature standing at -0.68 while the other is between backing vacuum gauge feedback and column temperature and its value is -0.61. Moreover, Column temperature and bottom temperature are also negatively correlated to column vacuum gauge feedback and chamber vacuum gauge feed back.

### 4.1.8 Correlation Analysis Conclusion

The summary of correlation analysis is shown in the table 4.1.

Build Done Cases
Build Failed Cases

	Beam Current	Bottom Temperature	Column Temperature	Filament Current	Current Height	Rake Current Feedback	Left t Regulator Pulse length	Right t Regulator Pulse length	Backing Vacuum Gauge feedback	Chamber Vacuum Gauge feedback	Column Vacuum Gauge feedback
Beam Current	1	Strong -	Moderate -	Strong +	Moderate -	Weak -	Weak -	Weak -	N/A	N/A	N/A
Bottom Temperature	Strong -	1	Weak +	Strong -	Moderate -	Weak -	Weak -	Weak -	Strong -	Weak -	Moderate -
Column Temperature	Strong -	Strong +	1	Moderate -	Moderate +	Weak -	Weak +	Weak -	Weak -	Weak -	Moderate -
Filament Current	Strong +	Moderate -	Strong -	1	Weak -	Weak -	Weak -	Weak -	N/A	N/A	N/A
Current Height	Moderate -	Moderate -	Strong +	Moderate -	1	Weak +	Weak -	Weak -	N/A	N/A	N/A
Rake Current Feedback	Moderate +	Weak +	Moderate -	Weak -	Weak -	1	Weak -	Weak -	N/A	N/A	N/A
Left t Regulator Pulse length	Weak -	Weak -	Strong +	Weak -	Weak -	Weak -	1	Weak -	N/A	N/A	N/A
Right t Regulator Pulse length	Weak -	Weak -	Weak +	Weak -	Weak -	Weak -	Weak -	1	N/A	N/A	N/A
Backing Vacuum Gauge feedback	N/A	Strong -	Weak +	N/A	N/A	N/A	N/A	N/A	1	Weak -	Moderate -
Chamber Vacuum Gauge feedback	N/A	Moderate -	Moderate +	N/A	N/A	N/A	N/A	N/A	Moderate +	1	Moderate -
Column Vacuum Gauge feedback	N/A	Strong -	Moderate +	N/A	N/A	N/A	N/A	N/A	Moderate +	Moderate +	1

Table 4.1: Summary of Correlation analysis

The upper triangle represents the build done cases, while the lower triangle represents the build failed cases.

The co-relation results obtained in the previous section provide an important insight about the most important parameters that are responsible for the final part quality. It is worth nothing that for build done parts all the correlations between the parameters are fairly moderate and in almost the same range for all the build done cases. However for build failed cases the behavior of correlation between the parameters was so extreme and their value was so scattered when compared to other build failed parts or build done parts. It is also pertinent to mention here that the beam current is by far the most significant parameter that gives an idea about the build process. Similarly the bottom and column temperatures are also very important. The results show that all the selected parameters have some sort of co-relation between them and preserve some uniqueness when moving form build done to build failed category, therefore they all can give important information regarding the prediction of the quality of the part under production. Therefore, this data set is used for the Machine learning algorithm for prediction in the next section

## 4.2 Results of Support Vector Machine (SVM)

While implementing the SVM, three kernel functions were applied separately, i.e; Polynomial, Gaussian and Sigmoid kernel. The shape of the data set is summarized in the table 4.2.

Data Set	
Number of Features	11
Number of Entries for type 0	5000
Number of Entries for type1	5000
Total Number of Entries	10000
Training Size	600
Test Size	200
Validation Size	200

Table 4.2: Shape of SVM data set

The results of all the three kernels applied are shown in the table 4.3.

Results												
	Polynomial Kernel				Gaussian Kernel				Sigmoid Kernel			
Output	Precision	Recall	F1-Score	Support	Precision	Recall	F1-Score	Support	Precision	Recall	F1-Score	Support
0	0.57	0.07	0.13	4515	0.59	0.56	0.57	4515	0.53	0.78	0.63	4515
1	0.50	0.95	0.66	4485	0.58	0.61	0.59	4485	0.57	0.29	0.38	4485
Avg./tot.	0.54	0.51	0.51	9000	0.58	0.58	0.58	9000	0.55	0.54	0.51	9000

Table 4.3: Results of SVM model

Gaussian kernel achieved a perfect 58 percent prediction rate while Sigmoid kernel achieved 51 percent. Therefore the Gaussian kernel performed slightly better. Polynomial kernel showed the least accurate results.

Overall the results obtained from SVM were absolutely not satisfactory. This is because the data set was very huge and typically the state vector machine (SVM) model performs better when the data set is small.

Therefore, other experiments were carried out by artificial neural network models and training and testing them against the variance of different parameters to obtain the satisfactory prediction results.

### 4.3 Results of Artificial Neural Networks (ANN)

The shape of data set used for training, testing and validation is summarized in the table 4.4.

Data Set	
Number of Features	11
Number of Entries for type 0	528046
Number of Entries for type 1	972912
Total Number of Entries	1390885
Training Size	834531
Test Size	278177
Validation Size	278177

Table 4.4: Shape of ANN data set

The best results were obtained by using this division of data into train, test and validate sets. 60 percent of the data was used for the training purpose, while for testing and validation 20 percent was used for each. Overall the total features were 11 and the total number of entries were 1390885. Out of it the total number of entries for build done parts were 972912 while for build failed parts the number was 528046. A total of 834531 entries of all the 11 features were used for training the model. for testing and training 278177 entries were used for each.

The results of the model are shown in the table 4.5.

Results		
Epochs=50, test size=10%, batch size=200, Model=Sequential, Hidden Layers=4, Activation Function=Relu and Sigmoid, ANN Model=Keras		
Mean Squared Error (MSE)	Model	Root Mean Squared Error (RMSE)
0.17810483276844025	Test Set Score	0.4254
0.17890693247318268	Train Set Score	0.4262
0.8948207	Predict test Set 1 (Actual Value =1)	0.7539
0	Predict test Set 2 (Actual Value =0)	0

Table 4.5: Results of ANN model

The model was tested for two metrics. The Mean squared Error (MSE) and the Root mean Squared Error (RMSE). The test set score for the mean squared error was achieved as 0.17810483276844025 while for root mean squared error it was 0.425437629. Clearly the test score of mean squared error is much more superior than the root mean aqua red error.

As far as the training score is concerned, it was 0.17890693247318268 in the case of mean squared error, while it was 0.426165998 in the case of root mean squared error. Again the mean squared error won over root mean squared error in the category of train score.

Then the model was tested with two sets of values against each feature. For the first set the predicted result was 0 and 0.8948207 for actual values of 0 and 1 respectively in the case of mean squared error. However, in the case of root mean squared error the predicted results were 0 and 0.7539 for the actual values of 0 and 1. Again in this category the mean squared error predicted better results than the root mean squared error.

## 4.4 Python Script

```
from sklearn.decomposition import PCA
from sklearn import preprocessing
import pandas as pd
import numpy as np
import matplotlib.pyplot as plt
from sklearn.model_selection import train_test_split
from sklearn.preprocessing import StandardScaler
from tensorflow.keras import Sequential
from tensorflow.keras.layers import Dense
from tensorflow.keras.optimizers import Adam
from tensorflow.keras.callbacks import EarlyStopping
from sklearn.model_selection import KFold
from sklearn.model_selection import cross_val_score
import datetime
import csv
import glob
import os
import pprint
import seaborn as sns

#Combining the data set
df1= pd.read_csv(r'C:\Users\ASUS\Desktop\Data Set\CSV_Bottom_Temperature(C).csv')
df2=pd.read_csv(r'C:\Users\ASUS\Desktop\Data Set\CSV_Column_Temperature(C).csv')
df3= pd.read_csv(r'C:\Users\ASUS\Desktop\Data Set\CSV_Beam_Current(mA).csv')
df4=pd.read_csv(r'C:\Users\ASUS\Desktop\Data Set\CSV_Filament_Current(A).csv')
df5=pd.read_csv(r'C:\Users\ASUS\Desktop\Data Set\CSV_Rake_CurrentFeedback(A).csv')
df6=pd.read_csv(r'C:\Users\ASUS\Desktop\Data Set\CSV_RightRegulator_PulseLenght(ms).csv')
df7=pd.read_csv(r'C:\Users\ASUS\Desktop\Data Set\CSV_LeftRegulator_PulseLenght(ms).csv')
df8=pd.read_csv(r'C:\Users\ASUS\Desktop\Data Set\CSV_CurrentHeight(mm).csv')

df9=pd.read_csv(r'C:\Users\ASUS\Desktop\Data Set\CSV_BackingVacuumGaugeFB(mBar).csv')
df10=pd.read_csv(r'C:\Users\ASUS\Desktop\Data Set\CSV_ChamberVacuumGaugeFB(mBar).csv')
```

```

df11=pd.read_csv(r'C:\Users\ASUS\Desktop\Data Set\CSV_ColumnVacuumGaugeFB.csv')

df1.columns = ['Time_Stamp', 'Bottom_Temperature']
df2.columns = ['Time_Stamp', 'Column_Temperature']
df3.columns = ['Time_Stamp', 'Beam_Current']
df4.columns = ['Time_Stamp', 'Filament_Current']
df5.columns = ['Time_Stamp', 'Rake_CurrentFeedback']
df6.columns = ['Time_Stamp', 'RightRegulator_PL']
df7.columns = ['Time_Stamp', 'LeftRegulator_PL']
df8.columns = ['Time_Stamp', 'CurrentHeight']

df9.columns = ['Time_Stamp', 'BackingVacuumGaugeFB']
df10.columns = ['Time_Stamp', 'ChamberVacuumGaugeFB']
df11.columns = ['Time_Stamp', 'ColumnVacuumGaugeFB']

df3["Beam_Current"] = df3.Beam_Current.str.replace(',','').astype(float)
df4["Filament_Current"] = df4.Filament_Current.str.replace(',','').astype(float)
df5['Rake_CurrentFeedback']=df5.Rake_CurrentFeedback.str.replace(',','').astype(float)
#df6['RightRegulator_PL']=df6.RightRegulator_PL.str.replace(',','').astype(float)
#df7['LeftRegulator_PL']=df7.LeftRegulator_PL.str.replace(',','').astype(float)
df8['CurrentHeight']=df8.CurrentHeight.str.replace(',','').astype(float)

df9['BackingVacuumGaugeFB']=df9.BackingVacuumGaugeFB.str.replace(',','').astype(float)
df10['ChamberVacuumGaugeFB']=df10.ChamberVacuumGaugeFB.str.replace(',','').astype(float)
df11['ColumnVacuumGaugeFB']=df11.ColumnVacuumGaugeFB.str.replace(',','').astype(float)

result1=pd.merge(df1, df2, on='Time_Stamp', how='outer')
result2=pd.merge(df3, df4, on='Time_Stamp', how='outer')
result3=pd.merge(df5, df6, on='Time_Stamp', how='outer')
result4=pd.merge(df7, df8, on='Time_Stamp', how='outer')
result5=pd.merge(df9, df10, on='Time_Stamp', how='outer')

result6=pd.merge(result1, result2, on='Time_Stamp', how='outer')
result7=pd.merge(result3, result4, on='Time_Stamp', how='outer')
result8=pd.merge(result5, df11, on='Time_Stamp', how='outer')

result9=pd.merge(result6, result7, on='Time_Stamp', how='outer')
result10=pd.merge(result8, result9, on='Time_Stamp', how='outer')

result10.sort_values(by=['Time_Stamp'], inplace=True, ascending=True)
#result10['Qualification_Category'] = '1'
result10= result10[['Time_Stamp', 'Bottom_Temperature', 'Column_Temperature',

```

```

        'Filament_Current', 'CurrentHeight', 'Rake_CurrentFeedback',
        'LeftRegulator_PL', 'RightRegulator_PL', 'Beam_Current',
        'BackingVacuumGaugeFB', 'ChamberVacuumGaugeFB',
        'ColumnVacuumGaugeFB']]
#result10.fillna(0, inplace=True)
result11=result10.drop(["Time_Stamp"], axis=1)
result11.to_csv(r'C:\Users\ASUS\Desktop\Out\BD\BD1.csv', index = False)

#Similarly all the cases were combine.

#After combining all the data against different cases, data was merged into a single CSV file.

path1 = r'C:\Users\ASUS\Desktop\Out\BD' # path
all_files1 = glob.glob(path1 + "/*.csv")

dfList1 = []
colnames1 = ['Bottom_Temperature', 'Column_Temperature', 'Filament_Current',
             'CurrentHeight', 'Rake_CurrentFeedback', 'LeftRegulator_PL',
             'RightRegulator_PL', 'Beam_Current', 'BackingVacuumGaugeFB',
             'ChamberVacuumGaugeFB', 'ColumnVacuumGaugeFB']
for filename in all_files1:
    df1 = pd.read_csv(filename, index_col=None, header=0)
    dfList1.append(df1)

concatDf1 = pd.concat(dfList1, axis=0, ignore_index=True)
concatDf1.columns =colnames1
newDf1= concatDf1 [['Bottom_Temperature', 'Column_Temperature',
                  'Filament_Current', 'CurrentHeight', 'Rake_CurrentFeedback',
                  'LeftRegulator_PL', 'RightRegulator_PL', 'Beam_Current',
                  'BackingVacuumGaugeFB', 'ChamberVacuumGaugeFB', 'ColumnVacuumGaugeFB']]

newDf1['Qualification_Category'] = '1'
newDf1.to_csv(r'C:\Users\ASUS\Desktop\Out\Combined\2AllBD.csv', index = False)

path2 = r'C:\Users\ASUS\Desktop\Out\BF' # path
all_files2 = glob.glob(path2 + "/*.csv")

dfList2 = []
colnames2 = ['Bottom_Temperature', 'Column_Temperature', 'Filament_Current',
             'CurrentHeight', 'Rake_CurrentFeedback', 'LeftRegulator_PL',
             'RightRegulator_PL', 'Beam_Current', 'BackingVacuumGaugeFB',

```

```

        'ChamberVacuumGaugeFB', 'ColumnVacuumGaugeFB']
for filename in all_files2:
    df2 = pd.read_csv(filename, index_col=None, header=0)
    dfList2.append(df2)

concatDf2 = pd.concat(dfList2, axis=0, ignore_index=True)
concatDf2.columns = colnames2
newDf2= concatDf2 [['Bottom_Temperature', 'Column_Temperature', 'Filament_Current',
                  'CurrentHeight', 'Rake_CurrentFeedback', 'LeftRegulator_PL',
                  'RightRegulator_PL', 'Beam_Current', 'BackingVacuumGaugeFB',
                  'ChamberVacuumGaugeFB', 'ColumnVacuumGaugeFB']]

newDf2['Qualification_Category'] = '0'
newDf2.to_csv(r'C:\Users\ASUS\Desktop\Out\Combined\1AllBF.csv', index = False)

path3 = r'C:\Users\ASUS\Desktop\Out\Combined' # path
all_files3 = glob.glob(path3 + "/*.csv")

dfList3 = []
colnames3 = ['Bottom_Temperature', 'Column_Temperature', 'Filament_Current', 'CurrentHeight',
             'Rake_CurrentFeedback', 'LeftRegulator_PL', 'RightRegulator_PL', 'Beam_Current',
             'BackingVacuumGaugeFB', 'ChamberVacuumGaugeFB', 'ColumnVacuumGaugeFB',
             'Qualification_Category']
for filename in all_files3:
    df3 = pd.read_csv(filename, index_col=None, header=0)
    dfList3.append(df3)

concatDf3 = pd.concat(dfList3, axis=0, ignore_index=True)
concatDf3.columns = colnames3
newDf3= concatDf3 [['Bottom_Temperature', 'Column_Temperature', 'Filament_Current',
                  'CurrentHeight', 'Rake_CurrentFeedback', 'LeftRegulator_PL',
                  'RightRegulator_PL', 'Beam_Current', 'BackingVacuumGaugeFB',
                  'ChamberVacuumGaugeFB', 'ColumnVacuumGaugeFB', 'Qualification_Category']]

newDf3.to_csv(r'C:\Users\ASUS\Desktop\Out\All.csv', index = False)

#Implementation of SVM algorithm

df= pd.read_csv(r'C:\Users\ASUS\Desktop\Out\All.csv')
print(df.dtypes)
print(len(df))

```

```
df.fillna(0, inplace=True)

print(len(df.loc[(df['Beam_Current']==0)]))

df_bd=df[df['Qualification_Category']==1]
df_bf=df[df['Qualification_Category']==2]

print(len(df_bd))
print(len(df_bf))

df_bd_downsampled = resample(df_bd, replace=False, n_samples=100000,random_state=0)
print(len(df_bd_downsampled))

df_bf_downsampled = resample(df_bf, replace=False, n_samples=100000,random_state=0)
print(len(df_bf_downsampled))

df_downsampled = pd.concat([df_bd_downsampled , df_bf_downsampled])
print(len(df_downsampled))

df_downsampled.to_csv(r'C:\Users\ASUS\Desktop\Out\df_downsampled.csv', index = False)

X=df_downsampled.drop('Qualification_Category', axis=1).copy()
print(X.head())

y=df_downsampled['Qualification_Category'].copy()
print(y.head())

X_train, X_test, y_train, y_test = train_test_split(X, y, train_size=0.7,random_state=42)
X_train_scaled = scale(X_train)
X_test_scaled = scale(X_test)

clf_svm = svm.SVC(kernel='linear')
clf_svm.fit(X_train_scaled, y_train)
y_pred = clf_svm.predict(X_test)

plot_confusion_matrix(clf_svm, X_test_scaled, y_test, values_format='d',
                      display_labels=["Build Done", "Build Failed"])

plt.show()
```

```
confidence = clf_svm.score(X_test, y_test)
print(confidence)

print(confusion_matrix(y_test, y_pred))
print(classification_report(y_test, y_pred))
print("Accuracy:", metrics.accuracy_score(y_test, y_pred))

#ANN for training accuracy

df= pd.read_csv(r'C:\Users\ASUS\Desktop\Out\All.csv')
df.fillna(0, inplace=True)

X=df.drop('Qualification_Category', axis=1)
y=df['Qualification_Category']

X_train, X_test, y_train, y_test = train_test_split(X, y, test_size=0.62, random_state=0)

#standardize the dataset
sc = StandardScaler()
sc.fit(X_train)
X_train = sc.transform(X_train)
X_test = sc.transform(X_test)
'''

print(f"Shape of train set is {X_train.shape}")
print(f"Shape of test set is {X_test.shape}")
print(f"Shape of train label is {y_train.shape}")
print(f"Shape of test labels is {y_test.shape}")
'''

model=Sequential()
model.add(Dense(28, input_dim=11, activation= 'relu'))
model.add(Dense(17, activation= 'relu'))
model.add(Dense(12, activation= 'relu'))
model.add(Dense(5, activation= 'relu'))
model.add(Dense(1, activation= 'sigmoid'))
```

```
model.compile(optimizer='adam', loss='binary_crossentropy', metrics=['accuracy'])

history = model.fit(X_train, y_train, epochs=20, batch_size=200, verbose=0)

print('accuracy:      ', history.history['accuracy'][-1])

plt.figure(figsize=(7, 3))
plt.plot(history.history['accuracy'], lw =2, ls = '-', label = 'Training accuracy')
plt.title('Training Accuracy')
plt.xlabel('Epochs')
plt.ylabel('Accuracy')
plt.legend()
plt.show()

#ANN for MSE

df= pd.read_csv(r'C:\Users\ASUS\Desktop\Out\All.csv')
df.fillna(0, inplace=True)
print(len(df))

X=df.drop('Qualification_Category', axis=1)
y=df['Qualification_Category']

X_train, X_test, y_train, y_test =
train_test_split(X, y, test_size=0.25, random_state=0)

#standardize the dataset
sc_X = StandardScaler()
sc_X .fit(X_train)
X_train = sc_X.transform(X_train)
X_test = sc_X.transform(X_test)

print(f"Shape of train set is {X_train.shape}")
print(f"Shape of test set is {X_test.shape}")
print(f"Shape of train label is {y_train.shape}")
print(f"Shape of test labels is {y_test.shape}")
num_features = len(X_train[1,:])

# ANN with Keras
```

```
classifier=Sequential()
classifier.add(Dense(28, input_dim=num_features, activation= 'relu'))
classifier.add(Dense(17, activation= 'relu'))
classifier.add(Dense(12, activation= 'relu'))
classifier.add(Dense(5, activation= 'relu'))
classifier.add(Dense(1, activation= 'sigmoid'))

classifier.compile(optimizer = 'adam', loss = 'mean_squared_error')
history_mse = classifier.fit(X_train, y_train,
                             epochs = 20, batch_size=200, verbose = 0, validation_split = 0.2)

print('Loss:      ', history_mse.history['loss'][-1],
      '\nVal_loss: ', history_mse.history['val_loss'][-1])

# EVALUATE MODEL IN THE TEST SET
score_mse_test = classifier.evaluate(X_test, y_test)
print('Test Score:', score_mse_test)

# EVALUATE MODEL IN THE TRAIN SET
score_mse_train = classifier.evaluate(X_train, y_train)
print('Train Score:', score_mse_train)

#Converting the first line of the dataset
linha1 = np.array([0 ,0,10.77546,0,-0.5769,0,0,35.7982,0,0,0]).reshape(1,-1)
linha2 = np.array([27 ,33,11.3,0.05,0.1153,
                  560,0,0.260417,6,0.002108,0.00000388]).reshape(1,-1)
# Scaling the first line to the same pattern used in the model
linha1 = sc_X.transform(linha1)
linha2 = sc_X.transform(linha2)
# Predicted value by model
y_pred_mse_1 = classifier.predict(linha1)
y_pred_mse_2 = classifier.predict(linha2)
print('Predicted value mse 1: ',y_pred_mse_1)
print('Real value: ', '1')
print('Predicted value mse 2: ',y_pred_mse_2)
print('Real value: ', '0')

plt.figure(figsize=(6, 4))
```

```
plt.plot(history_mse.history['loss'], lw=3, ls='--', label='Loss')
plt.plot(history_mse.history['val_loss'], lw=2, ls='-', label='Val Loss')
plt.xlabel('Epochs', fontsize=15)
plt.ylabel('Loss', fontsize=15)
plt.title('MSE')
plt.legend()
plt.show()
```

```
#ANN for RMSE
```

```
df= pd.read_csv(r'C:\Users\ASUS\Desktop\Out\All.csv')
df.fillna(0, inplace=True)
df['Qualification_Category'] = df['Qualification_Category'].astype(float)
```

```
X=df.drop('Qualification_Category', axis=1)
y=df['Qualification_Category']
```

```
X_train, X_test, y_train, y_test = train_test_split(X, y,
                                                    test_size=0.35, random_state=0)
```

```
#standardize the dataset
```

```
sc_X = StandardScaler()
sc_X .fit(X_train)
X_train = sc_X.transform(X_train)
X_test = sc_X.transform(X_test)
```

```
print(f"Shape of train set is {X_train.shape}")
print(f"Shape of test set is {X_test.shape}")
print(f"Shape of train label is {y_train.shape}")
print(f"Shape of test labels is {y_test.shape}")
num_features = len(X_train[1,:])
```

```
# ANN with Keras
```

```
classifier=Sequential()
classifier.add(Dense(28, input_dim=num_features, activation='relu'))
classifier.add(Dense(17, activation='relu'))
classifier.add(Dense(12, activation='relu'))
classifier.add(Dense(5, activation='relu'))
classifier.add(Dense(1, activation='sigmoid'))
```

---

```

def root_mean_squared_error(y_true, y_pred):
    return K.sqrt(K.mean(K.square(y_pred - y_true)))

classifier.compile(optimizer = 'adam', loss = root_mean_squared_error)

early_stopping_monitor = EarlyStopping(monitor='val_loss', patience=50)

history = classifier.fit(X_train, y_train, epochs = 20,
                        batch_size=200, callbacks = [early_stopping_monitor],
                        verbose = 0, validation_split = 0.2)

print('Loss:      ', history.history['loss'][-1], '\nVal_loss: ',
      history.history['val_loss'][-1])

# EVALUATE MODEL IN THE TEST SET
score_rmse_test = classifier.evaluate(X_test, y_test)
print('Test Score:', score_rmse_test)

# EVALUATE MODEL IN THE TRAIN SET
score_rmse_train = classifier.evaluate(X_train, y_train)
print('Train Score:', score_rmse_train)

linha1 = np.array([0, 0, 10.77546, 0, -0.5769, 0, 0,
                  35.7982, 0, 0, 0]).reshape(1, -1)
linha2 = np.array([27, 33, 11.3, 0.05, 0.1153, 560,
                  0, 0.260417, 6, 0.002108, 0.00000388]).reshape(1, -1)
# Scaling the first line to the same pattern used in the model
linha1 = sc_X.transform(linha1)
linha2 = sc_X.transform(linha2)
# Predicted value by model
y_pred_rmse_1 = classifier.predict(linha1)
y_pred_rmse_2 = classifier.predict(linha2)
print('Predicted value rmse 1: ', y_pred_rmse_1)
print('Real value: ', '1')
print('Predicted value rmse 2: ', y_pred_rmse_2)
print('Real value: ', '0')

plt.figure(figsize=(6, 4))
plt.plot(history.history['loss'], lw = 3, ls = '--', label = 'Loss')
plt.plot(history.history['val_loss'], lw = 2, ls = '-', label = 'Val Loss')

```

```
plt.xlabel('Epochs', fontsize=15)
plt.ylabel('Loss', fontsize=15)
plt.title('RMSE')
plt.legend()
plt.show()
```

---

---

## CHAPTER 5

---

# CONCLUSION AND FUTURE WORK

Conclusion of the experimental results are explained in section 5.1 and in section 5.2 the future possible work in continuation to this thesis is discussed.

### 5.0.1 Conclusion

A large number of applications of artificial intelligence and machine learning are available in the literature, specially for the in-situ monitoring and edge detection for the additive manufacturing, however, not much work has been done in the past for the characterization and classification using the prediction models. This really can be a successful pro-active and predictive approach to detect the quality flaws and defects before even they happen and can cause a major industrial breakthrough for the EBM technique.

In this thesis work, the effort has been carried out to address the characterization issue and develop some prediction models that are able to perform proactive and predictive task.

First of all the important parameters involved in the EBM additive manufacturing were analyzed. Then correlation between the parameters was carried out and the most significant parameters were selected to proceed towards the model development.

Two models were developed, one using the Support Vector Machine (SVM) and the second model was Artificial Neural Network (ANN). As a comparison the results obtain by the ANN model are far more superior than the SVM model. The main reason behind SVM not predicting good results can be the fact that SVM can manage small data sets very well but when the dimension of the data set increases, it decreases its accuracy. For larger data set ANN comes into play, and it is evident from the results of the ANN model that is giving much better results than ANN.

Also withing the ANN approach the metrics were calculated using two different approaches, i.e; the Mean Squared Error (MSE) and the Root Mean Squared Error (RMSE). Upon comparison of these two metrics it turned out that the MSE was giving the best results, that is to say, the loss of the MSE metric is 0.178 as compared to 0.426 for that of RMSE. Therefore, as a final result MSE metric was selected as the best one.

## 5.1 Future Work

Recent advancement in Artificial intelligence has a huge impact on the deployment of ML algorithms in the manufacturing sector. Particularly for additive manufacturing which can now be done in a better way than ever before. A significant leap can be achieved by improving the proposed model to further accuracy level for prediction in order to attain a proactive approach towards the quality monitoring in real time while manufacturing of the part with EBM. Several propositions can be presented for this work.

The accuracy of prediction can be improved to a further level by analysing and selecting more data for the model training. It will be a good idea to collect the data from an industry on regular basis and try to predict with more improved models.

Also the developed model can be tested in real time while getting the test data directly from the machine.

Moreover, the predictions made by the model can be helpful to optimize the manufacturing parameters in the real time scenario during the manufacturing EBM process.

---

# Bibliography

- [1] ASTM-International, "Standard Terminology for Additive Manufacturing Technologies," vol.F2792-12a, ed. West Conshohocken, PA: ASTM International, 2012.
- [2] ISO/ASTM 52900:2015 (E). Standard Terminology for Additive Manufacturing – General Principles – Terminology
- [3] Gibson, I., Rosen, D. W., Stucker, B. (2010). Additive manufacturing technologies (Vol. 238). New York: Springer.
- [4] Zaeh, M. F., Kahnert, M. (2009). The effect of scanning strategies on electron beam sintering. *Production Engineering*, 3(3), 217-224.
- [5] Rodriguez, E., Mireles, J., Terrazas, C. A., Espalin, D., Perez, M. A., Wicker, R. B. (2015). Approximation of absolute surface temperature measurements of powder bed fusion additive manufacturing technology using in situ infrared thermography. *Additive Manufacturing*, 5, 31- 39.
- [6] <http://www.arcam.com/technology/electron-beam-melting/hardware/>
- [7] Mahale, T. R. (2009). Electron beam melting of advanced materials and structures. North Carolina State University.
- [8] Sames, W. J., List, F. A., Pannala, S., Dehoff, R. R., Babu, S. S. (2016). The metallurgy and processing science of metal additive manufacturing. *International Materials Reviews*, 61(5), 315-360.
- [9] Korner, C. (2016). Additive manufacturing of metallic components by selective electron beam melting—a review. *International Materials Reviews*, 61(5), 361-377.
- [10] Schultz, H. (1994). *Electron beam welding*. Elsevier.
- [11] Gibson, I., Rosen, D. W., Stucker, B. (2010). Additive manufacturing technologies (Vol. 238). New York: Springer.
- [12] Krumeich, F. (2011). Properties of electrons, their interactions with matter and applications in electron microscopy. Laboratory of Inorganic Chemistry, disponível em
- [13] Mathew, A. *Lattice Vibrations–Phonons in Solid State*.
- [14] Everton, S. K., Hirsch, M., Stravroulakis, P., Leach, R. K., Clare, A. T. (2016). Review of in-situ process monitoring and in-situ metrology for metal additive manufacturing. *Materials Design*, 95, 431-445.
- [15] Grasso, M., Colosimo, B. M. (2017). Process defects and in situ monitoring methods in metal powder bed fusion: a review. *Measurement Science and Technology*, 28(4), 044005.
- [16] Zah, M. F., Lutzmann, S. (2010). Modeling and simulation of electron beam melting. *Production Engineering*, 4(1), 15-23.
- [17] Schwerdtfeger, J., Singer, R. F., Korner, C. (2012). In situ flaw detection by IR-imaging during electron beam melting. *Rapid Prototyping Journal*, 18(4), 259-263.

- [18] Boone, Nicholas Zhu, Chengxi Smith, C. Todd, I. Willmott, J.R.. (2018). Thermal near infrared monitoring system for electron beam melting with emissivity tracking. *Additive Manufacturing*. 22. 601-605. 10.1016/j.addma.2018.06.004.
- [19] Gong, X., Cheng, B., Price, S., Chou, K. (2013, November). Powder-bed electron-beam-melting additive manufacturing: powder characterization, process simulation and metrology. In *Proceedings of the ASME District F Early Career Technical Conference* (pp. 59-66).
- [20] Price, S., Cooper, K., Chou, K. (2012, August). Evaluations of temperature measurements by near-infrared thermography in powder-based electron-beam additive manufacturing. In *Proceedings of the Solid Freeform Fabrication Symposium* (pp. 761-773). University of Texas, Austin, TX.
- [21] Dinwiddie, R. B., Dehoff, R. R., Lloyd, P. D., Lowe, L. E., Ulrich, J. B. (2013, May). Thermographic in-situ process monitoring of the electron-beam melting technology used in additive manufacturing. In *SPIE Defense, Security, and Sensing* (pp. 87050K-87050K). International Society for Optics and Photonics.
- [22] Cheng, B., Price, S., Lydon, J., Cooper, K., Chou, K. (2014). On Process Temperature in Powder- Bed Electron Beam Additive Manufacturing: Model Development and Validation. *Journal of Manufacturing Science and Engineering*, 136(6), 061018.
- [23] Ridwan, S., Mireles, J., Gaytan, S. M., Espalin, D., Wicker, R. B. (2014). Automatic layerwise acquisition of thermal and geometric data of the electron beam melting process using infrared thermography. In *Proc. Int. Symp. Solid Freeform Fabrication* (Vol. 343).
- [24] Mireles, J., Terrazas, C., Gaytan, S., Roberson, D., Wicker, R. (2015). Closed-loop automatic feedback control in electron beam melting. *International Journal of Advanced Manufacturing Technology*, 78.
- [25] Raplee, J., Plotkowski, A., Kirka, M. M., Dinwiddie, R., Okello, A., Dehoff, R. R., Babu, S. S. (2017). Thermographic Microstructure Monitoring in Electron Beam Additive Manufacturing. *Scientific Reports*, 7, 43554.
- [26] Cordero, P. M., Mireles, J., Ridwan, S., Wicker, R. B. (2017). Evaluation of monitoring methods for electron beam melting powder bed fusion additive manufacturing technology. *Progress in Additive Manufacturing*, 2(1-2), 1-10.
- [27] Tuan D. Ngo, Alireza Kashani, Gabriele Imbalzano, Kate T.Q. Nguyen, David Hui, *Additive manufacturing (3D printing): A review of materials, methods, applications and challenges*, *Composites Part B: Engineering*, Volume 143, 2018, Pages 172-196, ISSN 1359-8368.
- [28] Shevchik SA, Kenel C, Leinenbach C, Wasmer K. Acoustic emission for in situ quality monitoring in additive manufacturing using spectral convolutional neural networks. *Addit Manuf* 2018;21:598–604.
- [29] Wasmer K, Le-Quang T, Meylan B, Shevchik SA. In situ quality monitoring in AM using acoustic emission: a machine learning approach. *J Mater Eng Perform* 2019;28(2):666–72.
- [30] Mallikharjun Marrey, Ehsan Malekipour, Hazim El-Mounayri, Eric J. Faierson, A Framework for Optimizing Process Parameters in Powder Bed Fusion (PBF) Process Using Artificial Neural Network (ANN), *Procedia Manufacturing*, Volume 34, 2019, Pages 505-515,ISSN 2351-9789,
- [31] Imani, F., Montazeri, M., Gaikwad, A., Rao, P., Yang, H., and Reutzler, E., 2018, "Layerwise In-Process Quality Monitoring in Laser Powder Bed Fusion," *ASME 2018 13th International Manufacturing Science and Engineering Conference*, ASME, College Station, USA.

- [32] Grasso, M., Gallina, F., and Colosimo, B. M., 2018, "Data Fusion Methods for Statistical Process Monitoring and Quality Characterization in Metal Additive Manufacturing," *Procedia CIRP*.
- [33] Liu, C., Roberson, D., and Kong, Z., 2017, "Textural Analysis-Based Online Closed-Loop Quality Control for Additive Manufacturing Processes," 2017 Industrial and Systems Engineering Conference, Blacksburg, VA, USA.
- [34] Yao, B., Imani, E., and Yang, H., 2018, "Markov Decision Process for Image-Guided Additive Manufacturing," *IEEE Robot. Autom. Lett.*, 3(4), pp. 2792–2798.
- [35] M.O. Alabi, K. Nixon, I. Botef, A survey on recent applications of machine learning with big data in additive manufacturing industry, *Am. J. Eng. Appl. Sci.* 11 (2018) 1114–1124.
- [36] D. Wu, C. Jennings, J. Terpenney, R.X. Gao, S. Kumara, A comparative study on machine learning algorithms for smart manufacturing: tool wear prediction using random forests, *J. Manuf. Sci. Eng.* 139 (7) (2017) 071018.
- [37] <https://www.mathworks.com/>
- [38] Nils J. Nilsson, INTRODUCTION TO MACHINE LEARNING, 1998, Robotics Laboratory Stanford University
- [39] L. P. Kaelbling, M. L. Littman, A.W. Moore, Reinforcement Learning: A Survey, 1996, *Journal of Artificial Intelligence Research*, Vol 4, (1996), 237-285, arXiv:cs/9605103
- [40] Baumann, F.W., A. Sekulla, M. Hassler, B. Himpel and M. Pfeil, 2018. Trends of machine learning in additive manufacturing. *Int. J. Rapid Manufact.*
- [41] Roberson III, D.M., 2016. Sensor-based online process monitoring in advanced manufacturing. Virginia Polytechnic Institute and State University. <http://hdl.handle.net/10919/72911>.
- [42] Wu, M., V.V. Phoha, Y.B. Moon and A. Belman, 2016. Detecting malicious defects in 3D printing process using machine learning and image classification. *Proceeding of the International Mechanical Engineering Congress and Exposition*, Nov. 11-17, Phoenix, Arizona, USA, pp: V014T07A004-V014T07A004. DOI: 10.1115/IMECE2016-67641
- [43] Gobert, C., E.W. Reutzel, J. Petrich, A.R. Nassar and S. Phoha, 2018. Application of supervised machine learning for defect detection during metallic powder bed fusion additive manufacturing using high resolution imaging. *Additive Manufact.*, 21: 517-528. DOI: 10.1016/j.addma.2018.04.005
- [44] Scime, L. and J. Beuth, 2018. Anomaly detection and classification in laser powder bed additive manufacturing process using a trained computer vision algorithm. *Additive Manufact.*, 19:114-126. DOI: 10.1016/j.addma.2017.11.009
- [45] Xinbo Qi, Guofeng Chen, Yong Li, Xuan Cheng, Changpeng Li, Applying Neural-Network-Based Machine Learning to Additive Manufacturing: Current Applications, Challenges, and Future Perspectives, *Engineering*, Volume 5, Issue 4, 2019, Pages 721-729, ISSN 2095-8099,
- [46] "Autodesk And Airbus", 2016. Pioneering bionic 3D printing: <https://www.airbus.com/newsroom/news/en/2016/03/Pioneering-bionic3D-printing.html>
- [47] L. Scime, J. Beuth, A multi-scale convolutional neural network for autonomous anomaly detection and classification in a laser powder bed fusion additive manufacturing process, *Addit. Manuf.* 24 (2018) 273–286.
- [48] C. Wang, X. Tan, E. Liu, S.B. Tor, Process parameter optimization and mechanical properties for additively manufactured stainless steel 316L parts by selective electron beam melting, *Mater. Des.* 147 (2018) 157–166.

- [49] F. Caiazzo, A. Caggiano, Laser direct metal deposition of 2024 Al alloy: trace geometry prediction via machine learning, *Materials*. 11 (3) (2018) 444.
- [50] G. Tapia, S. Khairallah, M. Matthews, W.E. King, A. Elwany, Gaussian processbased surrogate modeling framework for process planning in laser powder-bed fusion additive manufacturing of 316L stainless steel, *Int. J. Adv. Manuf. Tech.* 94 (9–12) (2018) 3591–3603.
- [51] A. Garg, J.S.L. Lam, Measurement of environmental aspect of 3-D printing process using soft computing methods, *Measurement* 75 (2015) 210–217.
- [52] M. Zhang, C.-N. Sun, X. Zhang, P.C. Goh, J. Wei, D. Hardacre, H. Li, High cycle fatigue life prediction of laser additive manufactured stainless steel: a machine learning approach, *Int. J. Fatigue* 128 (105194) (2019).
- [53] K. Aoyagi, H. Wang, H. Sudo, A. Chiba, Simple method to construct process maps for additive manufacturing using a support vector machine, *Addit. Manuf.* 27 (2019) 353–362.
- [54] C. Wang, X.P. Tan, S.B. Tor, C.S. Lim, Machine learning in additive manufacturing: State-of-the-art and perspectives, *Additive Manufacturing*, Volume 36, 2020, 101538, ISSN 2214-8604,
- [55] B. Kappes, S. Moorthy, D. Drake, H. Geerlings, and A. Stebner, "Machine Learning to Optimize Additive Manufacturing Parameters for Laser Powder Bed Fusion of Inconel 718," in *Proceedings of the 9th International Symposium on Superalloy 718 Derivatives: Energy, Aerospace, and Industrial Applications*, Springer, Cham, 2018, pp. 595–610.
- [56] W. Zhang, A. Mehta, P. S. Desai, and C. F. H. III, "Machine Learning Enabled Powder Spreading Process Map for Metal Additive Manufacturing", in *2017 Solid Freeform Fabrication Symposium Proceedings*, 2017.
- [57] Galati, Manuela Iuliano, Luca. (2017). A literature review of powder-based electron beam melting focusing on numerical simulations. *Additive Manufacturing*. 19. 10.1016/j.addma.2017.11.001.
- [58] Y. Lecun, L. Bottou, Y. Bengio and P. Haffner, "Gradient-based learning applied to document recognition," in *Proceedings of the IEEE*, vol. 86, no. 11, pp. 2278-2324, Nov. 1998. doi: 10.1109/5.726791
- [59] A. Waibel, "Prosodic knowledge sources for word hypothesization in a continuous speech recognition system," *ICASSP '87. IEEE International Conference on Acoustics, Speech, and Signal Processing*, Dallas, TX, USA, 1987, pp. 856-859. doi: 10.1109/ICASSP.1987.1169848